LOW-SPEED CHARACTERISTICS OF A VARIABLE-SWEEP SUPERSONIC TRANSPORT MODEL WITH A BLENDED ENGINE FUSELAGE AND ENGINE-MOUNTED TAILS

By Vernard E. Lockwood and Wilson E. Thompson

Langley Research Center
Langley Station, Hampton, Va.

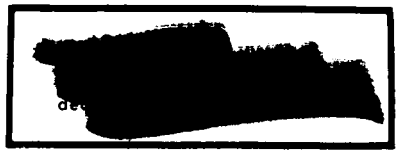

NATIONAL AERONAUTICS AND SPACE ADMINISTRATION

[redacted]

LOW-SPEED CHARACTERISTICS OF A VARIABLE-SWEEP SUPERSONIC TRANSPORT MODEL WITH A BLENDED ENGINE FUSELAGE AND ENGINE-MOUNTED TAILS*

By Vernard E. Lockwood and Wilson E. Thompson
Langley Research Center

SUMMARY

An investigation has been made at low speeds to determine the longitudinal and lateral stability and pitch control characteristics of a model of a proposed supersonic transport airplane configuration designated SCAT 14. The geometric variables studied were wing panel sweep, wing twist, and variations in sweep and deflection of the fixed area between the fuselage and the movable wing. Lateral stability data were obtained for one model configuration through a range of leading-edge sweep angles from 13.5° to 75°. The investigation was made in the Langley 300-MPH 7- by 10-foot tunnel at a Mach number of 0.18 which corresponds to a Reynolds number per foot of 1.24×10^6.

The results showed the basic model was longitudinally stable throughout the angle-of-attack and sweep range investigated for a moment reference located at the wing pivot station; however, a reduction in stability occurred at angles of attack greater than 8°. Varying the wing angle from 13.5° to 75° gave a rearward shift in the aerodynamic center of about 5.5 percent of the fuselage length and reduced the untrimmed maximum lift-drag ratio from 14.3 to 6.6. A change from the 70° wing-fuselage flaps to the 75° flaps resulted in pitch-up for wing sweep angles of 25° and 45°, a reduction in aerodynamic-center variation with sweep, and lower values of maximum lift-drag ratio.

Deflection of the 70° wing-fuselage flap gave stabilizing moments at high angles of attack and also resulted in reduced aerodynamic-center variation with panel sweep. Varying the wing sweep angle from 13.5° to 75° delayed the onset of directional instability from angles of attack of 18° to 23.5°.

INTRODUCTION

This paper contains the results of a low-speed investigation of a supersonic transport model designated SCAT 14. The configuration had a variable-sweep wing with an outboard pivot and in this respect is similar to the model reported on in

*Title, Unclassified.

reference 1. However, the aft fuselage design and powerplant geometry differ materially from that of the reference model. The present configuration had a blended engine-fuselage arrangement with the intake duct located beneath the fuselage. The horizontal tails were mounted on the sides of the engines.

The investigation was concerned primarily with the effect of wing geometry on the longitudinal characteristics. The geometric variables studied were wing panel sweep, wing twist, and variations in sweep and deflection of the fixed area between the movable wing and the fuselage. Tail-off data were also obtained to aid in understanding the complete model results. Lateral stability data were obtained for one model configuration through a range of leading-edge sweep angles from 13.5° to 75°.

The investigation was made in the Langley 300-MPH 7- by 10-foot tunnel at a Mach number of 0.18 which corresponds to a Reynolds number of 1,240,000 per foot.

SYMBOLS

The force and moment data contained herein are referred to the axis system shown in figure 1. The reference dimensions used in reducing the data based on the 75° swept wing are area, 7.00 square feet; chord, 31.35 inches; and span, 38.25 inches. The moment reference point is located at the wing pivot station (fuselage station 50.00) unless otherwise specified.

b wing span, in.

C_D drag coefficient, $\frac{\text{Drag}}{qS}$

C_L lift coefficient, $\frac{\text{Lift}}{qS}$

ΔC_L increment in lift coefficient

C_{L_α} slope of lift curve at $C_L = 0$

C_l rolling-moment coefficient, $\frac{\text{Rolling moment}}{qSb}$

$$C_{l_\beta} = \left(C_{l,\beta=5^\circ} - C_{l,\beta=-5^\circ}\right)\Big/\Delta\beta$$

ΔC_{l_β} increment in C_{l_β} due to addition of vertical tail

C_m pitching-moment coefficient, $\frac{\text{Pitching moment}}{qSc_{ref}}$

ΔC_m increment in pitching-moment coefficient

$\Delta C_m / \Delta \delta_h$ horizontal control effectiveness parameter

$\partial C_m / \partial C_L$ slope of pitching-moment-coefficient curve at $C_L = 0$

C_n yawing-moment coefficient, $\frac{\text{Yawing moment}}{qSb}$

$C_{n_\beta} = \left(C_{n,\beta=5^\circ} - C_{n,\beta=-5^\circ}\right) / \Delta\beta$

ΔC_{n_β} increment in C_{n_β} due to addition of vertical tail

C_Y side-force coefficient, $\frac{\text{Side force}}{qS}$

$C_{Y_\beta} = \left(C_{Y,\beta=5^\circ} - C_{Y,\beta=-5^\circ}\right) / \Delta\beta$

ΔC_{Y_β} increment in C_{Y_β} due to addition of vertical tail

c_{ref} reference chord, in.

L/D lift-drag ratio

$(L/D)_{max}$ maximum lift-drag ratio

q dynamic pressure, lb/sq ft

S	reference wing area, sq ft
x,y	coordinates of wing-fuselage flap, in.
y_l	lower surface ordinate of wing-fuselage flap, in.
y_u	upper surface ordinate of wing-fuselage flap, in.
α	angle of attack of fuselage reference line, deg
β	angle of sideslip, deg
$\Delta\beta$	increment in sideslip angle between $\beta = \pm 5^\circ$, corrected for balance and strut deflection, deg
Γ_h	horizontal-tail dihedral (positive up), deg
δ_h	horizontal-tail deflection, deg
δ_{WF}	wing-fuselage flap deflection (positive when leading edge is down), deg
Λ	wing leading-edge sweep angle, deg

Configuration designations:

F	fuselage
H	horizontal tail
s	sharp leading edge for wing-fuselage flap
r	round leading edge for wing-fuselage flap
V	vertical tail
W_1	wing with planar lower surface
W_2	wing with linear twist (2° nose-down at tip)
WF	wing-fuselage flap (see fig. 2)

MODEL

The model configuration features a variable-sweep wing with an outboard pivot location, a four-engine side-by-side arrangement which blends into the

fuselage at the rear of the model from an inlet located beneath the fuselage, and horizontal surfaces mounted from the sides of the engine ducts. A three-view drawing of the model is presented in figure 2(a) and photographs of the model mounted in the Langley 300-MPH 7- by 10-foot tunnel are shown in figure 3. Various model dimensions are given in tables I and II.

Fuselage cross sections drawn to model scale are presented in figure 4. It should be noted that the sections in the vicinity of the intake duct are solid, no provisions being made for internal flow.

Two sets of wings were used in the investigation, one untwisted W_1 and one twisted W_2. Wing 2 was twisted linearly about the 50-percent chord line from spanwise station 20.21 to 40.00. Both wings had identical airfoil sections which were developed from an NACA 65A006 section. The ordinates of this section were sheared upward to provide a flat bottom except in the immediate vicinity of the leading edge where the nose sections were rounded to provide a radius equal to 0.007 chord.

The model was provided with replaceable fillets between the fuselage and the movable wing which served to provide changes in planform, deflection, and leading-edge contour. The fillets or wing-fuselage flaps are shown in figures 2(b) and 2(c) and are described by the leading-edge sweep, the leading-edge contour (s = sharp; r = round), and the deflection of flap in a plane perpendicular to the hinge line as shown in figure 2(a) (for example, WF = $70^\circ s0^\circ$). Only the flap with the 70° sharp leading edge was deflected. When deflected, the break in the upper surface of the flap was faired over to provide a smooth transition between adjoining surfaces. The horizontal tail is shown in figure 2(a); additional dimensions are given in table I. The tail dihedral angle was zero except where noted otherwise.

TESTS AND CORRECTIONS

The investigation was made in the Langley 300-MPH 7- by 10-foot tunnel with the model strut supported from the floor of the tunnel as shown in figure 3. Forces and moments were measured by an internally mounted six-component strain-gage balance attached to the support strut. To insure a turbulent boundary-layer transition strips approximately 1/8 inch wide of No. 100 carborundum grains were attached to the model surfaces at the 7-percent chord station.

The investigation was made at a dynamic pressure of 45.6 pounds per square foot which corresponds to a Mach number of 0.18 and a Reynolds number per foot of 1.24×10^6. All configurations were investigated through a range of angle of attack at 0° sideslip, and selected configurations were also investigated at a sideslip angle of $\pm 5^\circ$. The drag data were corrected to correspond to a pressure at the base of the engine nacelles equal to free-stream static pressure.

The jet-boundary corrections calculated for the drag and angle of attack by the method of reference 2 are as follows:

$$C_D = C_{D,measured} + \left(0.0114C_L^2\right)$$

$$\alpha = \alpha_{measured} + \left(0.652C_L\right)$$

The jet-boundary corrections to the pitching-moment data were found to be negligible. The data were also corrected for wind-tunnel blockage by the method presented in reference 3. The angles of attack and sideslip were corrected for deflection of the balance and sting under load. The effect of the support strut on the model characteristics is unknown but because of the thinness of this strut it is thought that the corrections to the data would be small.

PRESENTATION OF DATA

The data obtained in the wind tunnel of the subject model are presented in the following figures:

	Figure
Longitudinal characteristics:	
Effect of wing sweep and horizontal tail.	
W_1; WF = 70°r0°	5 to 6
W_2; WF = 70°r0°	7
Effect of wing-fuselage flap geometry. W_2; δ_h = 0°	8
Effect of horizontal tail at various wing sweeps.	
W_2; WF = 75°s0°	9
Effect of wing sweep. W_2; WF = 70°s0°	10
Effect of wing-fuselage flap deflection at various wing sweeps.	
W_2; WF = 70°s	11
Effect of horizontal tail at various wing-sweep and wing-fuselage flap deflections. W_2; WF = 70°s	12 to 14
Effect of wing sweep on the increment in pitching-moment coefficient due to addition of horizontal tail ΔC_m and horizontal control effectiveness $\Delta C_m/\Delta\delta_h$. W_1; WF = 70°r0°	15
Effect of model geometry on variation of $\partial C_m/\partial C_L$, C_{L_α}, and $(L/D)_{max}$ with sweep.	
Effect of horizontal tail	16
Effect of wing twist	17
Effect of wing-fuselage flap geometry	18
Effect of wing-fuselage flap deflection	19

DISCUSSION

Longitudinal Stability

The results of investigations of the basic model are discussed and comparisons are made of the effect of changes in model geometry on the aerodynamic characteristics. The moment coefficient data are referred to the wing pivot location except where stated otherwise.

Basic model.- The data of figure 5(a) show the basic model (FW_1HV; WF = 70°r0°) is longitudinally stable throughout the angle of attack and sweep range investigated for the moment reference located at the wing pivot station. For intermediate sweep angles (25° to 55°) a reduction of stability occurred at angles of attack above 8°. The reduced stability or pitch-up characteristic is also noted in the tail-off data (FW_1V) of figure 5(b). Tuft studies made during the investigation show that the pitch-up is the result of separated flow over the outboard panel. The flow separation begins at an angle of attack of about 8°, and, except for a short span next to the wing pivot, complete separation occurs on the wing panel at an angle of attack of 12°. The pitch-up tendencies of the wing-fuselage combination are compensated to a large extent by the presence of a low horizontal tail as shown in figure 15. The increment in pitching-moment coefficient ΔC_m due to the horizontal tail increases with angle of attack and is generally independent of wing sweep angle. Also presented is the horizontal control effectiveness parameter $\Delta C_m/\Delta\delta_h$ determined from figure 6. It is noted that the control effectiveness which generally decreases between $\alpha = 0^\circ$ and $\alpha = 12^\circ$ results in less stability with the horizontal tail deflected at angles of attack greater than 12°.

The variation of basic model stability with wing sweep for low lift coefficients is shown in figure 16. This model, like other variable sweep configurations having a relatively large fixed area ahead of the moment reference, shows a reduction in stability at high sweep angles. (For example, see ref. 1.) The maximum change in the aerodynamic-center location occurs between the 13.5° and the 65° wing sweep angle and amounts to about 18.5 percent of the reference chord. Between wing sweep angles of 13.5° and 75° the aerodynamic-center

variation is reduced to 15.7 percent of the reference chord or about 5.5 percent of the fuselage length.

The summary of low angle-of-attack characteristics (fig. 16) shows the usual reduction in lift-curve slope C_{L_α} and untrimmed $(L/D)_{max}$ with sweep; the values of $(L/D)_{max}$ varied from 14.3 with $\Lambda = 13.5^\circ$ to 6.6 with $\Lambda = 75^\circ$ for configuration FW_1HV.

Wing 2.- A comparison of figure 6 with figure 7 shows no significant difference between wing 1 and wing 2 in the variation of C_m with C_L; in fact, the small amount of twist (2° nose down on W_2) gave almost identical values of $\partial C_m/\partial C_L$ as is shown in figure 17. Some small differences were noted, however, for the lift-curve slope C_{L_α} and $(L/D)_{max}$ between the two wings.

Wing-fuselage flap geometry.- A comparison of the aerodynamic characteristics of three wing-fuselage flap variations is presented in figure 8 for configuration FW_2HV. The pitching-moment characteristics were not affected significantly by the leading-edge radius of the 70° wing-fuselage flap but were affected by the increased area and sweep of the larger flap, $WF = 75^\circ s0^\circ$. At low angles of attack reduced stability margins occurred for each wing sweep angle and an overall reduction in aerodynamic-center variation between 25° and 75° wing sweep. (See fig. 18.) At the high angles of attack pitch-up tendencies were indicated for wing sweeps of 25° and 45°, and a reduced stability level was indicated for a wing sweep of 75°. (See fig. 8.) For a more direct comparison of the high-lift pitch characteristics of the two flap configurations, the values of C_m for $WF = 75^\circ s0^\circ$ were adjusted to give the same level of low-lift stability as flap $WF = 70^\circ s0^\circ$ had at $\Lambda = 25^\circ$. These adjusted values of C_m are indicated by the flagged symbols in figure 8; the pitch-up tendencies, although reduced, are still apparent in the transferred data. Most of this pitch-up tendency results directly from the added lift, only a small amount being attributed to reduced tail effectiveness. (See fig. 20.)

A change in the wing-fuselage flap also resulted in a small change in C_{L_α} and $(L/D)_{max}$ as is shown in figure 18. The lift-curve slope C_{L_α} was increased and values of $(L/D)_{max}$ were reduced for the range of sweep angles investigated.

Wing-fuselage flap deflection.- The data of figure 11 show that deflection of the wing-fuselage flap was an effective device for increasing model stability at high angles of attack. It is noted from figures 11 and 14 that 29° deflection of the wing-fuselage flap ($WF = 70^\circ s29^\circ$) reduces pitch-up tendencies and gives variations of C_m with C_L which are fairly linear over the design sweep range $\Lambda = 25^\circ$ to 75°. Increments in pitching-moment and lift coefficients due to the deflection of the flap (fig. 21) show that the stabilizing tendency is due in part to the loss of lift over the flapped area and in part to the additive lift of the horizontal tail. At high angles of attack the loss in lift is generally

less with the horizontal tail on than with the horizontal tail off; at low angles of attack positive increments in lift were obtained with the tail on.

The low-lift characteristics of the configuration are summarized in figure 19. These data generally show reductions in $\partial C_m/\partial C_L$ and C_{L_α}. Increases in $(L/D)_{max}$ are indicated for some configurations where the flap was deflected.

Tail dihedral.- A comparison of the longitudinal characteristics of the model with $\Gamma_h = -28.5^\circ$ with those models with $\Gamma_h = 0^\circ$ is shown in figures 9 and 13. No significant change in the pitch characteristics is noted for the negative tail dihedral.

Lateral Stability

Directional stability parameters are presented in figure 22 for model configuration FW_2HV and $WF = 70^\circ s0^\circ$. Increasing the wing sweep angle delayed the onset of directional instability from $\alpha = 18^\circ$ at $\Lambda = 13.5^\circ$ to $\alpha = 23.5^\circ$ at $\Lambda = 75^\circ$. This effect is due primarily to an increase in vertical-tail contribution arising from a favorable effect of sweep on the wing-induced sidewash at the vertical tail as shown in figure 24. Wing sweep also has a favorable effect on the stability of the wing-body combination as shown by the increasing values of C_{n_β} for increasing values of wing sweep in figure 23.

The effective dihedral parameter C_{l_β} given in figures 22 and 23 varied in a manner generally similar to that for other variable-sweep configurations of this type. For wings of low sweep, the effective dihedral increased up to wing stall angle and then decreased; this decrease was followed by increasing dihedral effect as the angle of attack was increased further. The wing of high sweep $\Lambda = 75^\circ$ gave increasing dihedral effect up to an angle of attack of 24°.

SUMMARY OF RESULTS

Results of a preliminary low-speed stability and control investigation on a model of a supersonic transport airplane configuration designated SCAT 14 are summarized as follows:

1. The basic model was longitudinally stable throughout the angle of attack and sweep range investigated for a moment reference located at the wing pivot station; however, for intermediate sweep angles (25° to 55°) a reduction of stability occurred at angles of attack greater than 8°. Varying the wing sweep angle from 13.5° to 75° gave a rearward shift in the aerodynamic center of about 5.5 percent of the fuselage length and reduced the untrimmed lift-drag ratio from 14.3 to 6.6.

2. A change from the 70° wing-fuselage flaps to the 75° flaps which increased the wing lifting area adjacent to the fuselage resulted in pitch-up

for wing sweep angles of 25° and 45°, a reduction in aerodynamic-center variation with sweep, and lower values of maximum lift-drag ratio.

3. Deflecting the 70° wing-fuselage flap 29° gave stabilizing moments at high angles of attack over the sweep range investigated. Deflection of the flap also reduced the aerodynamic-center variation with sweep and provided small increases in maximum lift-drag ratio.

4. Varying the wing-sweep angle from 13.5° to 75° delays the onset of directional instability from angles of attack of 18° to 23.5°.

Langley Research Center,
National Aeronautics and Space Administration,
Langley Station, Hampton, Va., August 12, 1964.

REFERENCES

1. Lockwood, Vernard E.; McKinney, Linwood W.; and Lamar, John E.: Low-Speed Aerodynamic Characteristics of a Supersonic Transport Model With a High-Aspect-Ratio Variable-Sweep Warped Wing. NASA TM X-979, 1964.

2. Gillis, Clarence L.; Polhamus, Edward C.; and Gray, Joseph L., Jr.: Charts for Determining Jet-Boundary Corrections for Complete Models in 7- by 10-Foot Closed Rectangular Wind Tunnels. NACA WR L-123, 1945. (Formerly NACA ARR L5G31.)

3. Herriot, John G.: Blockage Corrections for Three-Dimensional-Flow Closed-Throat Wind Tunnels, With Consideration of the Effect of Compressibility. NACA Rept. 995, 1950. (Supersedes NACA RM A7B28.)

TABLE I.- MODEL DIMENSIONS

Reference:	
Area, sq ft	7.00
Span, in.	38.25
Chord, in.	31.36
Fuselage:	
Length, in.	89.00
Base area of engine, sq ft	0.1365
Horizontal tail:	
Leading-edge sweep, deg	60.0
Trailing-edge sweep, deg	28.6
Root chord, in.	13.70
Tip chord, in.	4.20
Span (panel), in.	8.00
Span (overall), in.	28.00
Exposed area (total), sq ft	0.970
Vertical tail:	
Leading-edge sweep, deg	70.0
Trailing-edge sweep, deg	42.0
Root chord, in.	22.52
Tip chord, in.	4.60
Span, in.	9.68
Exposed area, sq ft	1.000
WF = $70^{o}s0^{o}$, WF = $70^{o}r0^{o}$:	
Area, sq ft	0.389
WF = $75^{o}s0^{o}$:	
Area, sq ft	0.714

TABLE II.- WING AREAS AND ASPECT RATIOS WITH CONSIDERATION FOR VARIOUS WING-FUSELAGE FLAPS

[Wing areas based on extension of leading and trailing edges to plane of symmetry]

Λ, deg	b, in.	Without WF flap		70° WF flap		75° WF flap	
		Area, sq ft	Aspect ratio	Area, sq ft	Aspect ratio	Area, sq ft	Aspect ratio
13.5	81.96	5.053	9.232	6.898	6.763	7.474	6.242
25	78.46	5.035	8.491	6.704	6.377	7.369	5.801
35	73.44	5.201	7.202	6.760	5.540	7.424	5.045
45	66.68	5.420	5.697	6.757	4.570	7.484	4.125
55	58.34	5.796	4.078	6.932	3.410	7.590	3.114
65	48.66	6.513	2.525	7.179	2.291	7.823	2.102
75	38.18	8.199	1.235	7.707	1.313	8.378	1.208

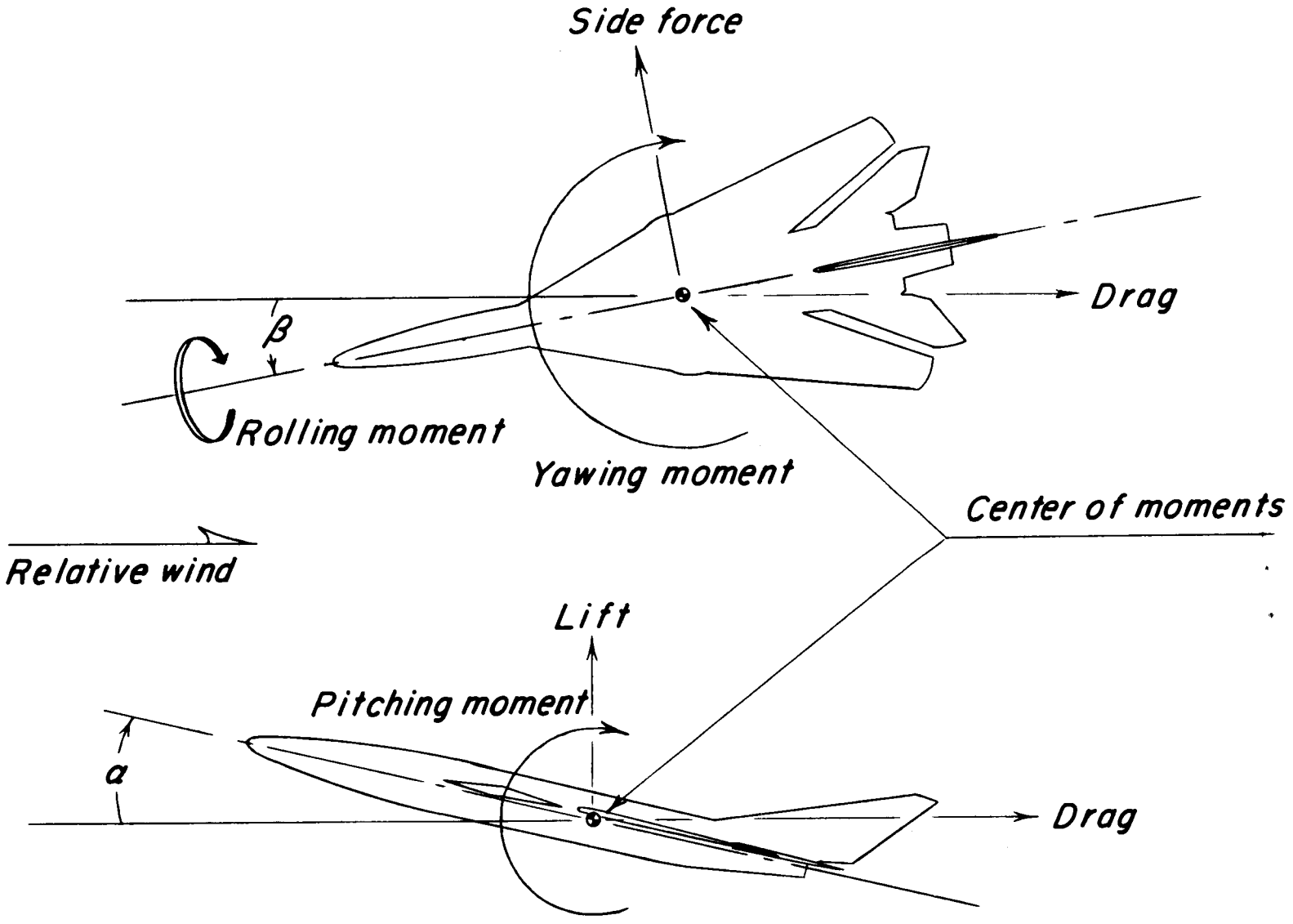

Figure 1.- Sketch of axis system used for presentation of data.

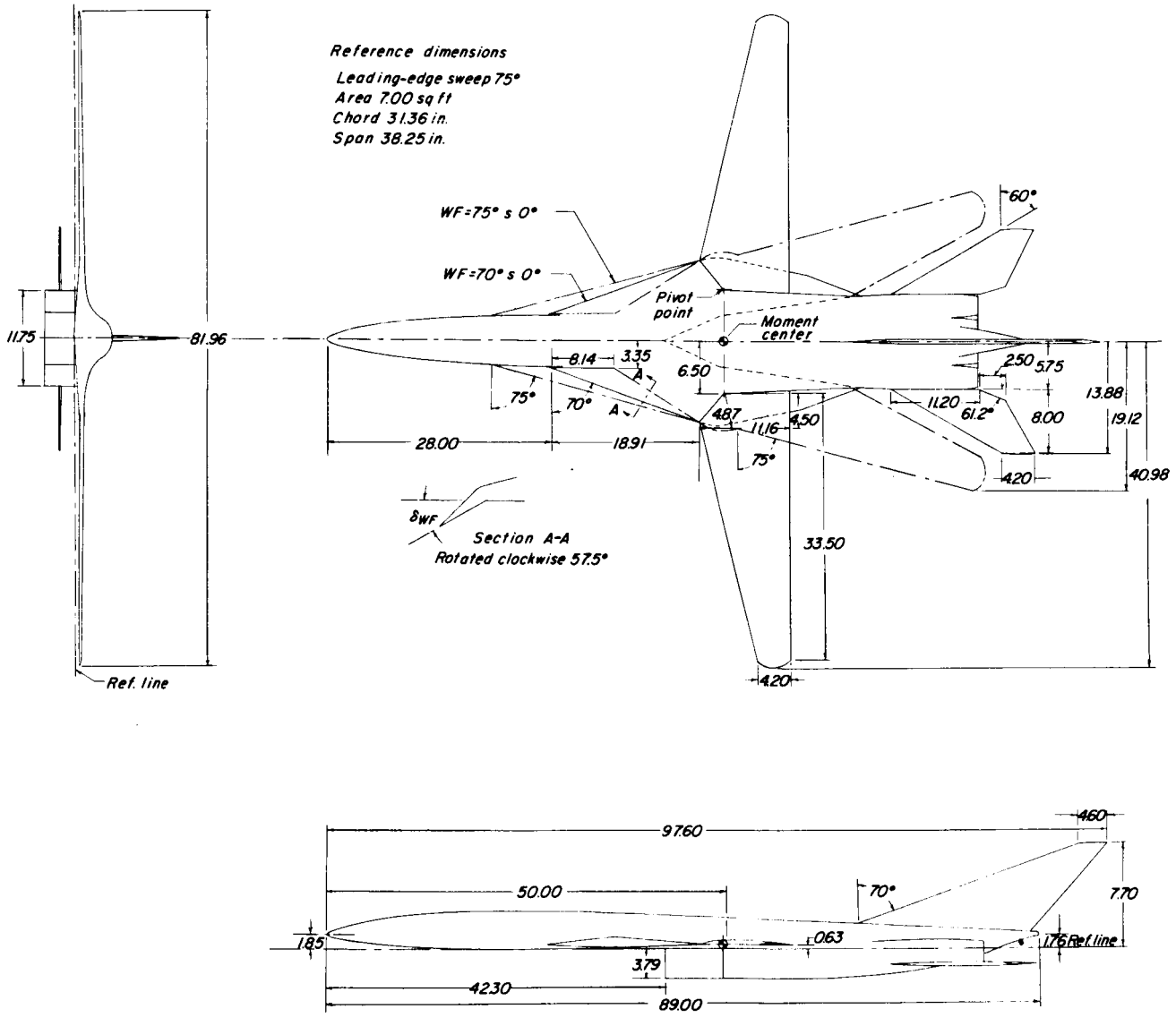

(a) Three-view drawing.

Figure 2.- Drawing of model tested. All linear dimensions are in inches.

70° WING-FUSELAGE FLAP ORDINATES

Section A-A			Section B-B			Section C-C		
x, in.	y_u, in.	y_l, in.	x, in.	y_u, in.	y_l, in.	x, in.	y_u, in.	y_l, in.
0	0	0	0	0	0	0	0	0
1.000	.200	-.010	1.000	.130	-.016	.600	.070	-.010
2.000	.374	-.030	2.000	.260	-.034	1.200	.132	-.024
3.000	.520	-.050	3.000	.372	-.060	2.000	.208	-.046
4.000	.660	-.080	4.000	.464	-.088	3.000	.290	-.072
5.000	.774	-.110	5.000	.550	-.112	3.460	.330	-.090
6.000	.874	-.136	5.630	.600	-.130			
7.000	.970	-.160						
8.140	1.060	-.210						

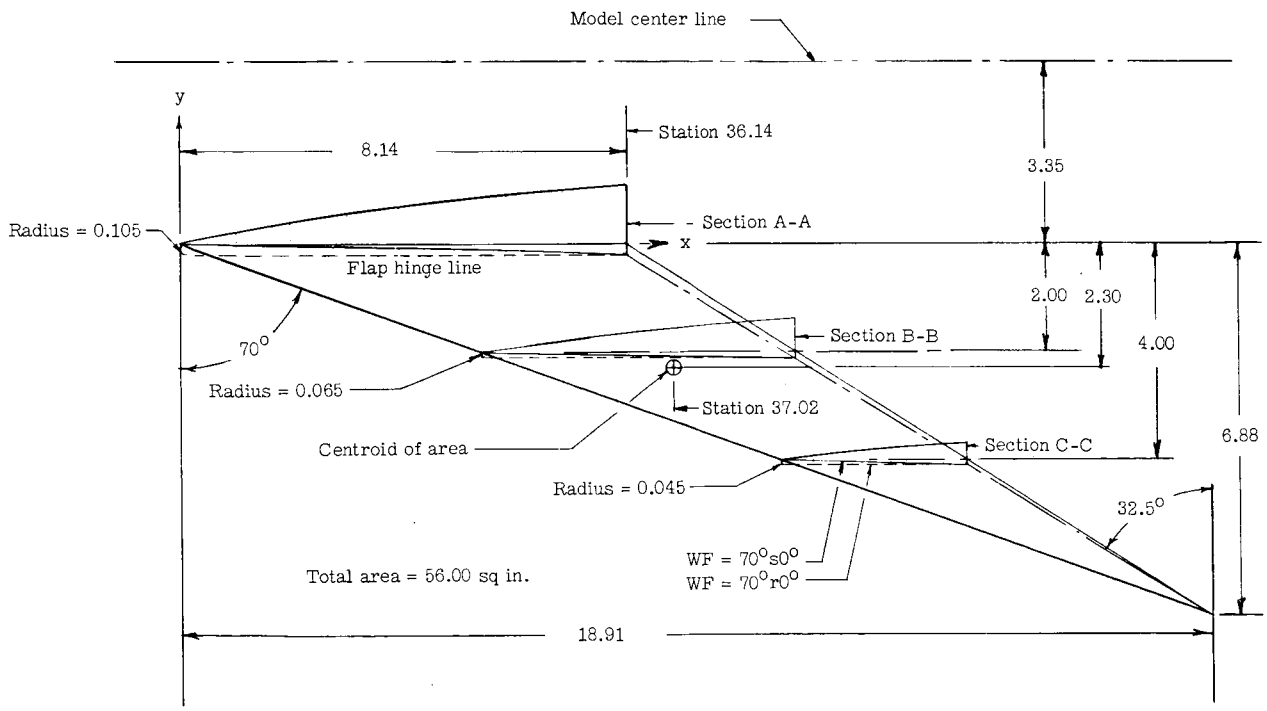

(b) Details of 70° wing-fuselage flap. WF = 70°s0° and WF = 70°r0°.

Figure 2.- Continued.

75° WING-FUSELAGE FLAP ORDINATES

Section A-A			Section B-B			Section C-C		
x, in.	y_u, in.	y_l, in.	x, in.	y_u, in.	y_l, in.	x, in.	y_u, in.	y_l, in.
0	0	0	0	0	0	0	0	0
1.000	.070	-.014	1.000	.056	-.012	1.000	.053	-.014
2.000	.142	-.028	2.000	.114	-.024	2.000	.106	-.028
3.000	.212	-.042	3.000	.170	-.036	3.000	.158	-.044
4.000	.284	-.056	4.000	.228	-.048	4.000	.210	-.056
5.000	.354	-.070	5.000	.282	-.062	5.000	.264	-.072
6.000	.426	-.084	6.000	.340	-.074	6.000	.316	-.088
7.000	.496	-.098	7.000	.396	-.086	6.270	.330	-.090
8.000	.568	-.112	8.000	.452	-.098			
9.000	.638	-.126	9.000	.506	-.110			
10.000	.710	-.140	10.000	.566	-.122			
11.000	.780	-.154	10.630	.600	-.130			
12.000	.850	-.168						
13.000	.922	-.182						
14.000	.392	-.196						
14.950	1.060	-.210						

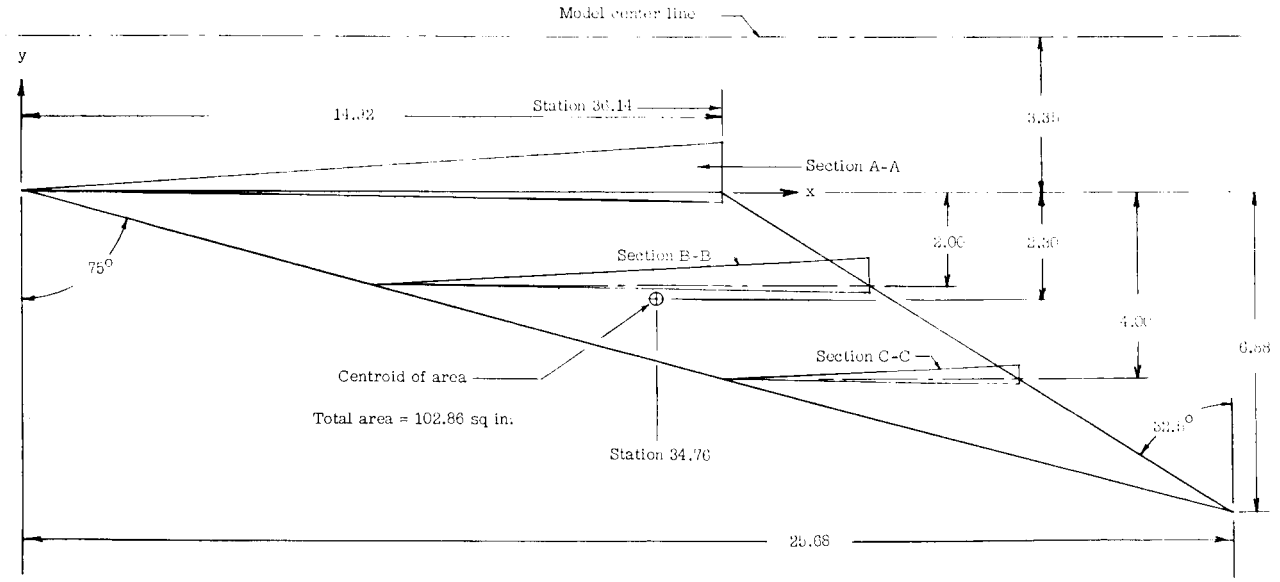

(c) Details of 75° wing-fuselage flap, WF = 75°s0°.

Figure 2.- Concluded.

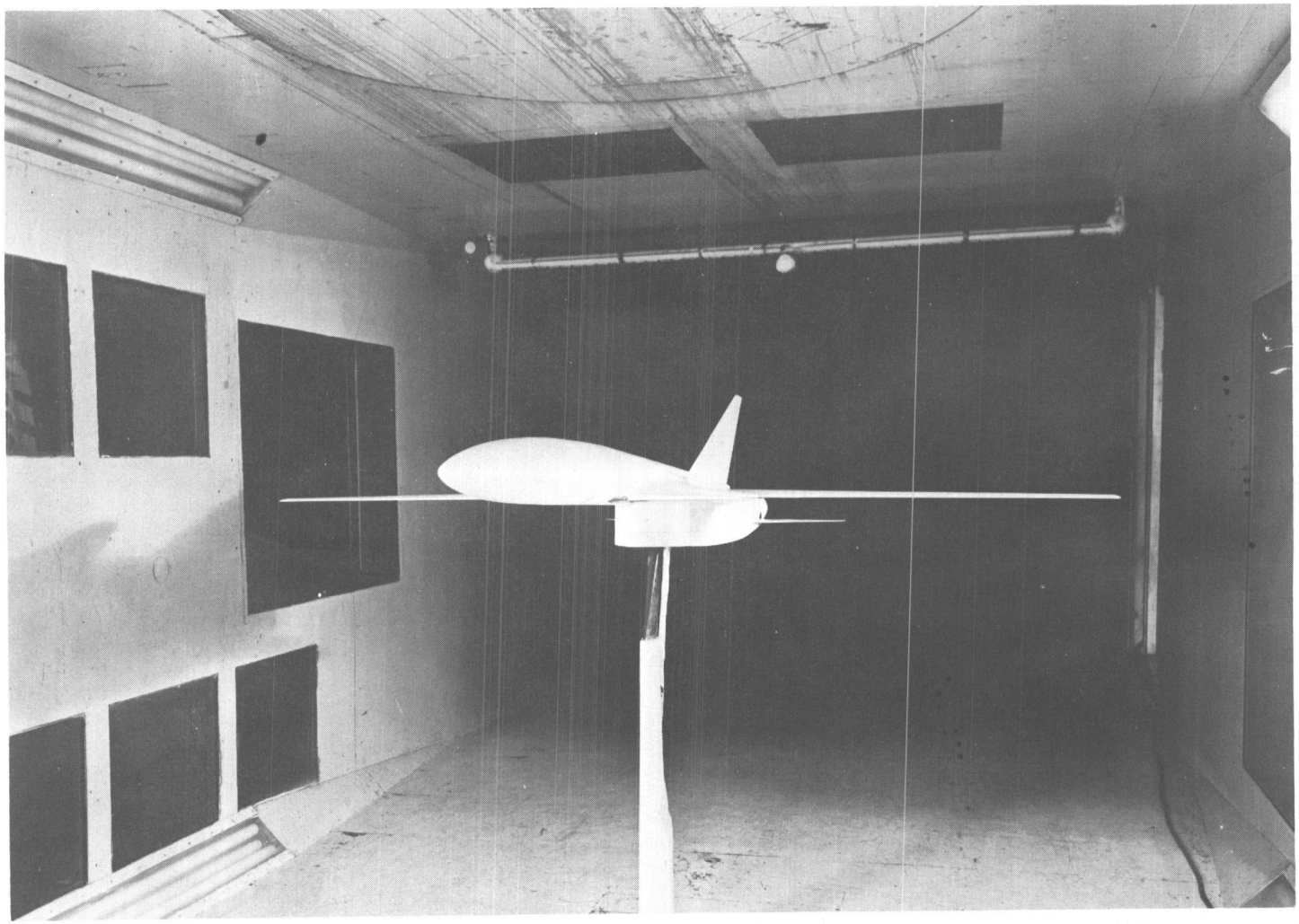

(a) Front view with wings fully extended (leading-edge sweep 13.5°). L-61-8078

Figure 3.- Model installed in the Langley 300-MPH 7- by 10-foot tunnel.

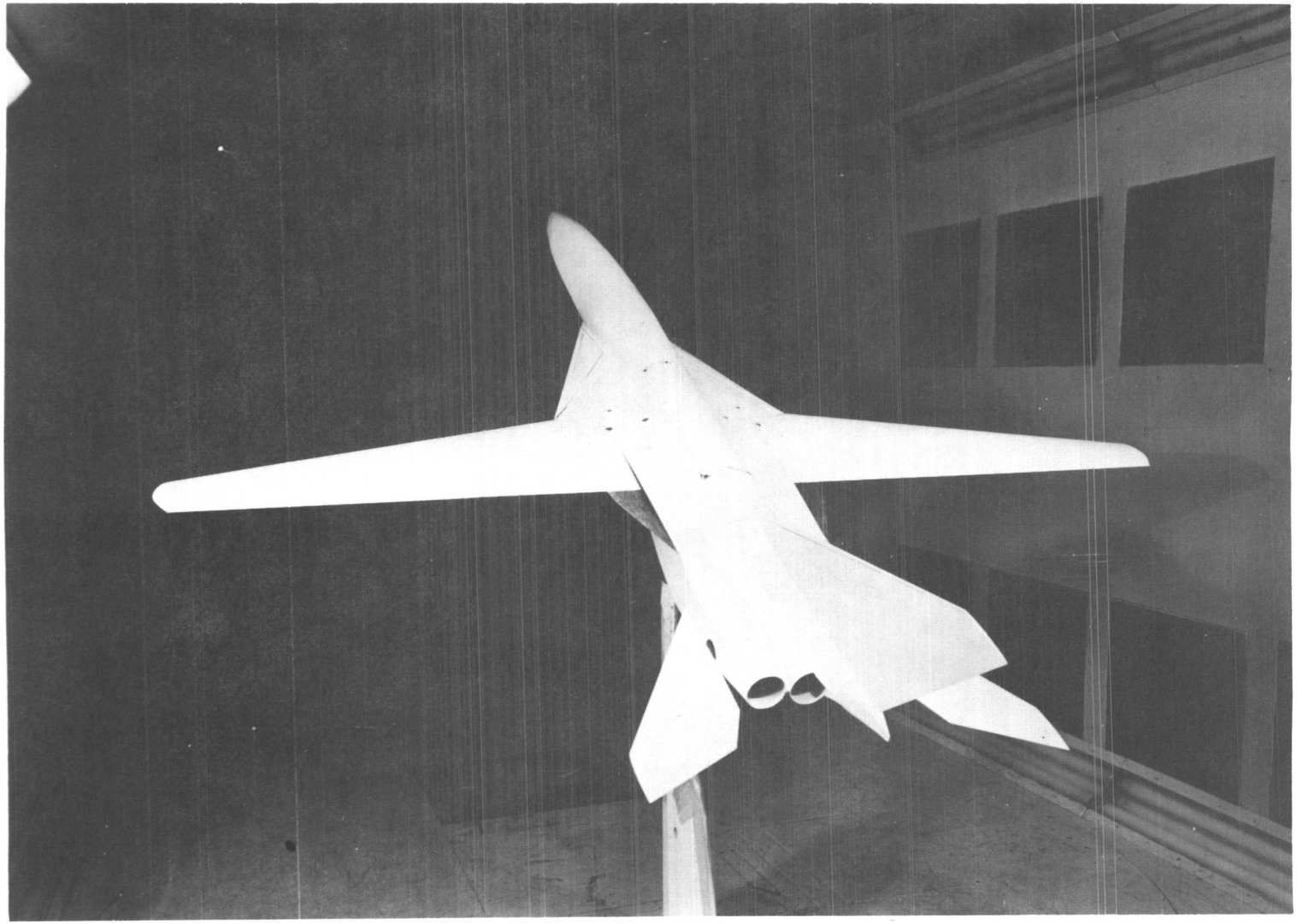

(b) Rear view with wings fully extended. L-61-8079

Figure 3.- Continued.

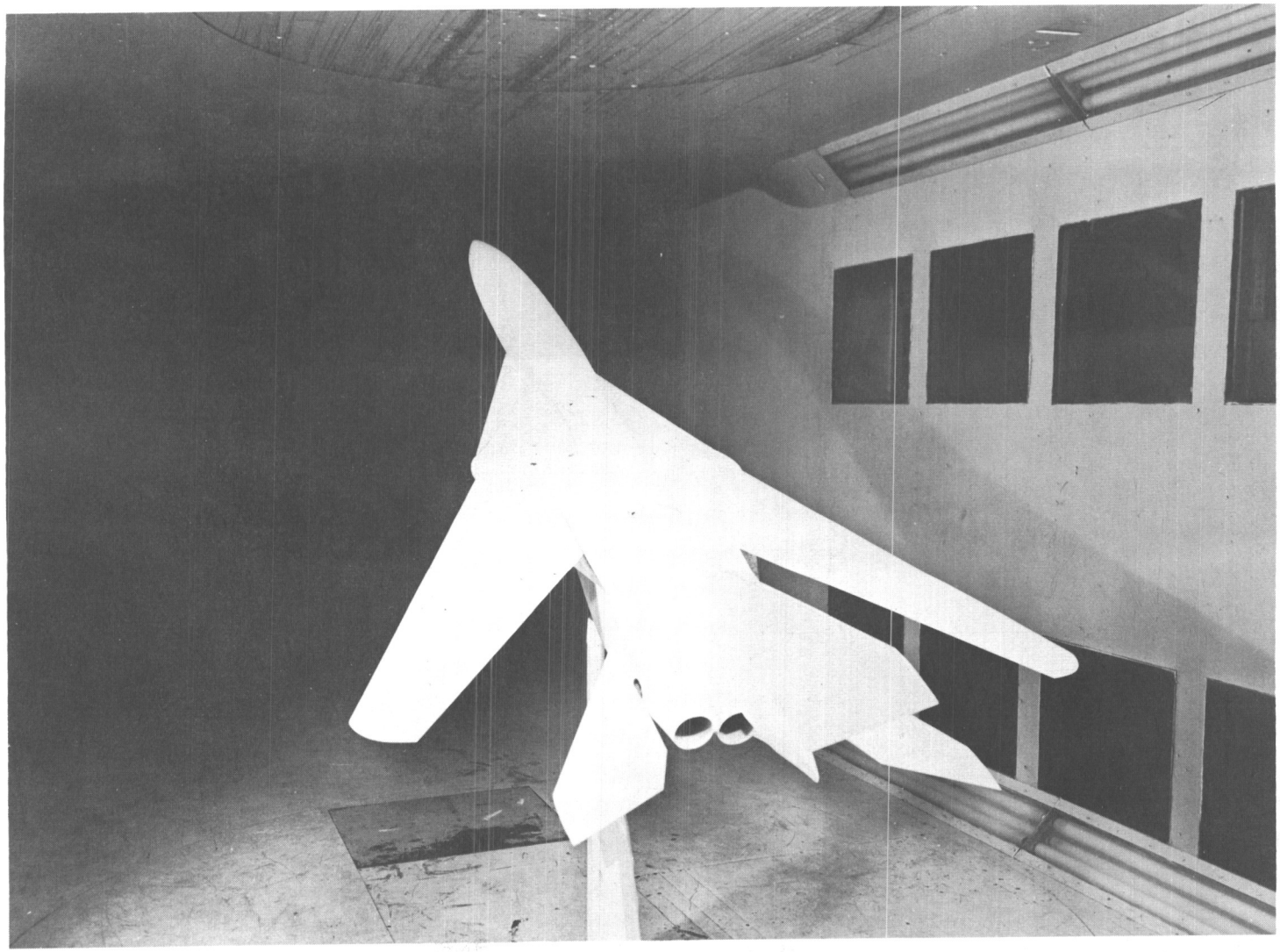

(c) Rear view with wing leading edges swept 65°.

L-61-8080

Figure 3.- Concluded.

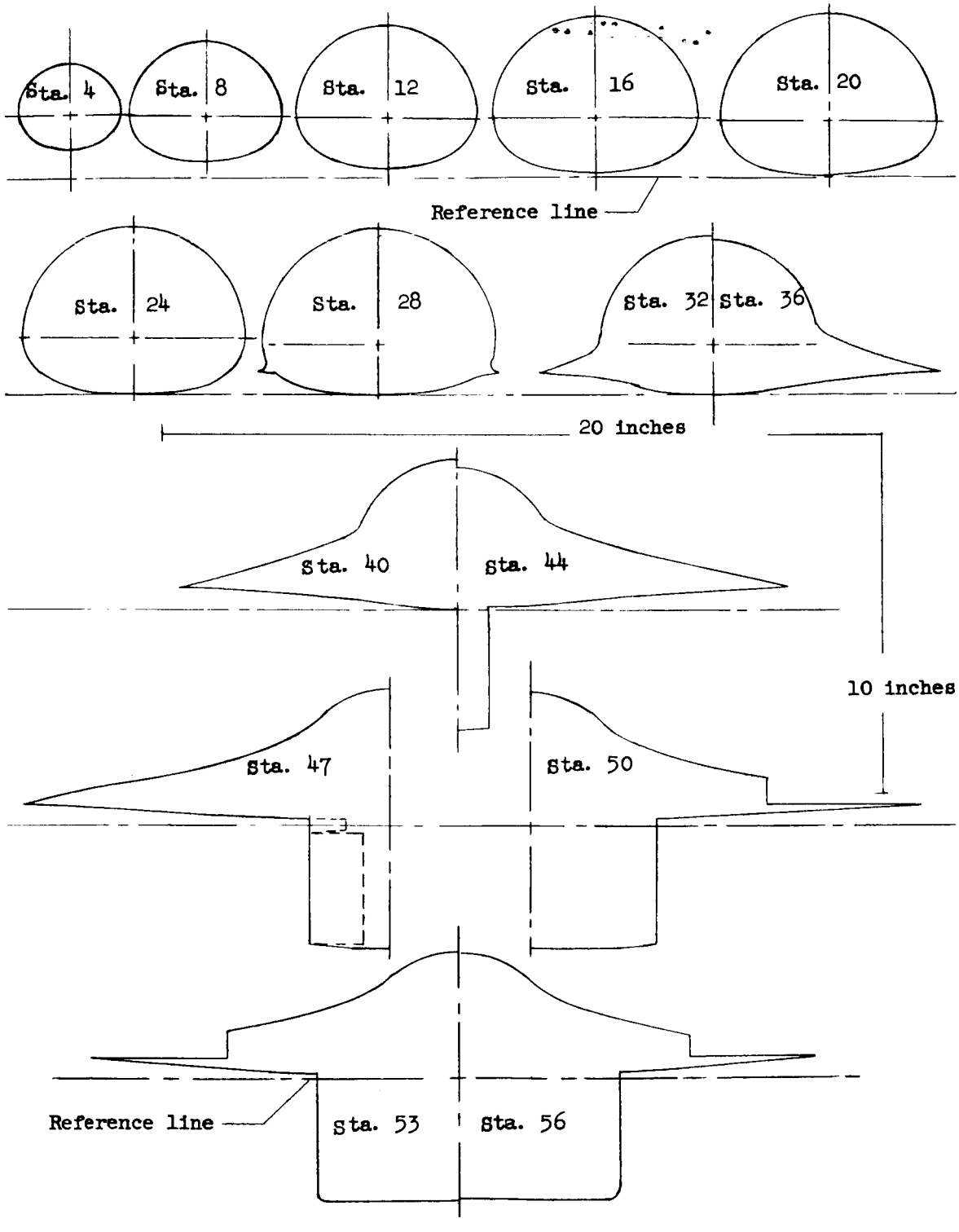

Figure 4.- Model fuselage cross sections.

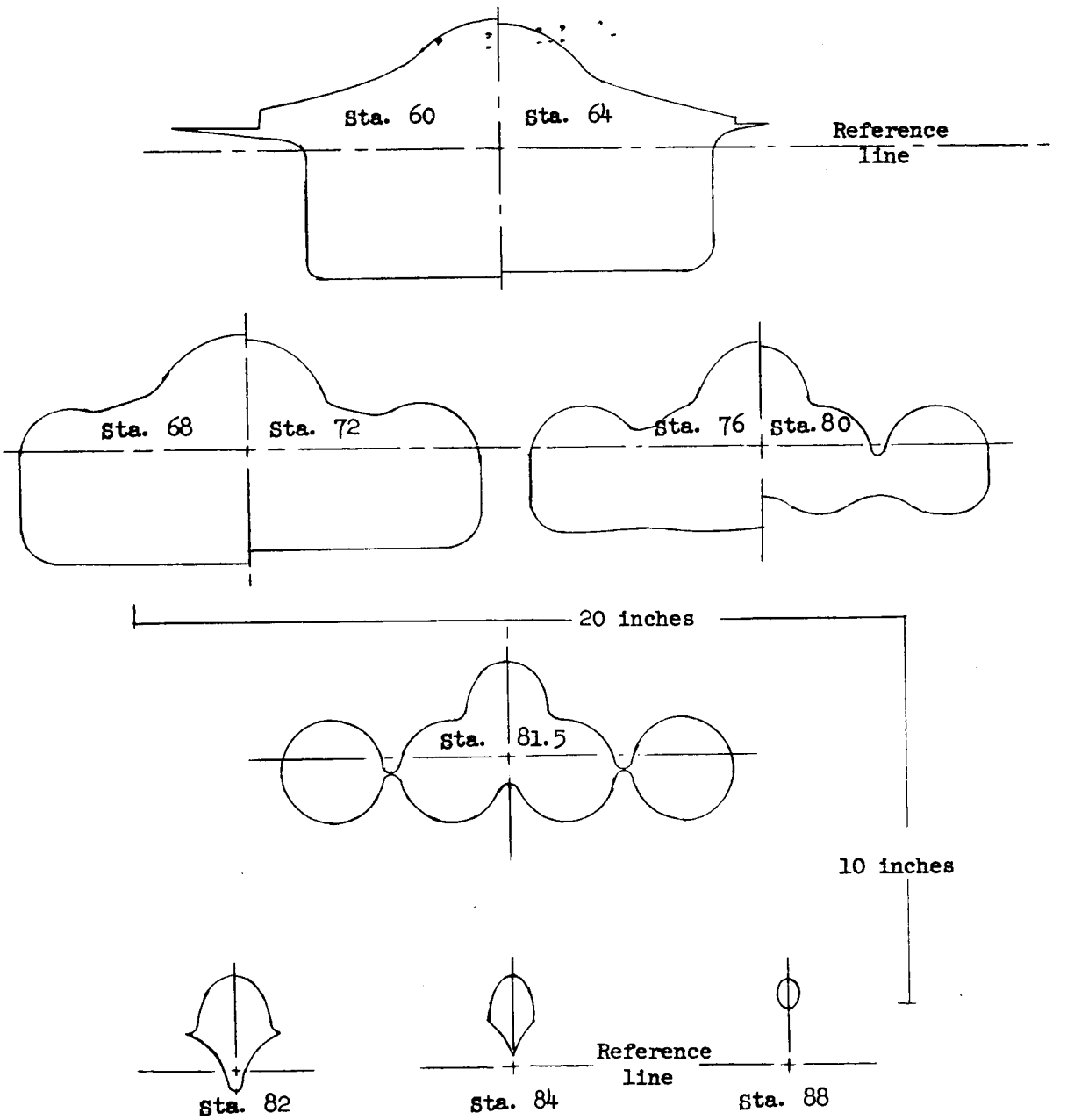

Figure 4.- Concluded.

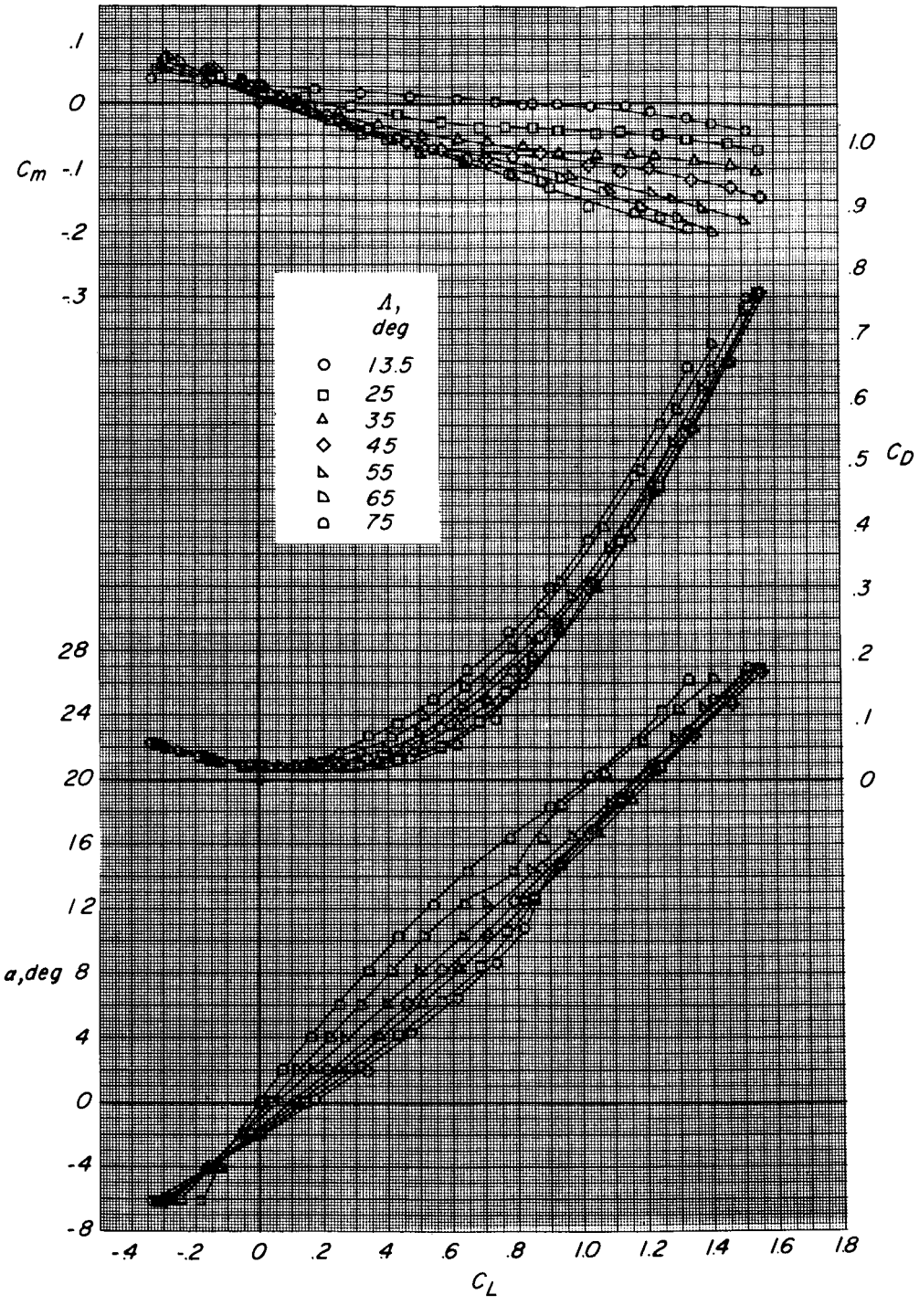

(a) FW_1HV.

Figure 5.- Effect of wing sweep on aerodynamic characteristics in pitch. $\delta_h = 0^\circ$; WF = 70°r0°.

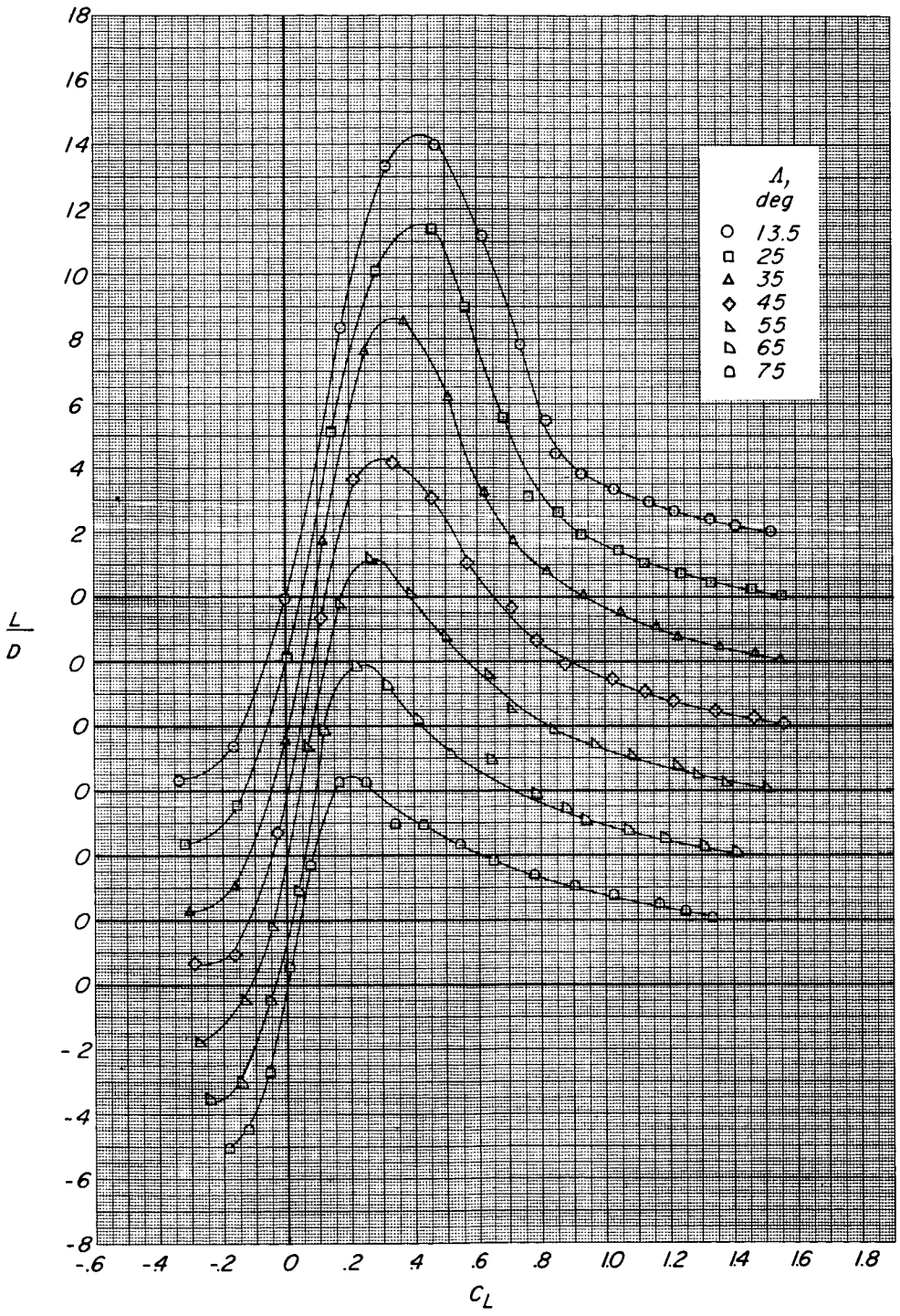

(a) Concluded.

Figure 5.- Continued.

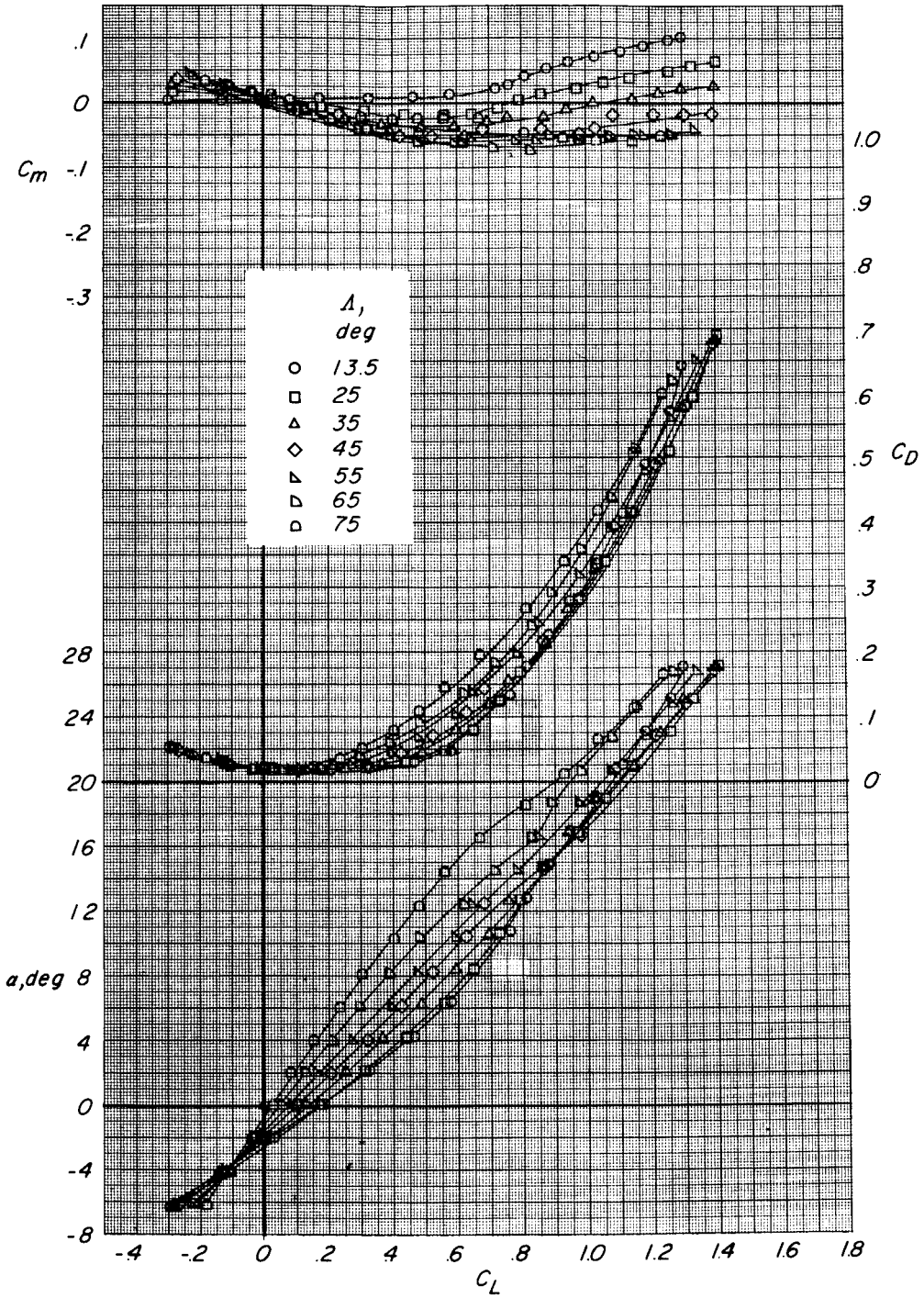

(b) FW_1V.

Figure 5.- Continued.

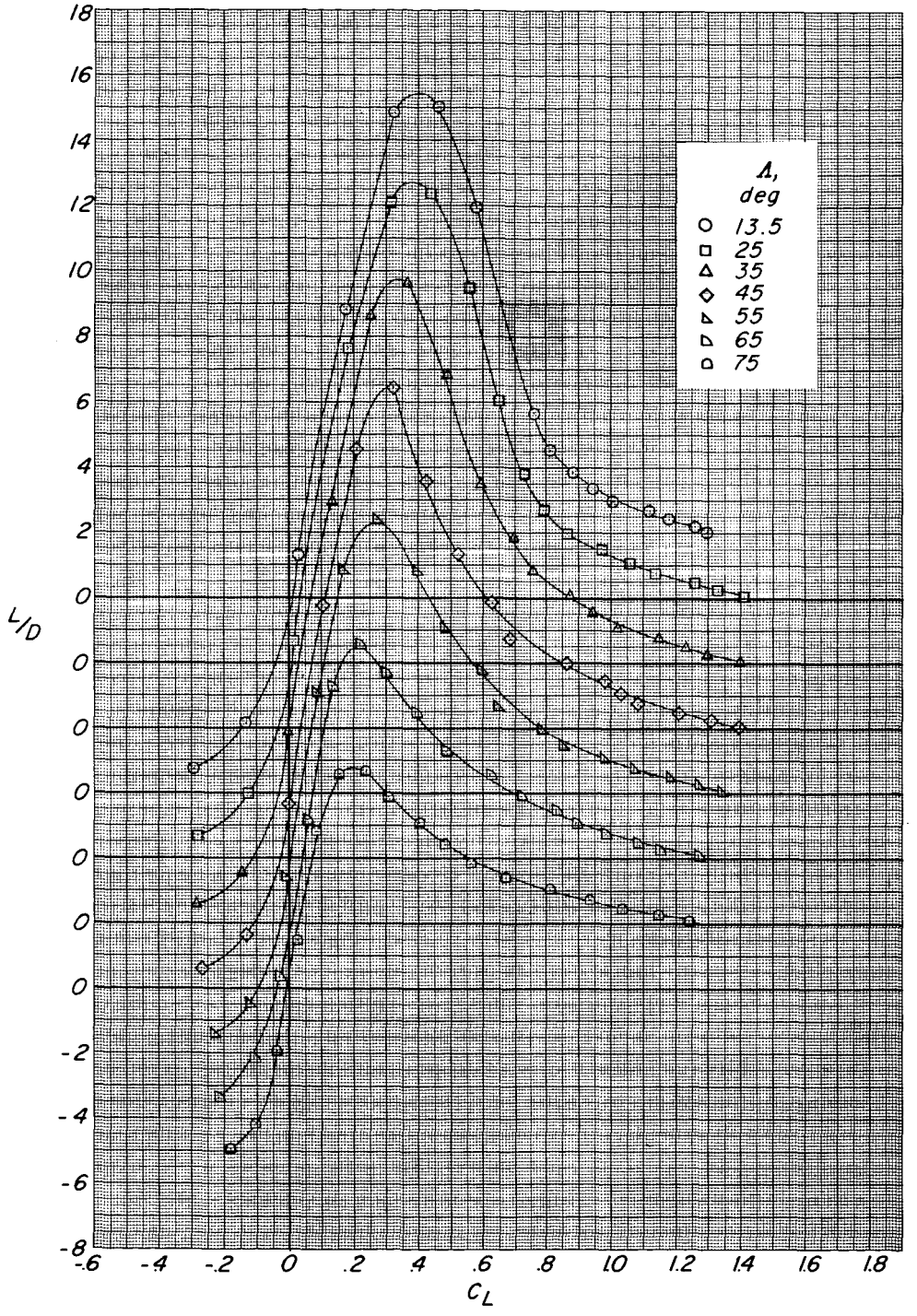

(b) Concluded.

Figure 5.- Concluded.

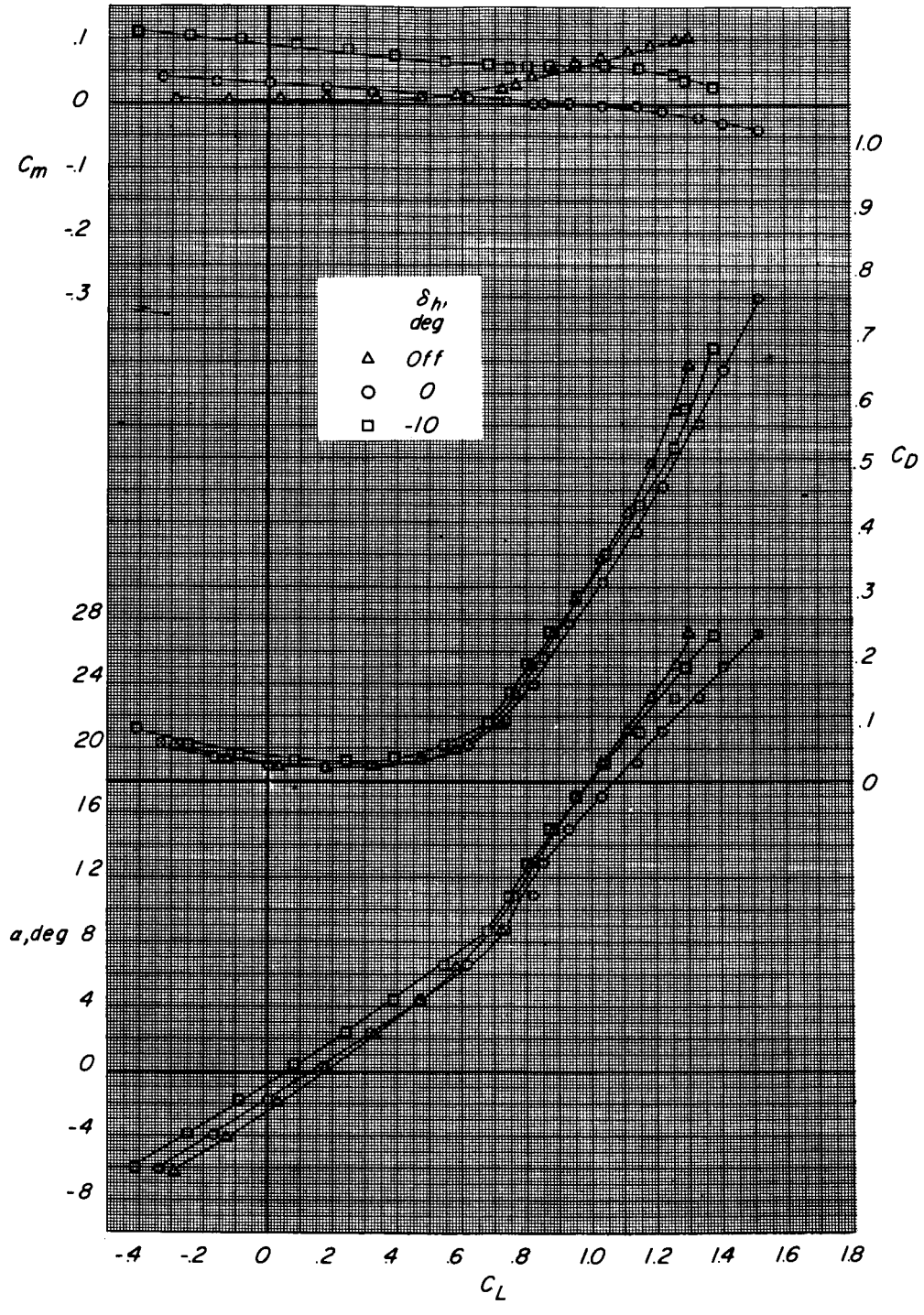

(a) $\Lambda = 13.5^{\circ}$.

Figure 6.- Effect of horizontal tail on aerodynamic characteristics in pitch. FW_1HV; WF = $70^{\circ}r0^{\circ}$.

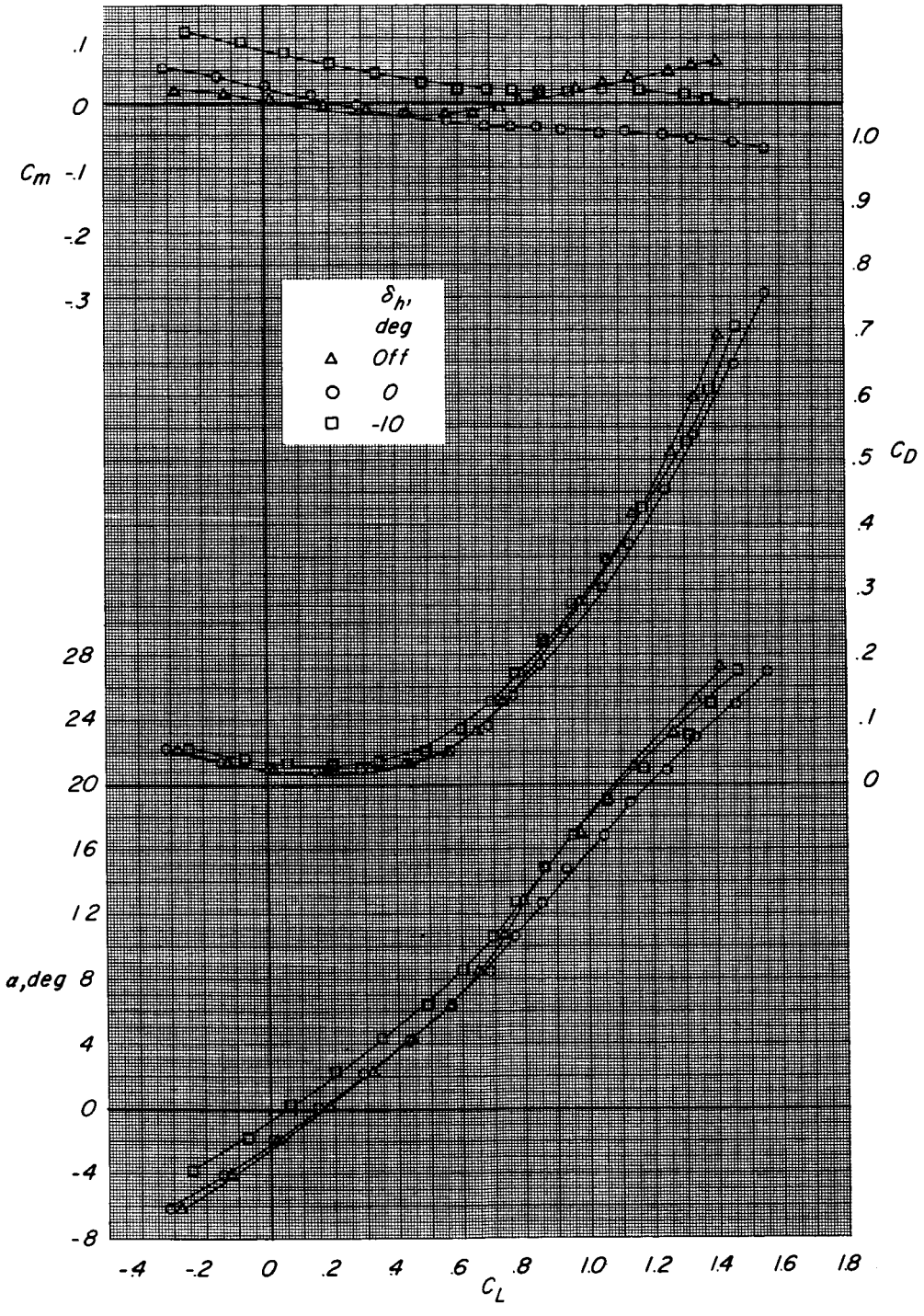

(b) $\Lambda = 25°$.

Figure 6.- Continued.

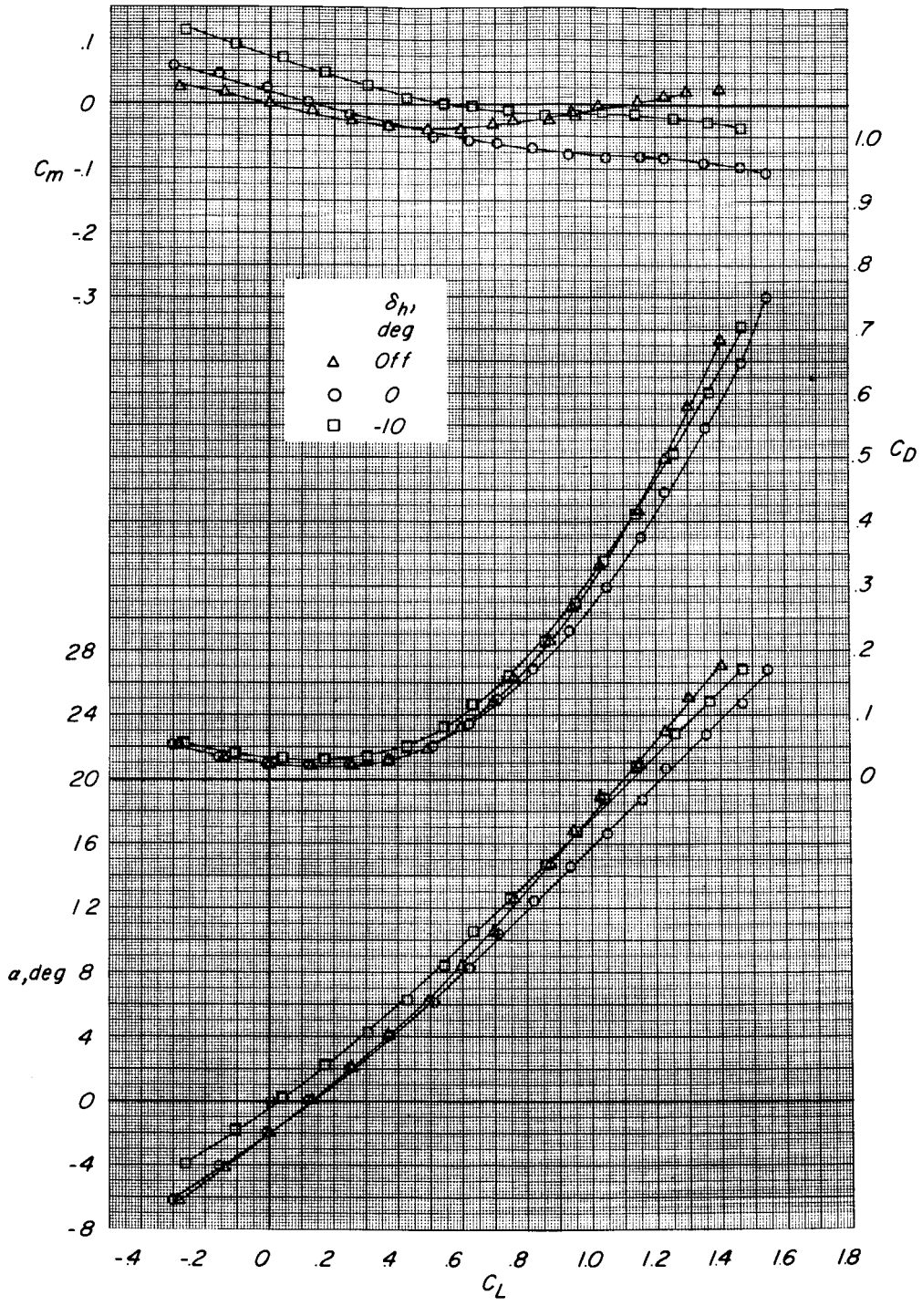

(c) $\Lambda = 35^\circ$.

Figure 6.- Continued.

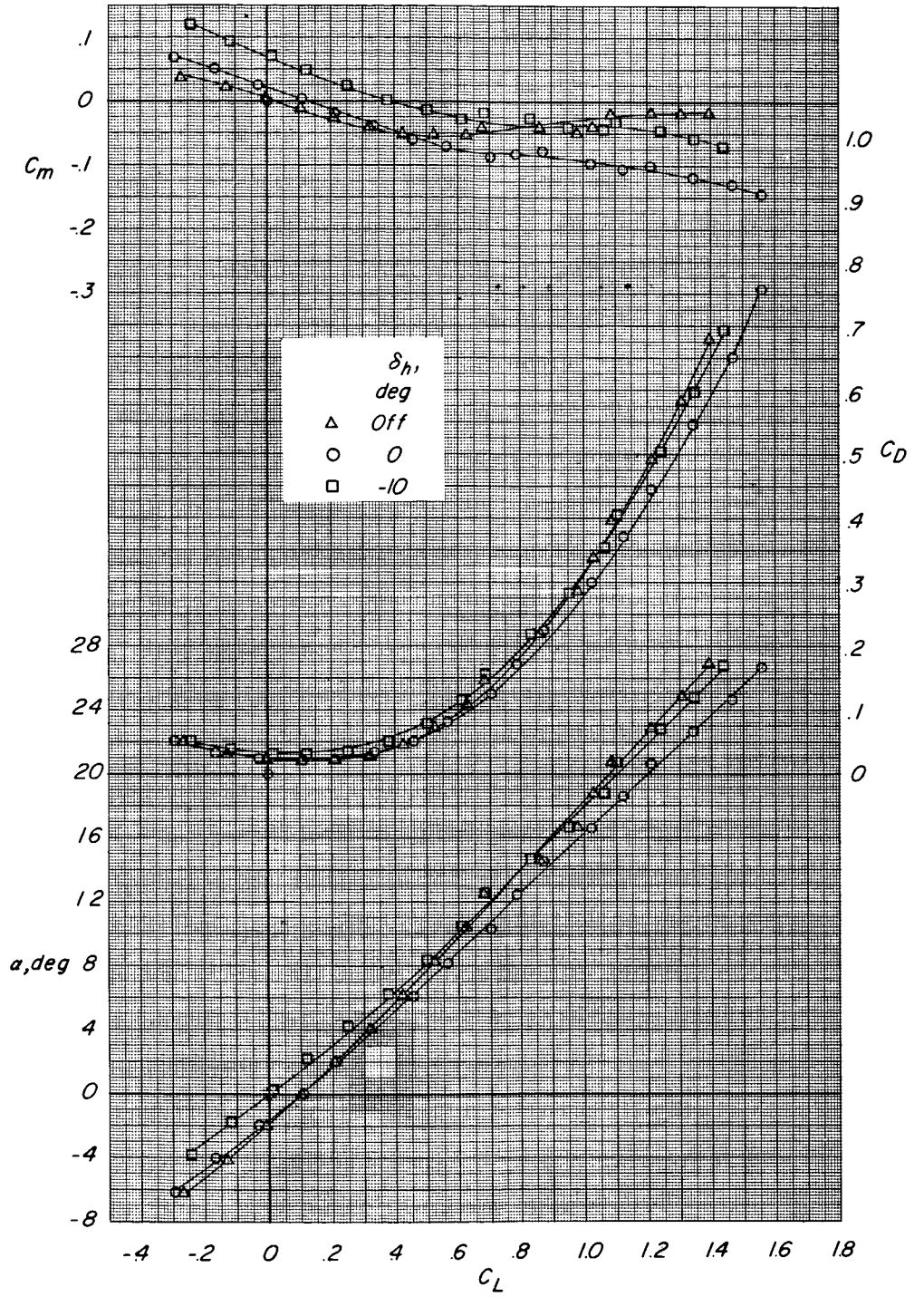

(d) $\Lambda = 45°$.

Figure 6.- Continued.

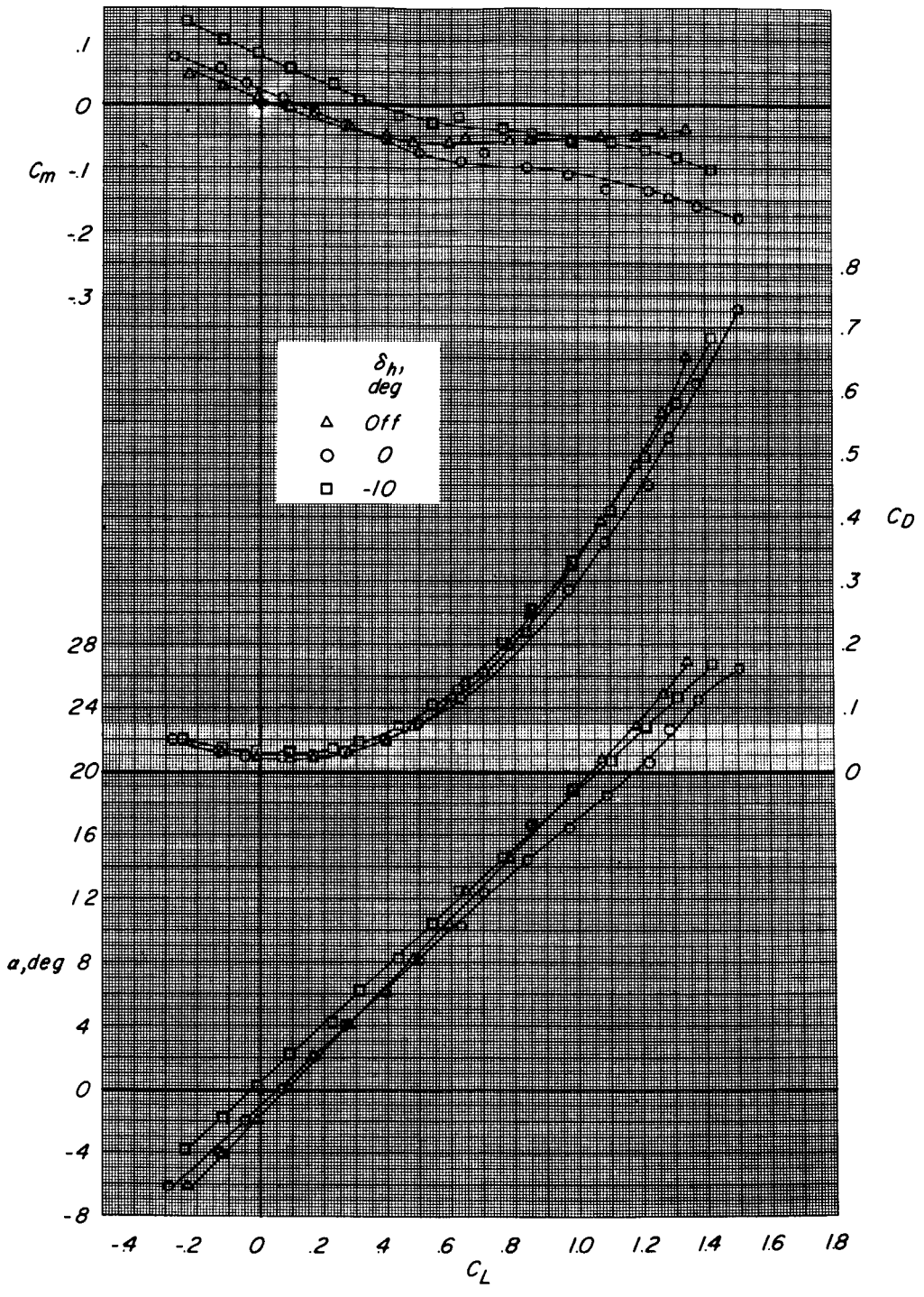

(e) $\Lambda = 55^{\circ}$.

Figure 6.- Continued.

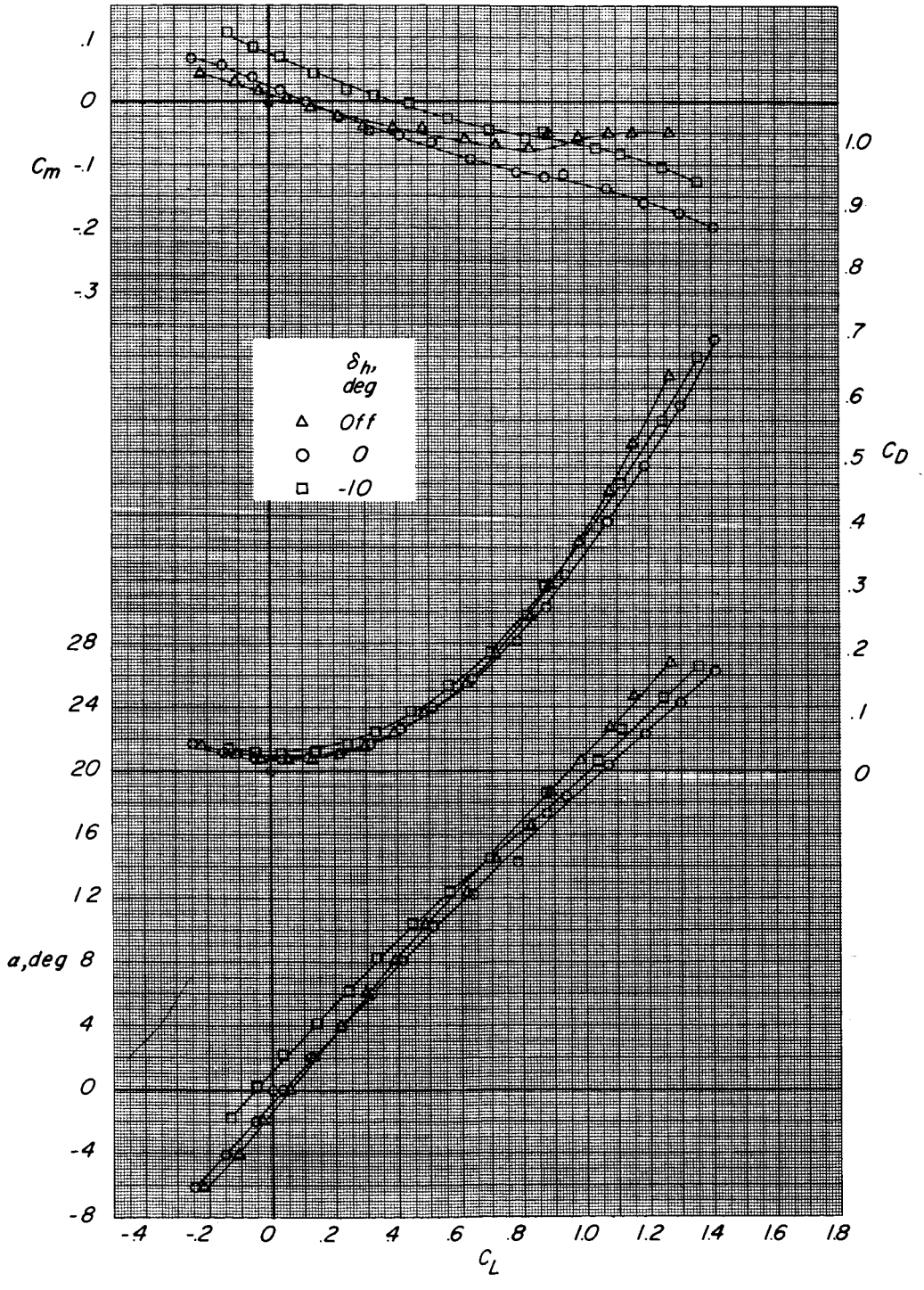

(f) $\Lambda = 65°$.

Figure 6.- Continued.

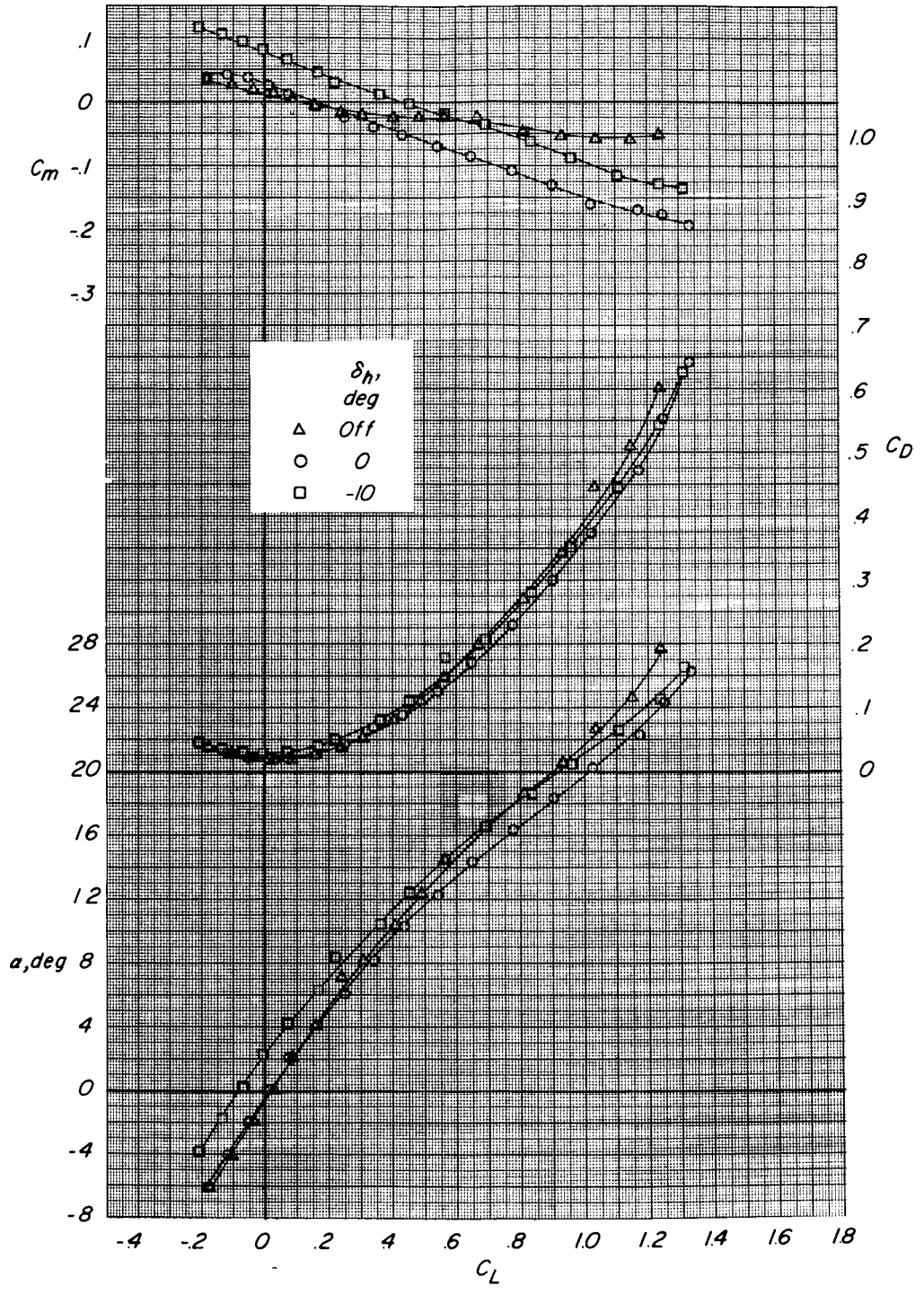

(g) $\Lambda = 75°$.

Figure 6.- Concluded.

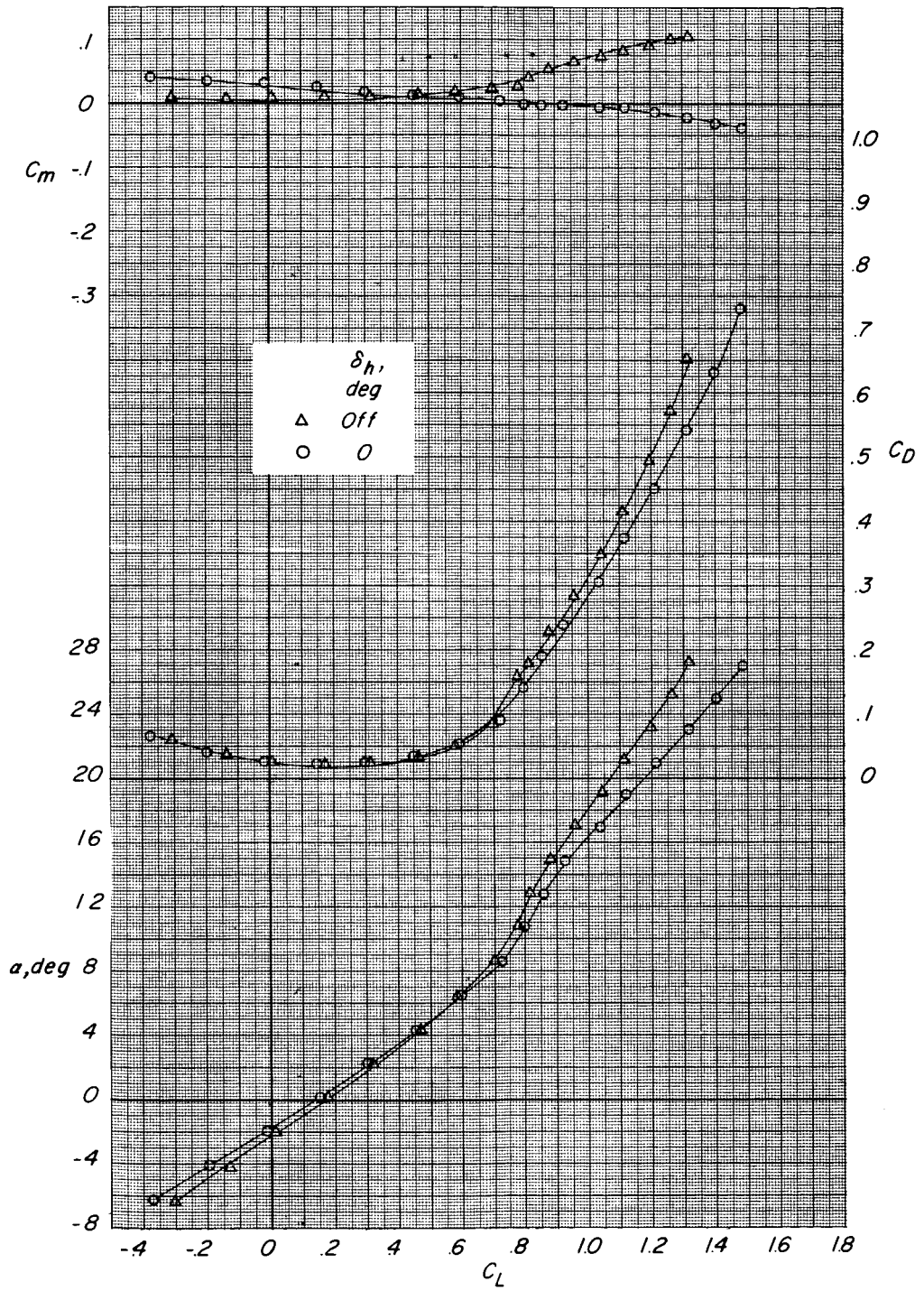

(a) $\Lambda = 13.5^{\circ}$.

Figure 7.- Effect of tail on aerodynamic characteristics in pitch. FW_2HV; WF = 70°r0°.

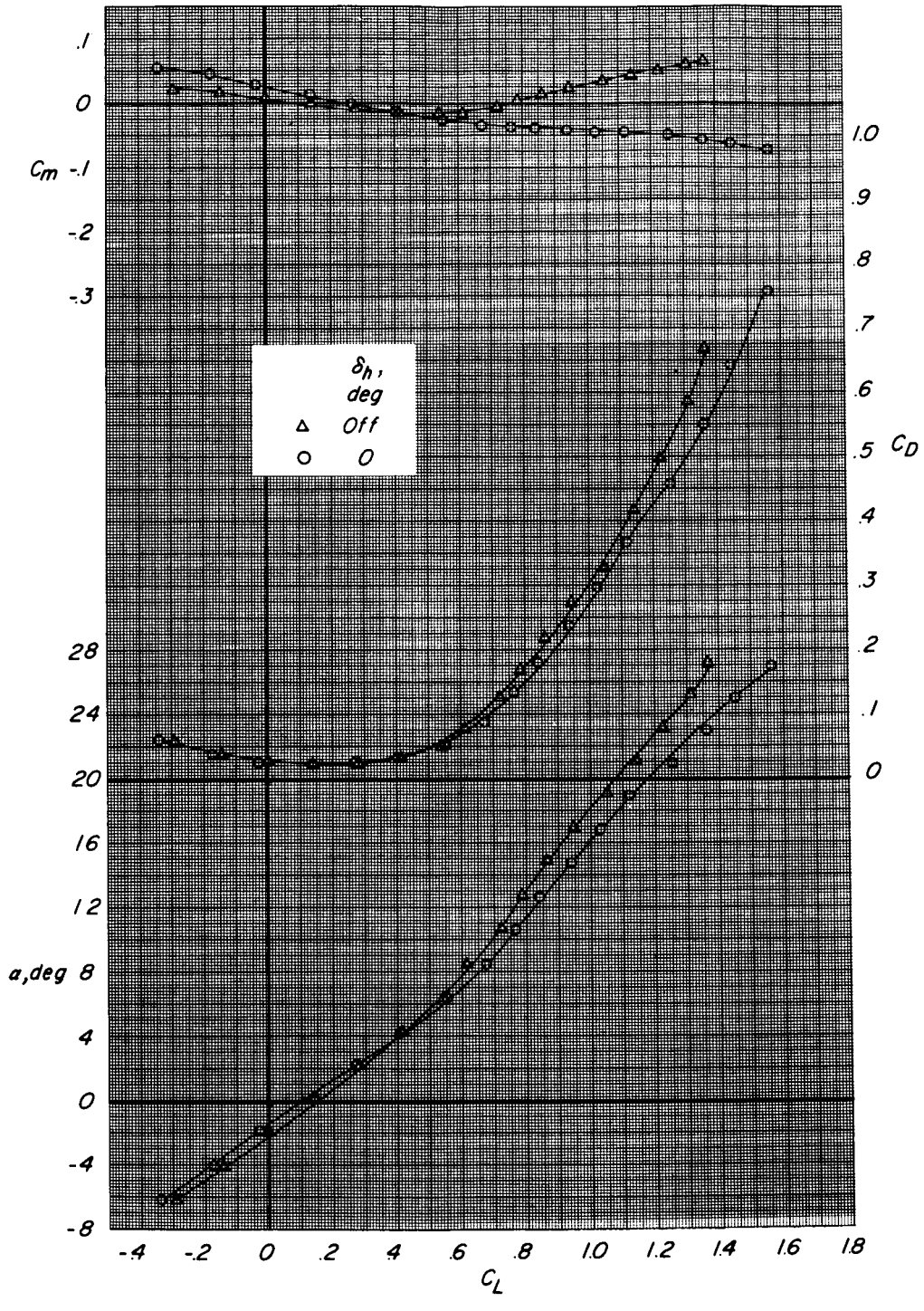

(b) $\Lambda = 25^{\circ}$.

Figure 7.- Continued.

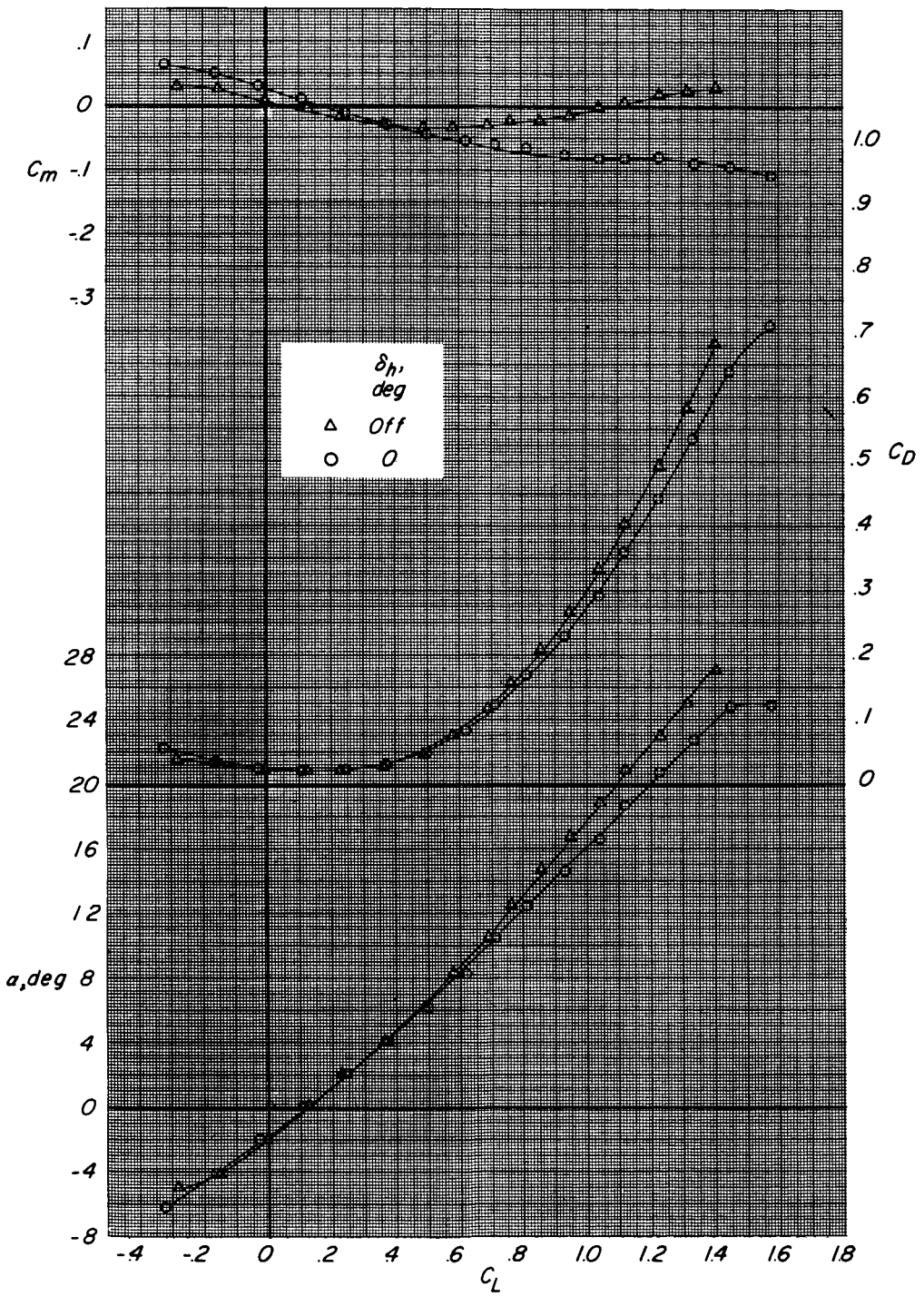

(c) $\Lambda = 35^\circ$.

Figure 7.- Continued.

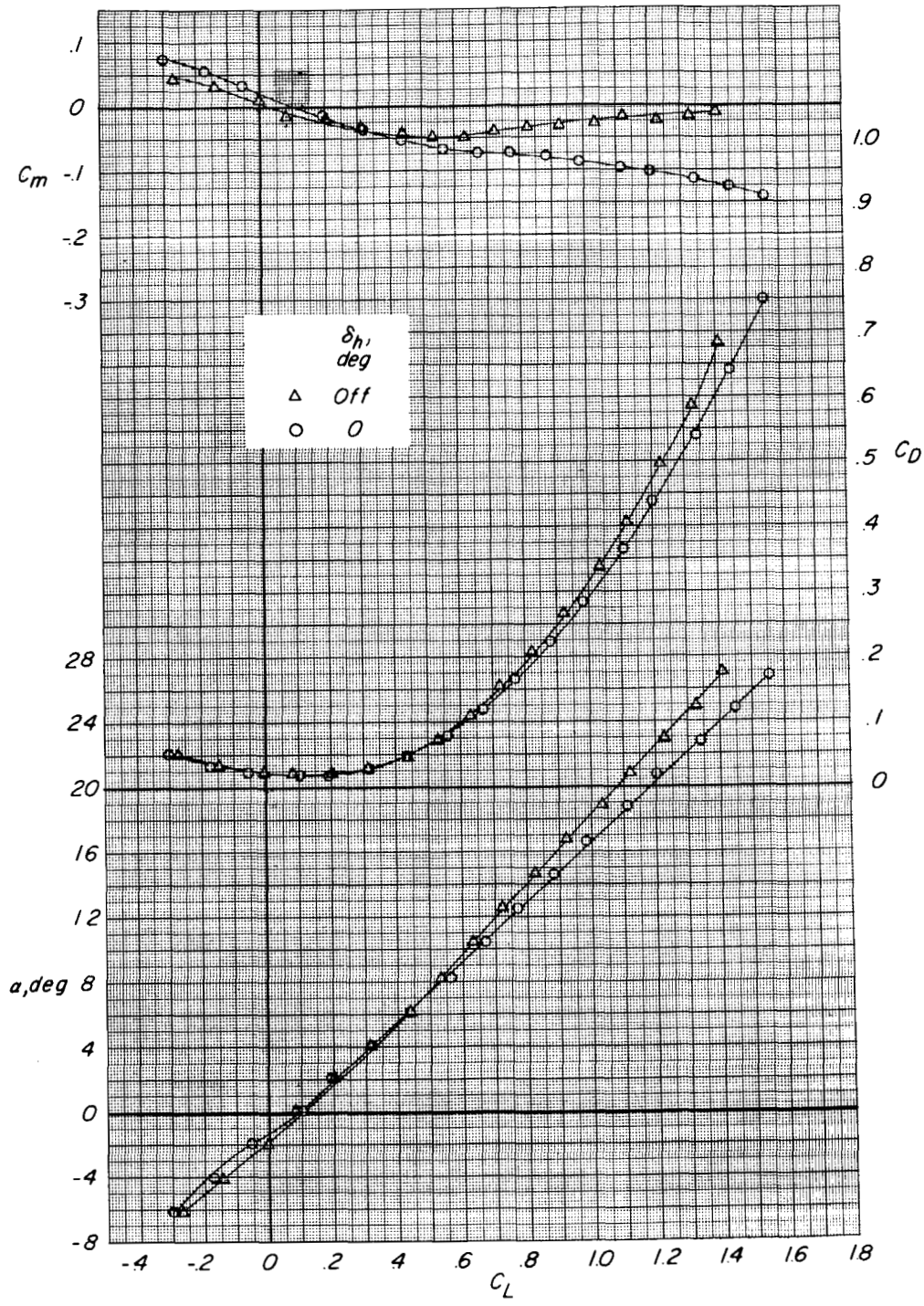

(d) $\Lambda = 45°$.

Figure 7.- Continued.

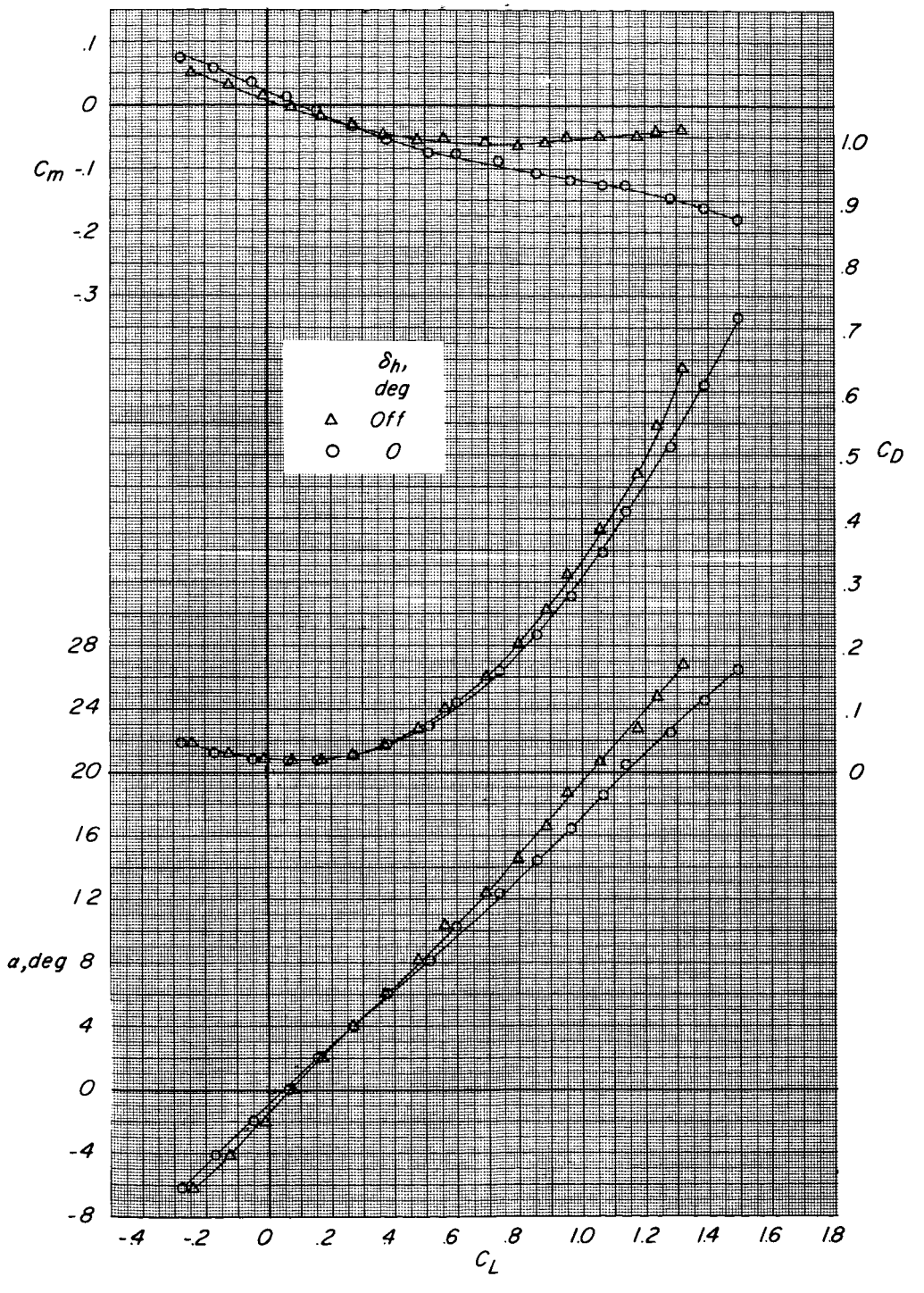

(e) $\Lambda = 55°$.

Figure 7.- Continued.

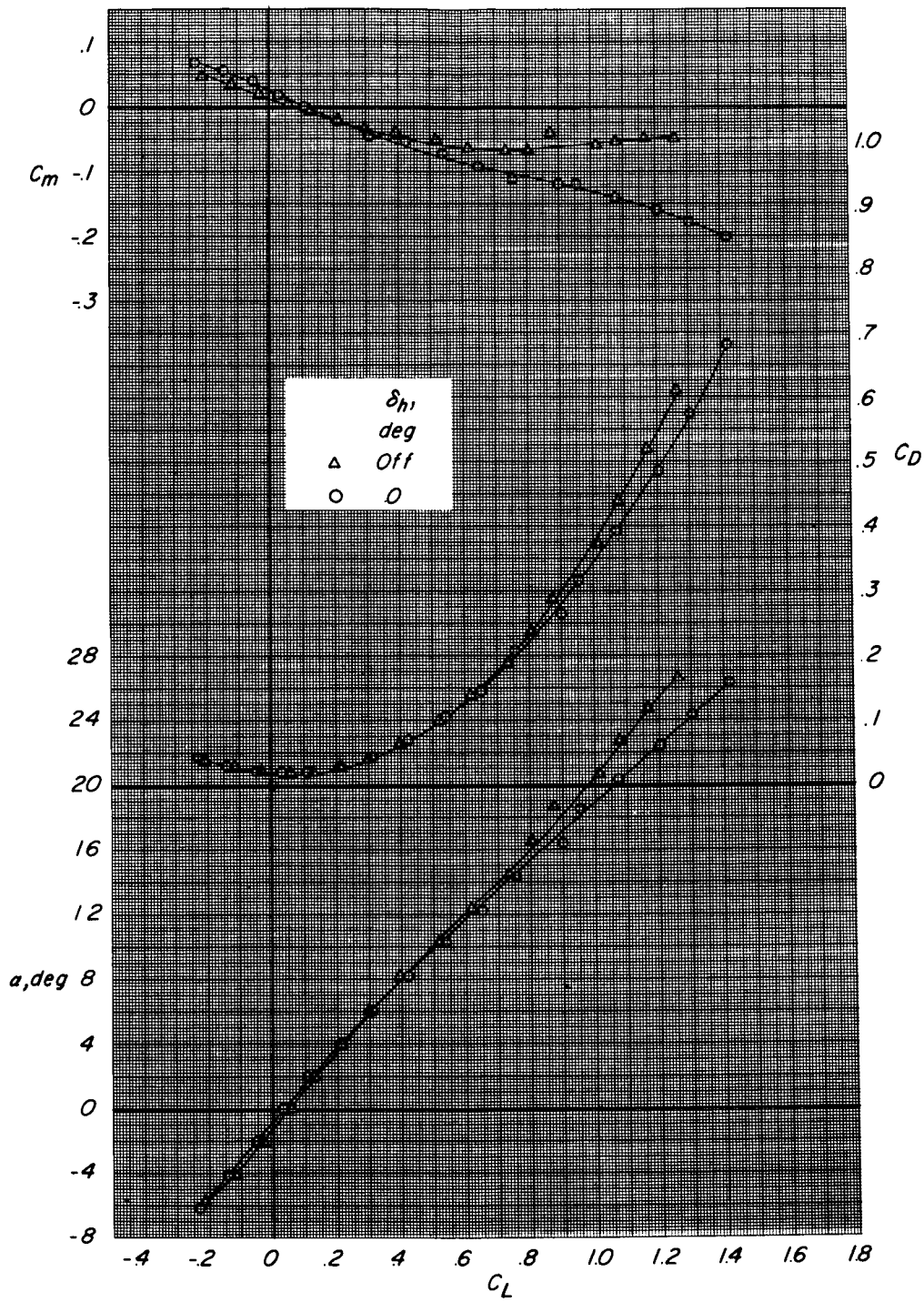

(f) $\Lambda = 65^\circ$.

Figure 7.- Continued.

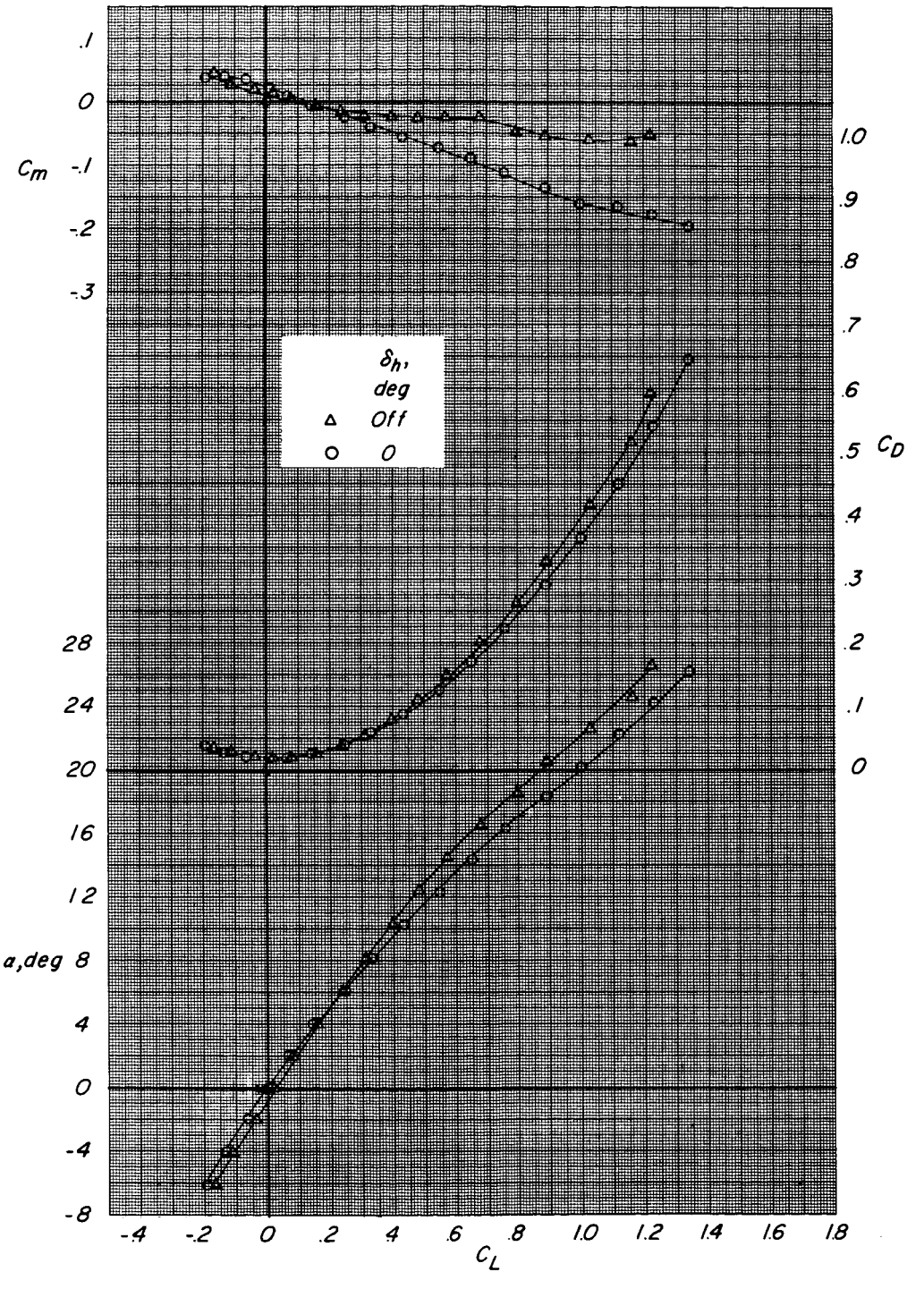

(g) $\Lambda = 75^{\circ}$.

Figure 7.- Concluded.

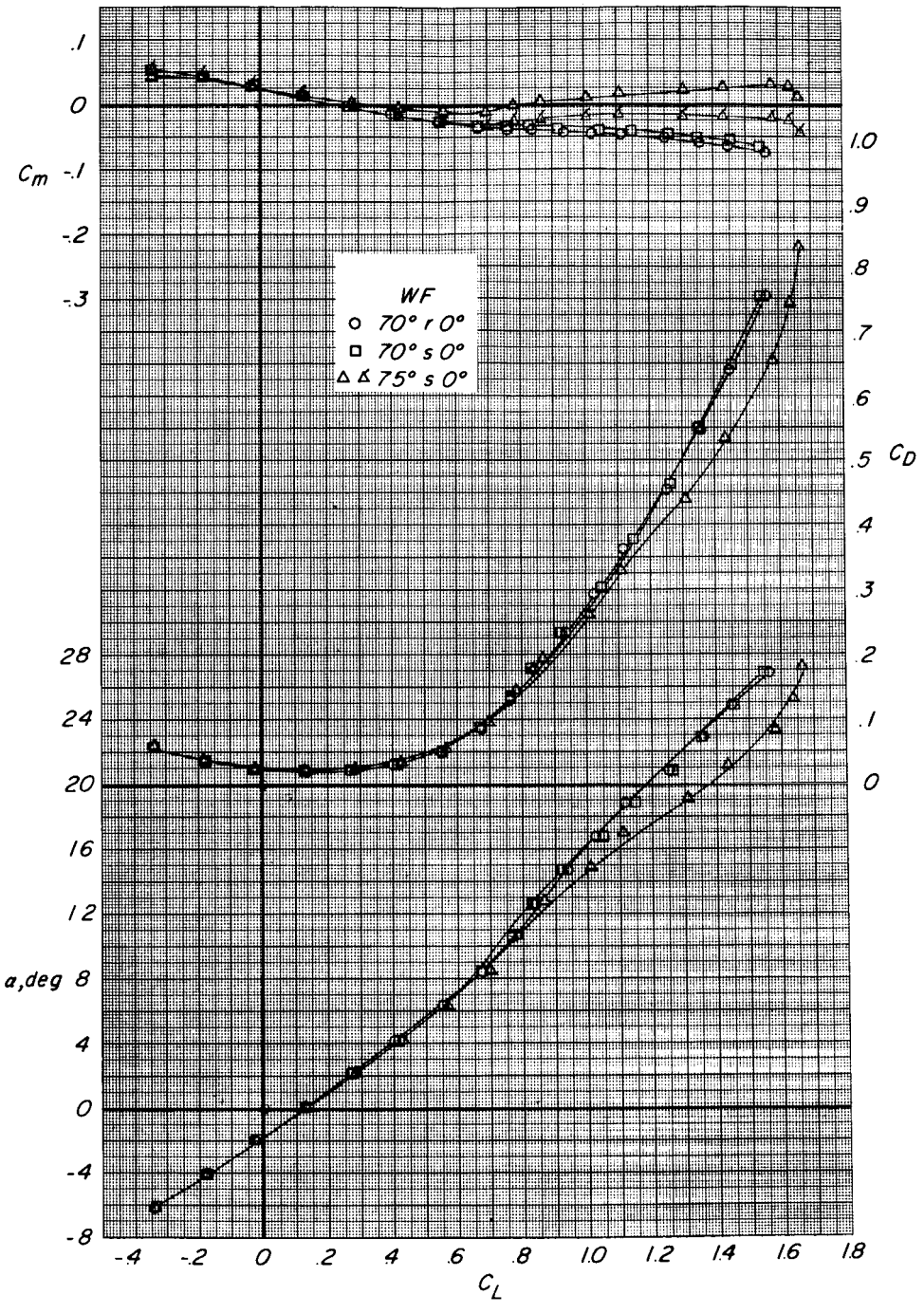

(a) $\Lambda = 25^{\circ}$.

Figure 8.- Effect of wing-fuselage flap geometry on aerodynamic characteristics in pitch. FW_2HV; $\delta_h = 0^{\circ}$. Flagged symbols indicate moment reference at $0.03c_{ref}$ ahead of wing pivot station.

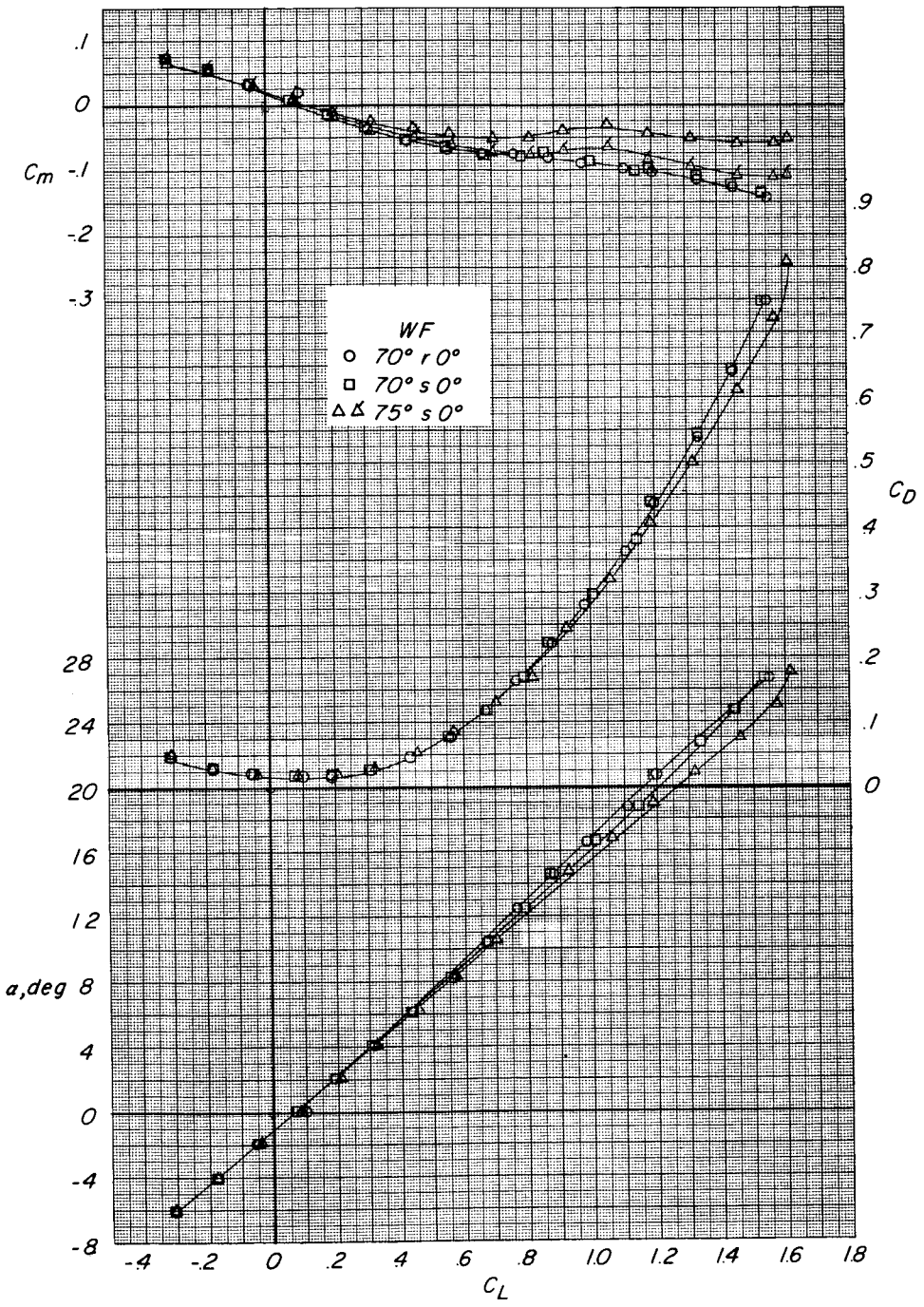

(b) $\Lambda = 45^{\circ}$.

Figure 8.- Continued.

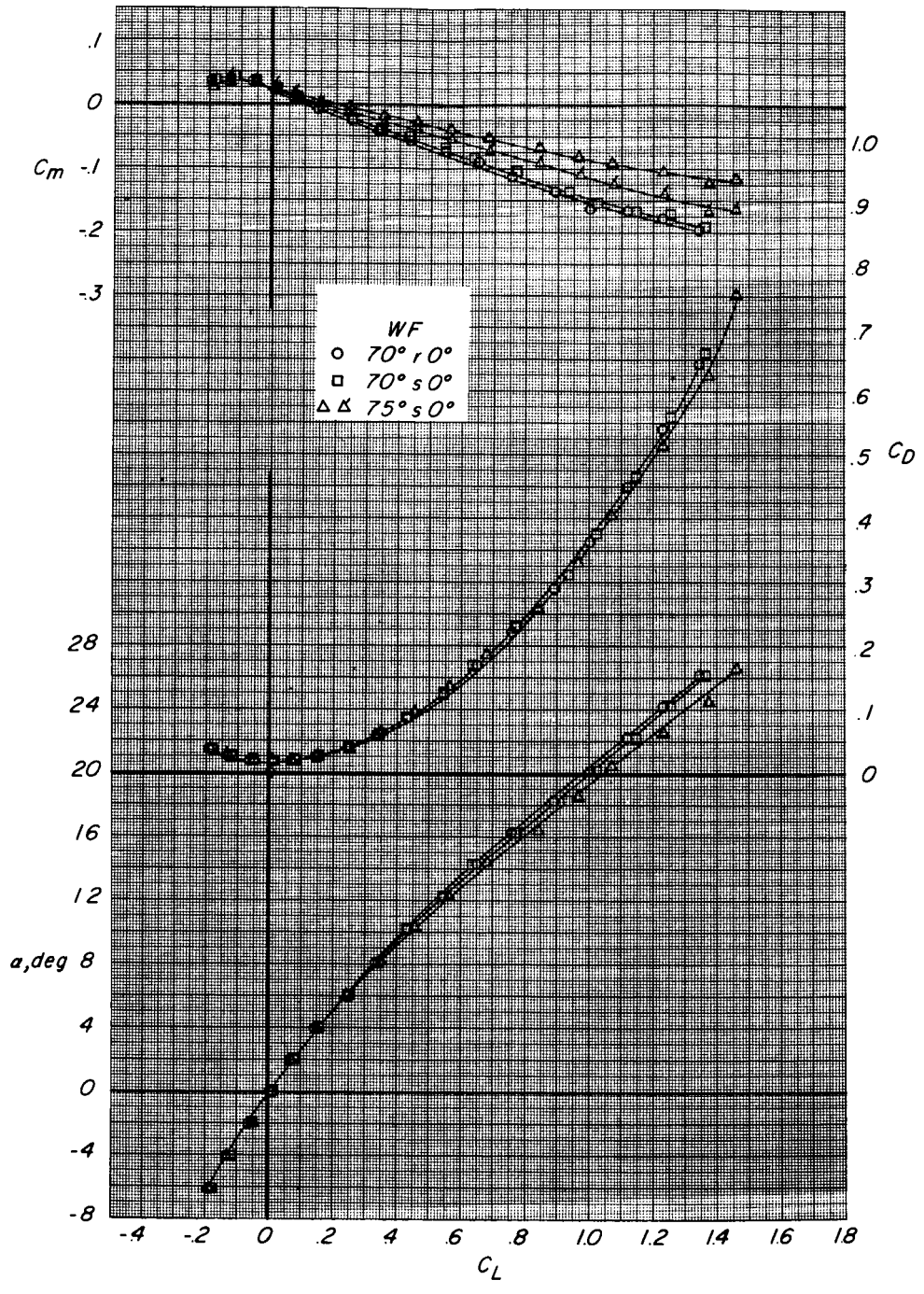

(c) $\Lambda = 75^{\circ}$.

Figure 8.- Concluded.

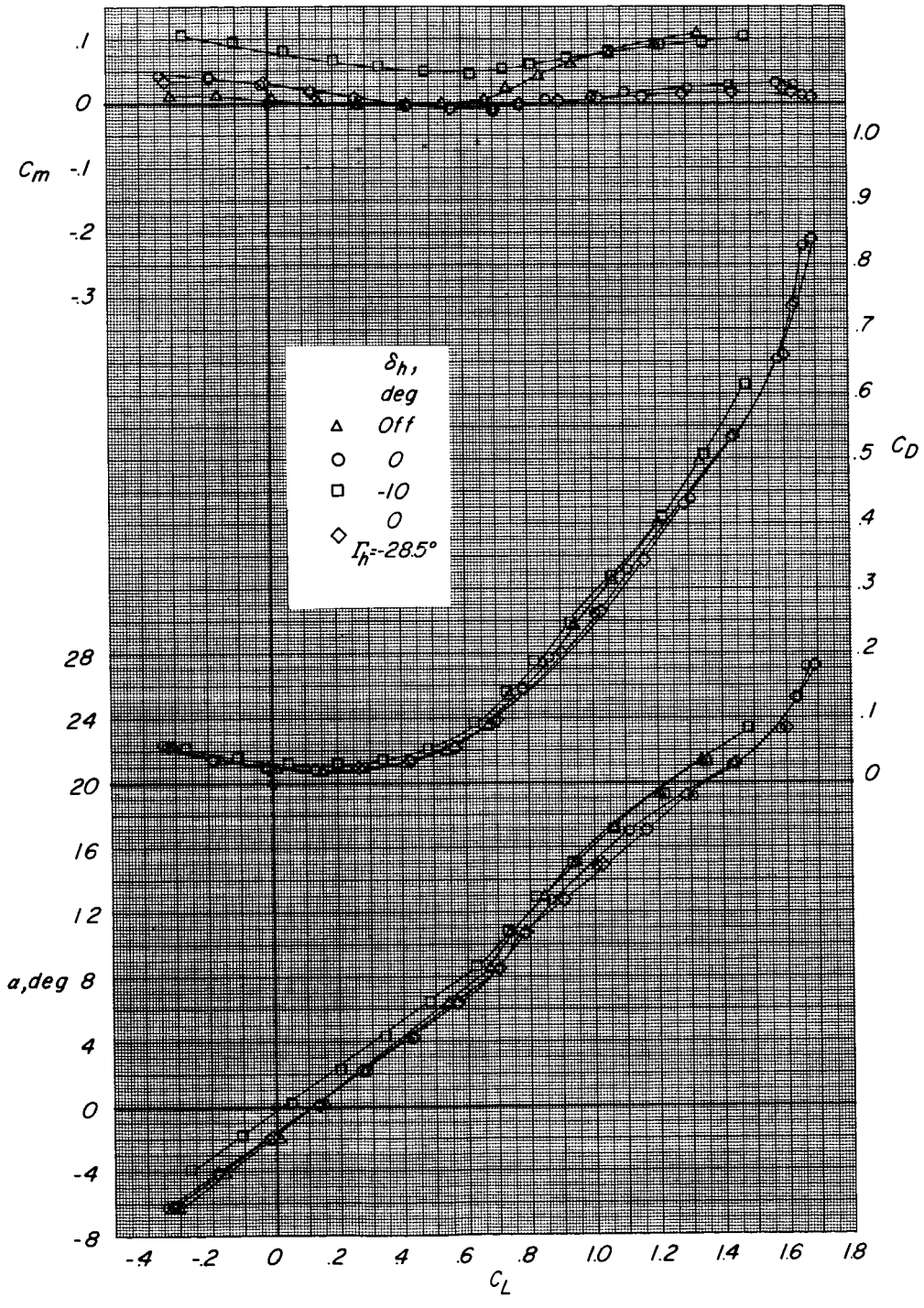

(a) $\Lambda = 25^\circ$.

Figure 9.- Effect of horizontal tail on aerodynamic characteristics in pitch. FW_2HV; WF = 75°s0°.

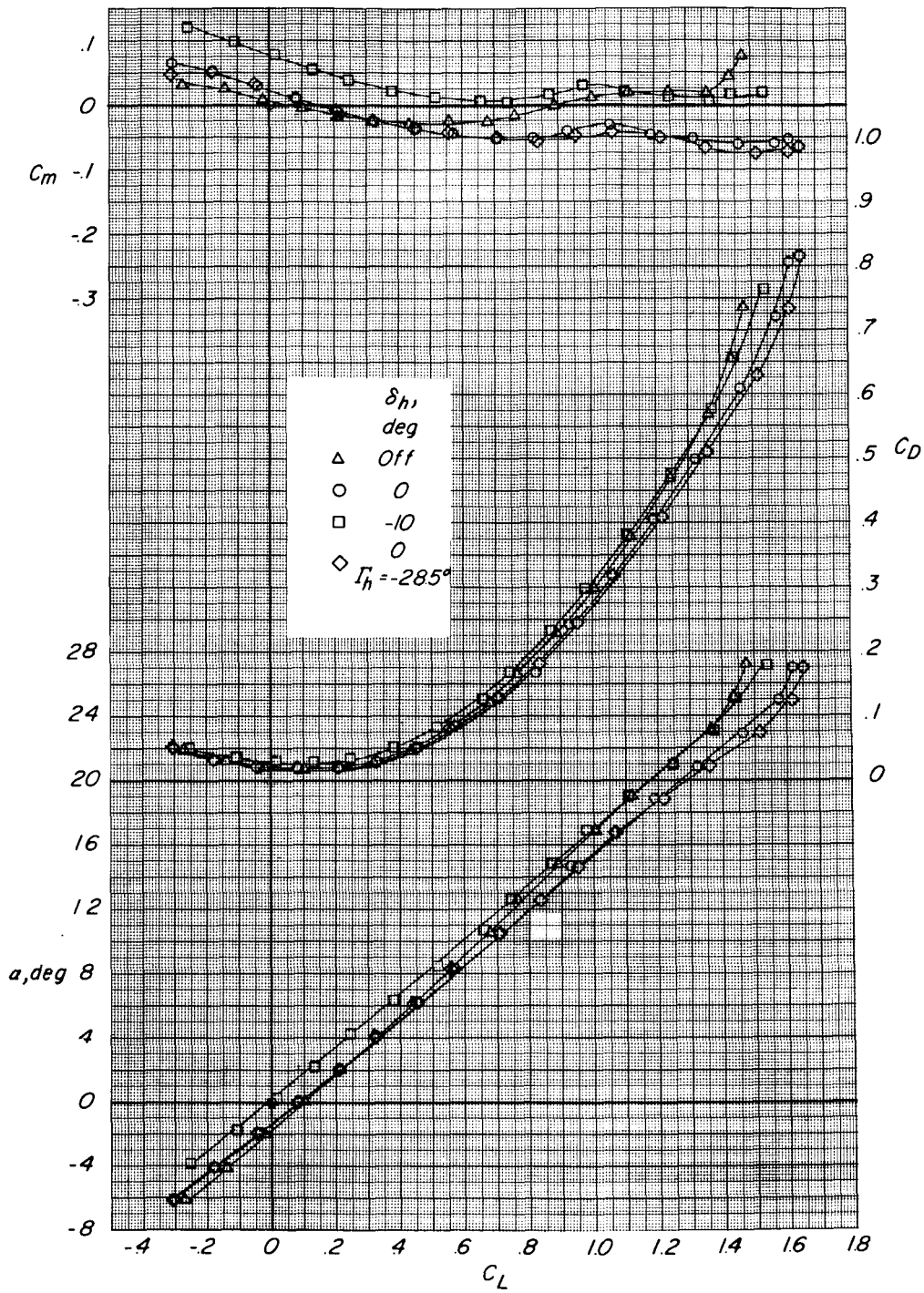

(b) $\Lambda = 45°$.

Figure 9.- Continued.

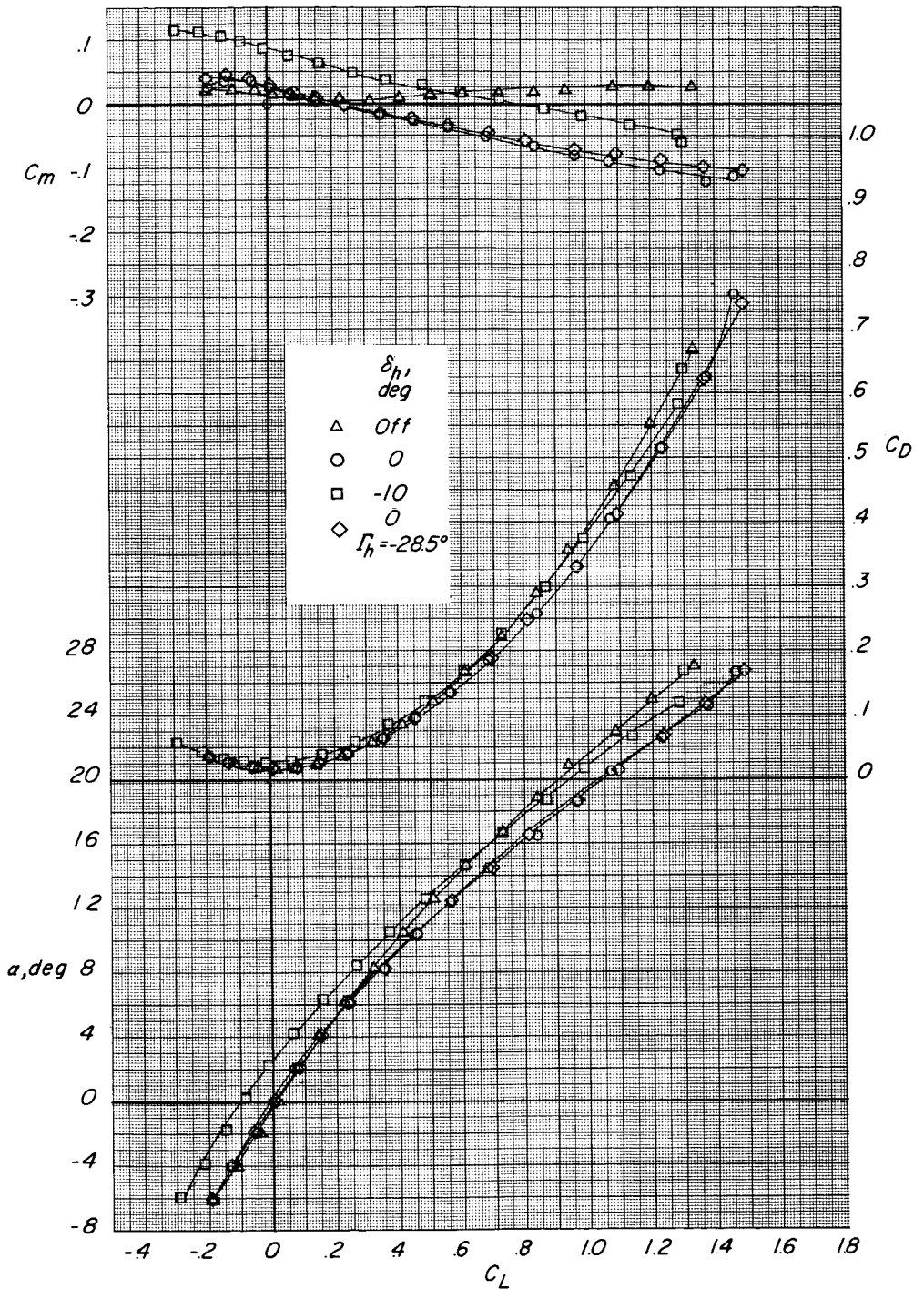

(c) $\Lambda = 75^\circ$.

Figure 9.- Concluded.

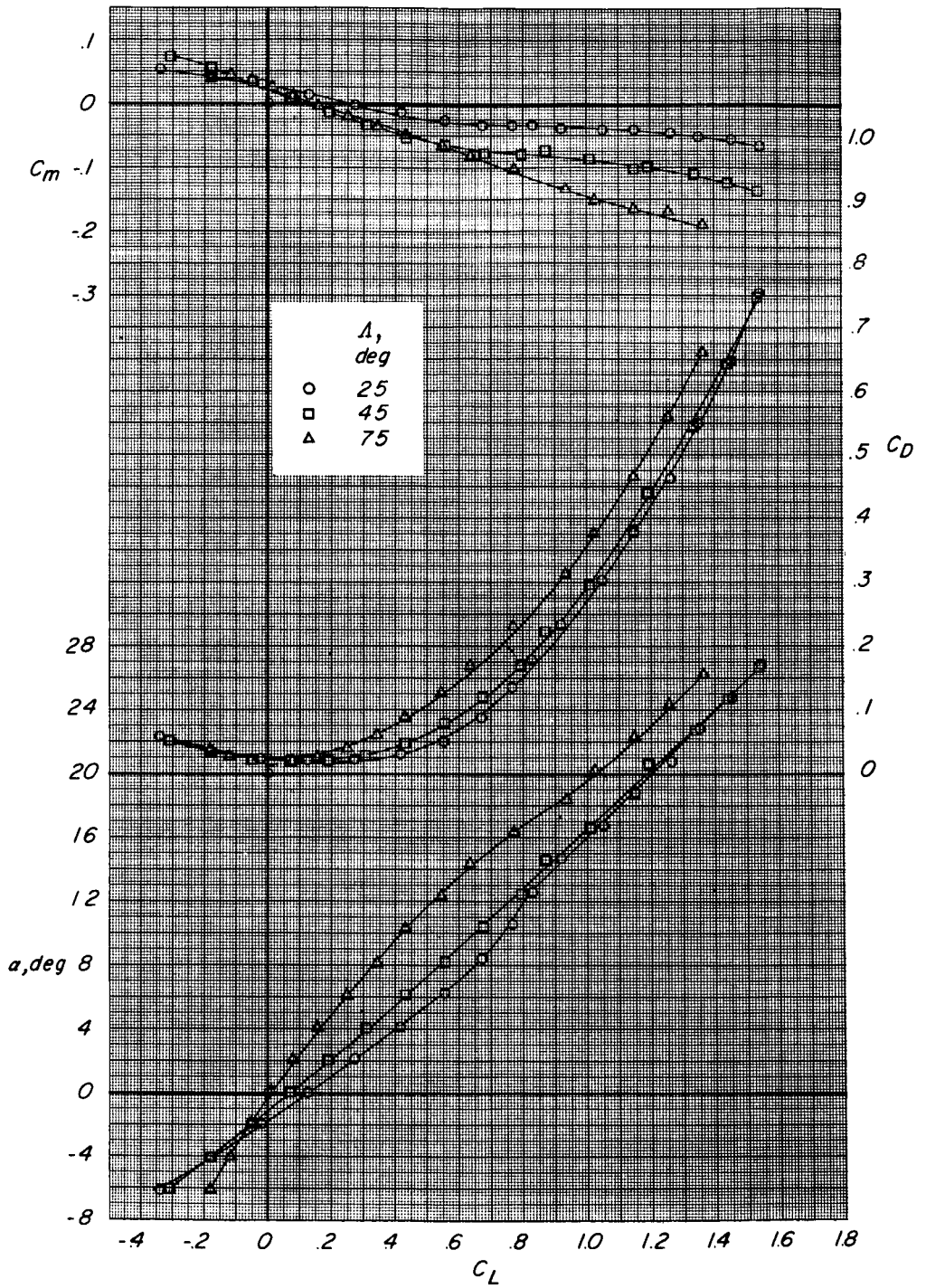

(a) FW_2HV.

Figure 10.- Effect of wing sweep on aerodynamic characteristics in pitch. $\delta_h = 0^\circ$; WF = $70^\circ s0^\circ$.

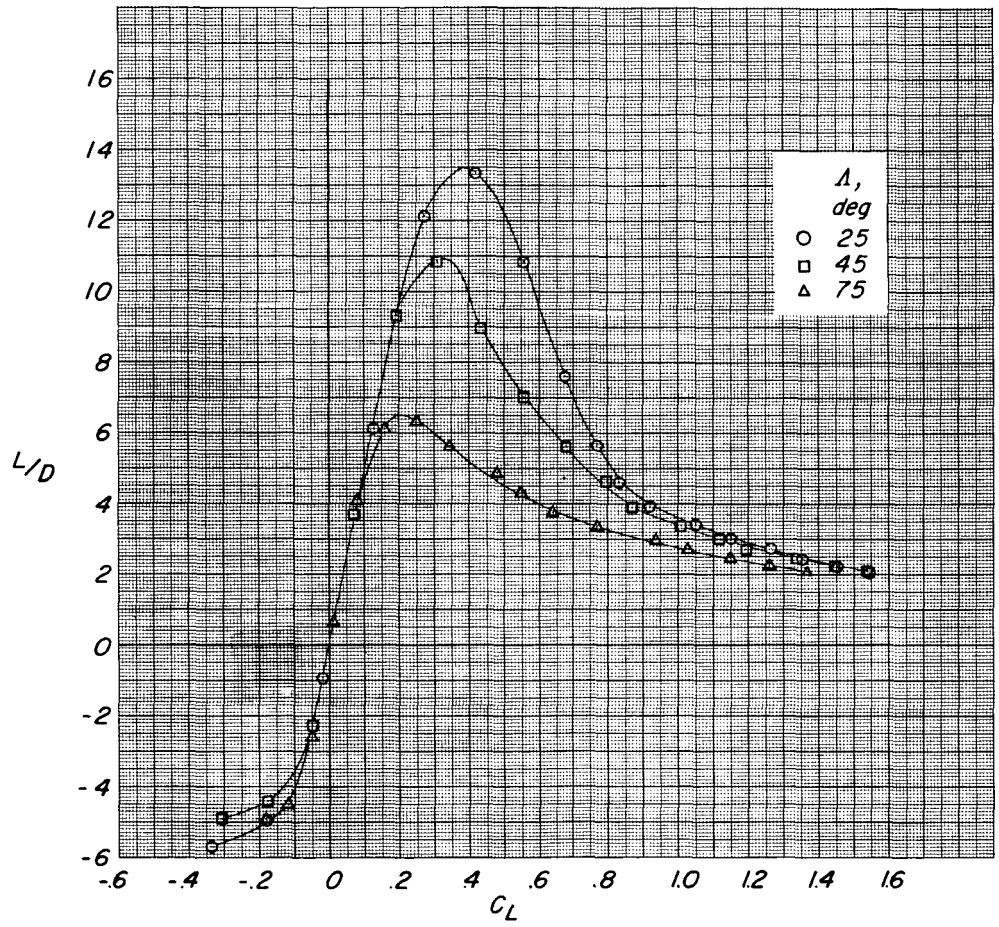

(a) Concluded.

Figure 10.- Continued.

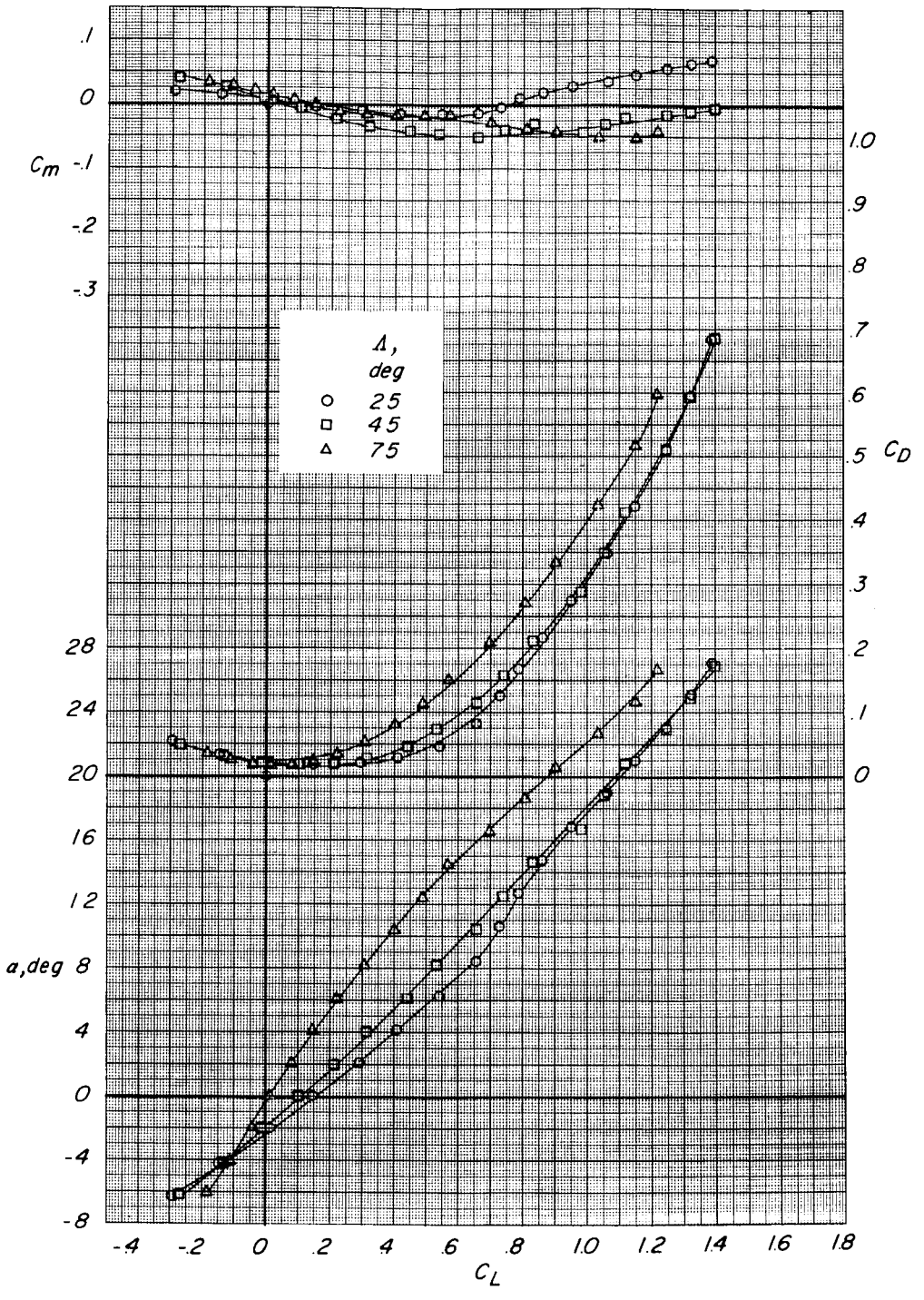

(b) FW_2V.

Figure 10.- Continued.

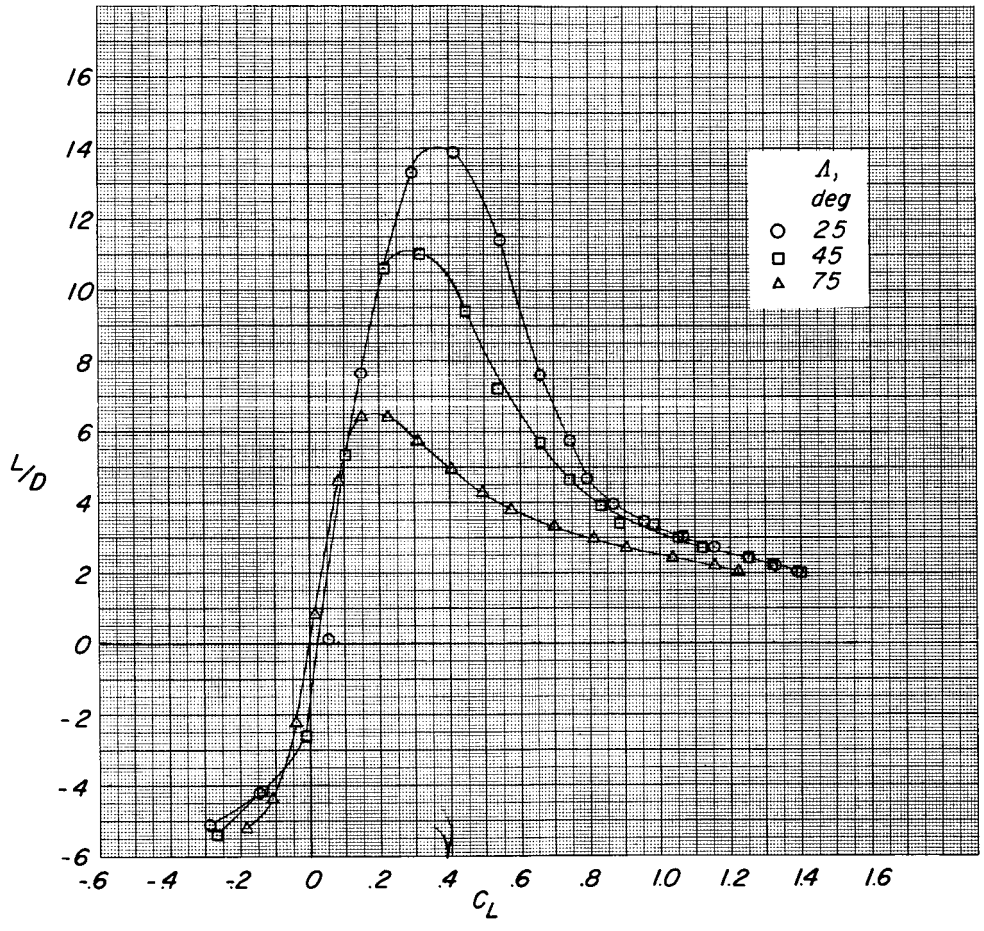

(b) Concluded.

Figure 10.- Concluded.

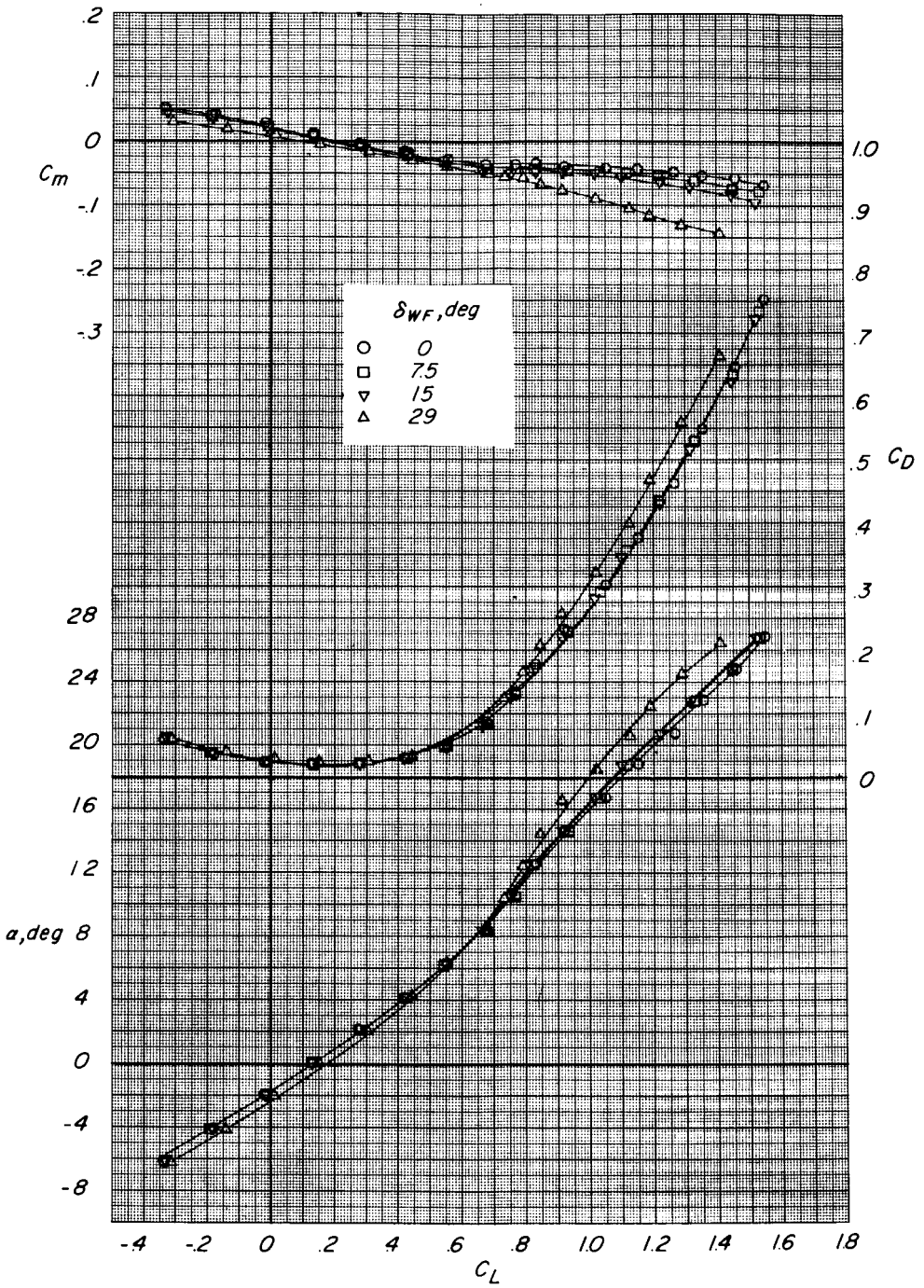

(a) $\Lambda = 25^{\circ}$.

Figure 11.- Effect of wing-fuselage flap deflection (WF = 70°s) on aerodynamic characteristics in pitch. FW_2HV; $\delta_h = 0^{\circ}$.

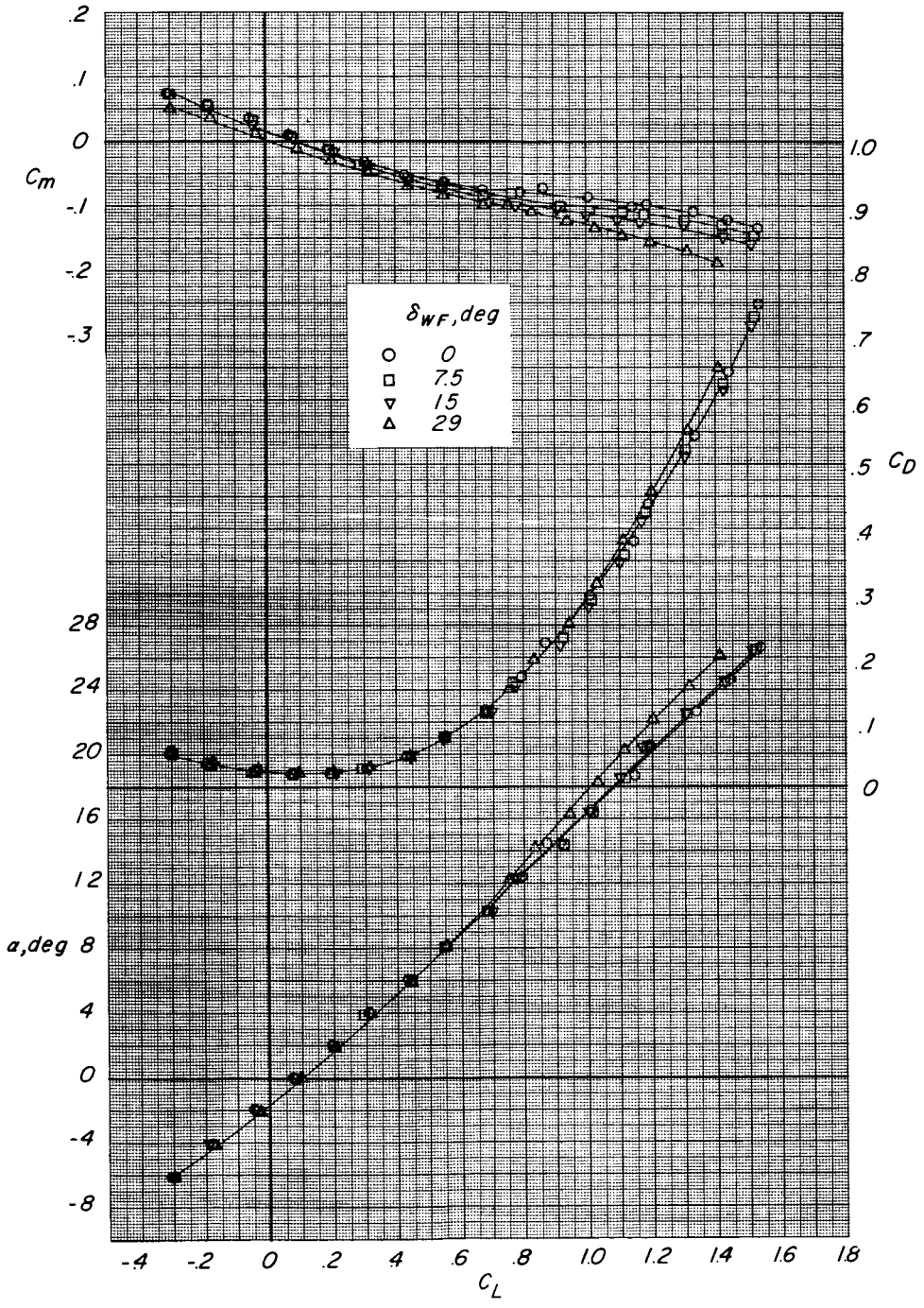

(b) $\Lambda = 45^\circ$.

Figure 11.- Continued.

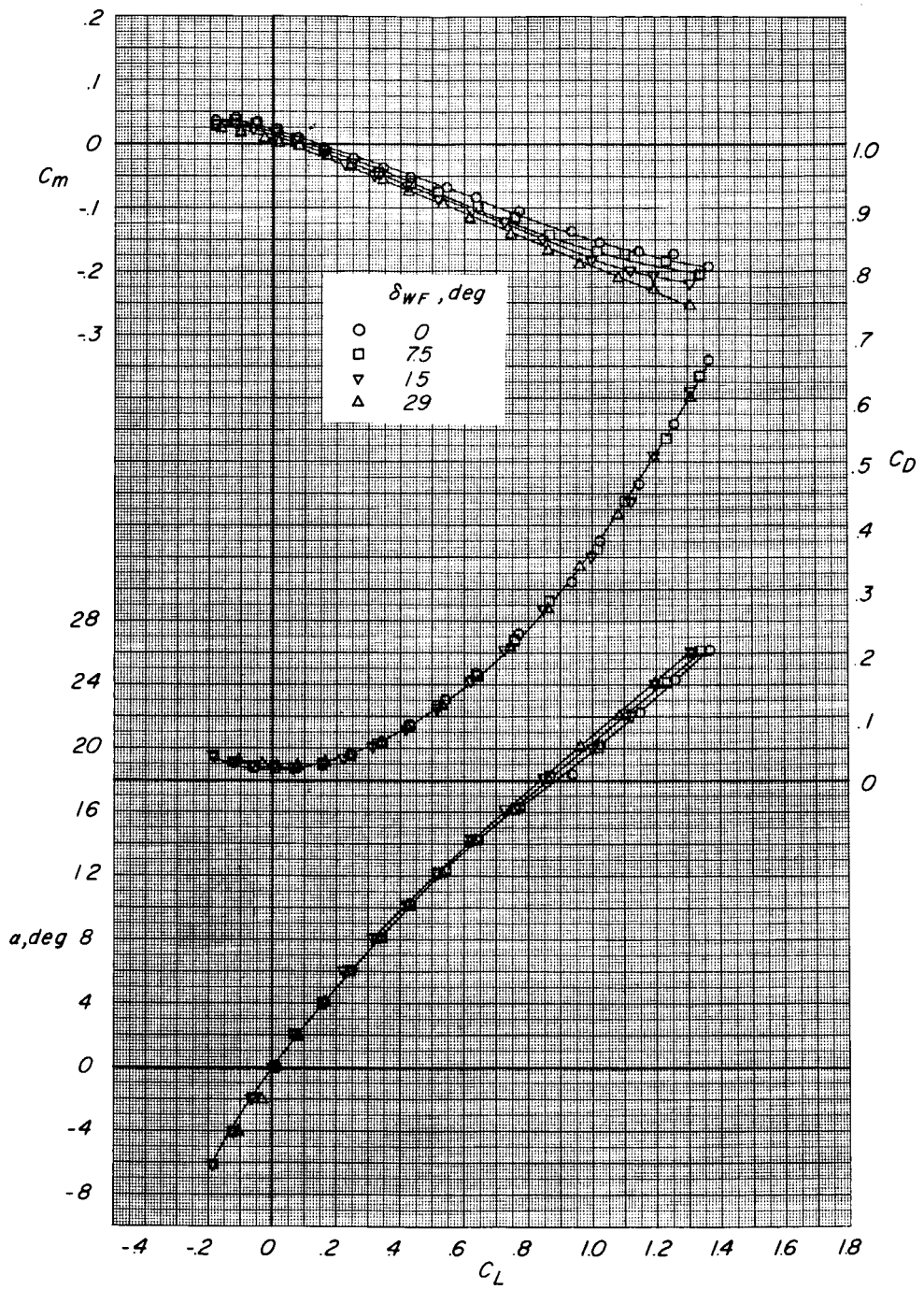

(c) $\Lambda = 75^{\circ}$.

Figure 11.- Concluded.

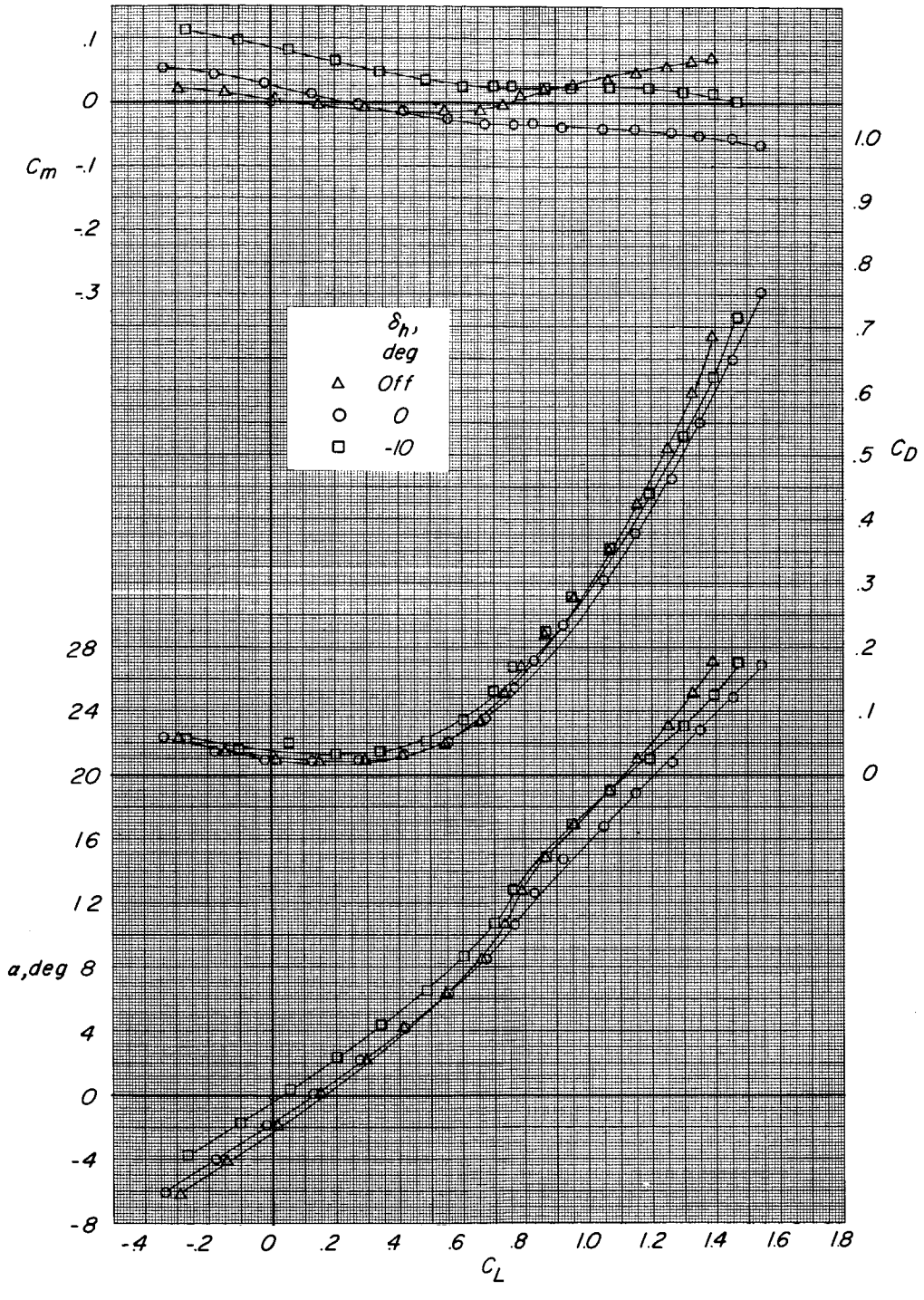

(a) $\Lambda = 25^\circ$.

Figure 12.- Effect of horizontal tail on aerodynamic characteristics in pitch. FW_2HV; WF = $70^\circ s0^\circ$.

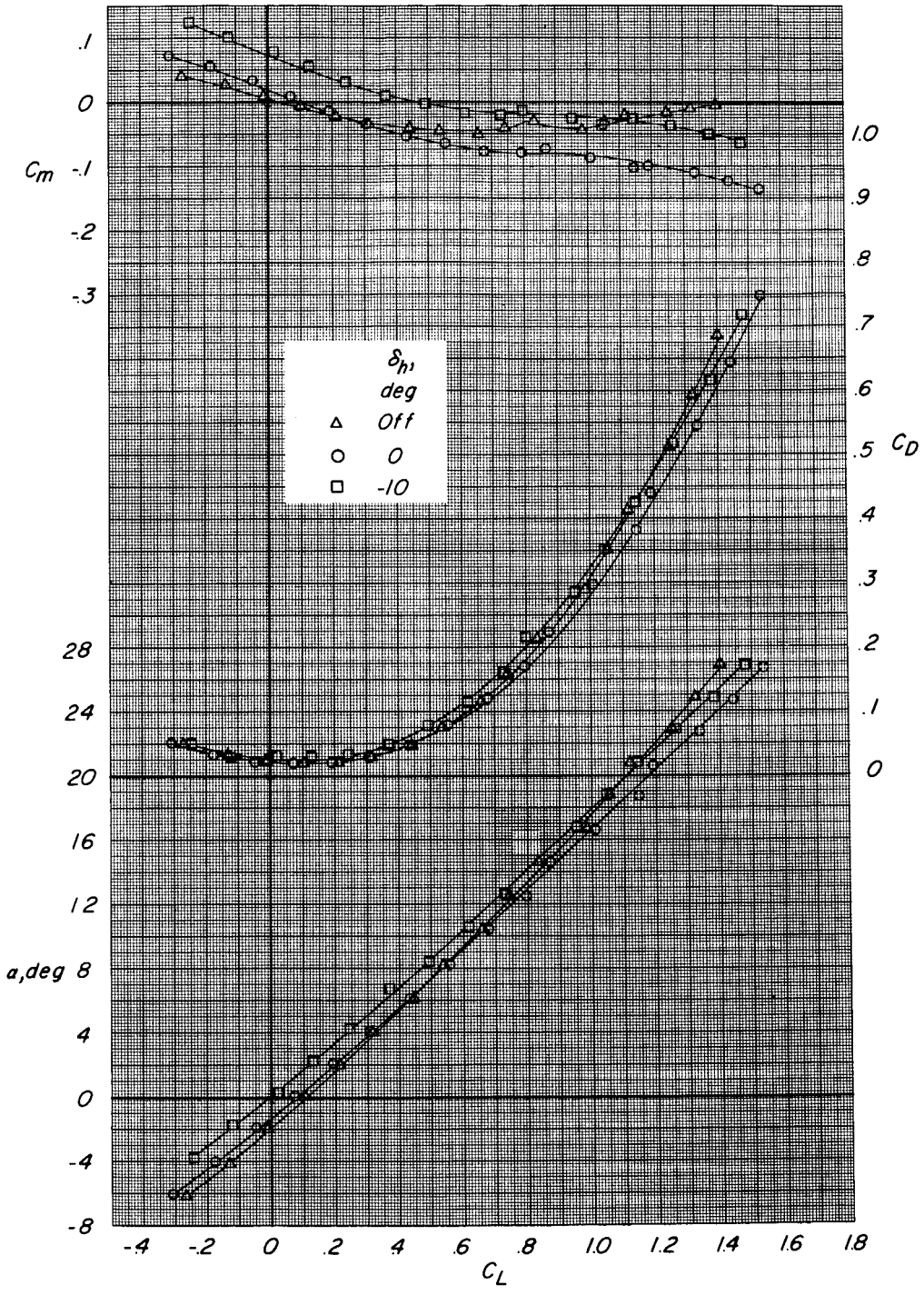

(b) $\Lambda = 45^\circ$.

Figure 12.- Continued.

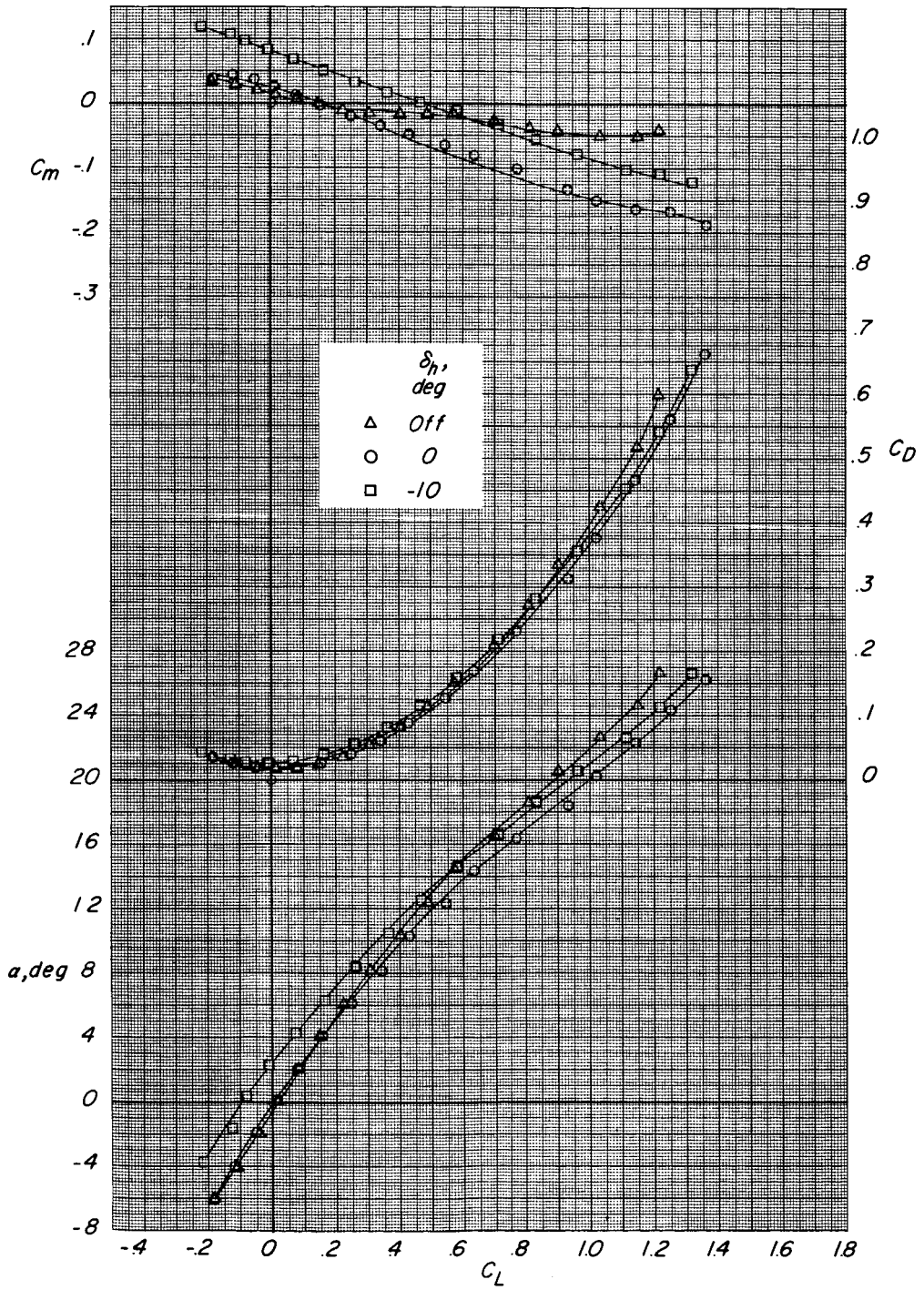

(c) $\Lambda = 75^\circ$.

Figure 12.- Concluded.

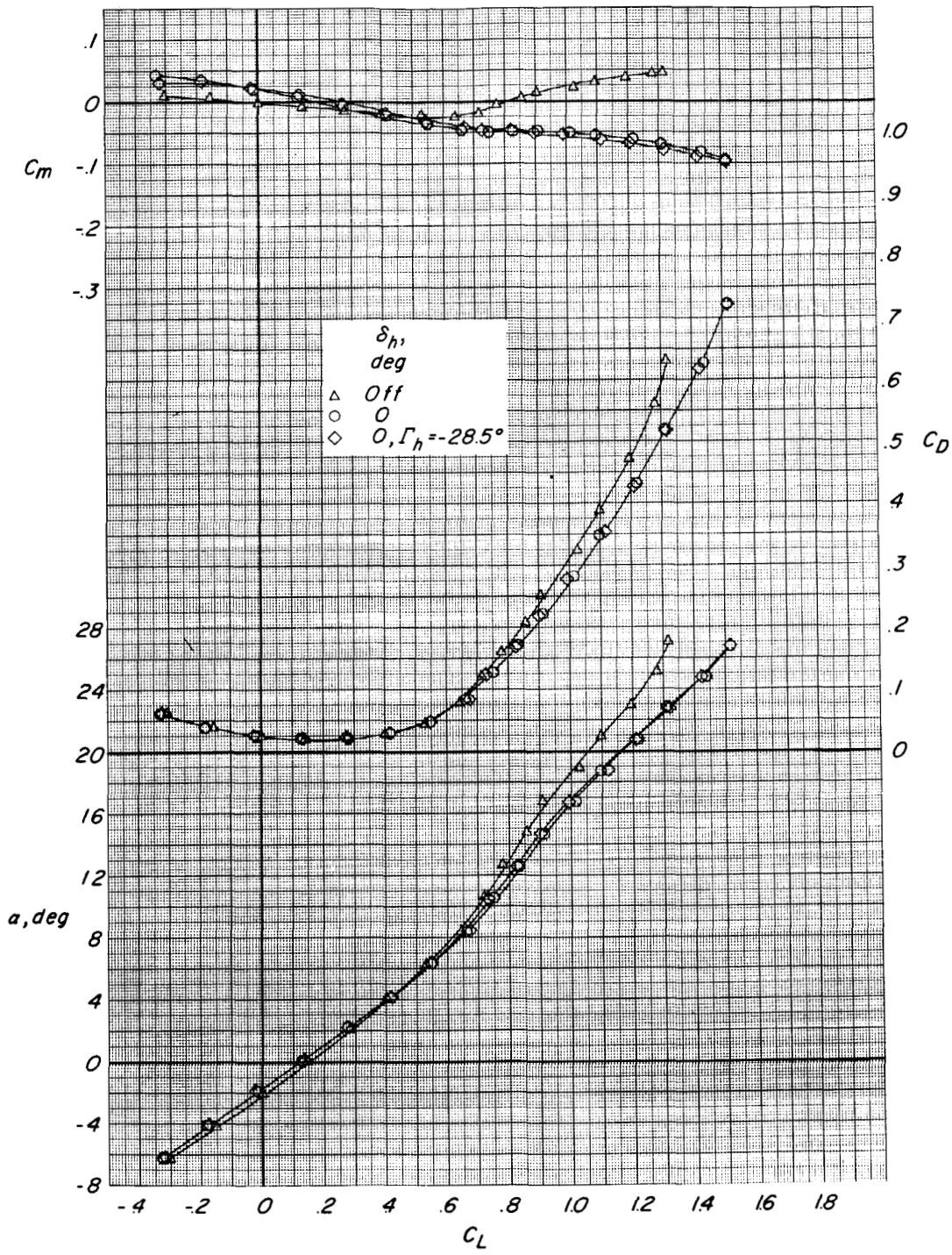

(a) $\Lambda = 25^{\circ}$.

Figure 13.- Effect of horizontal tail on aerodynamic characteristics in pitch. FW_2HV; WF = $70^{\circ}s15^{\circ}$.

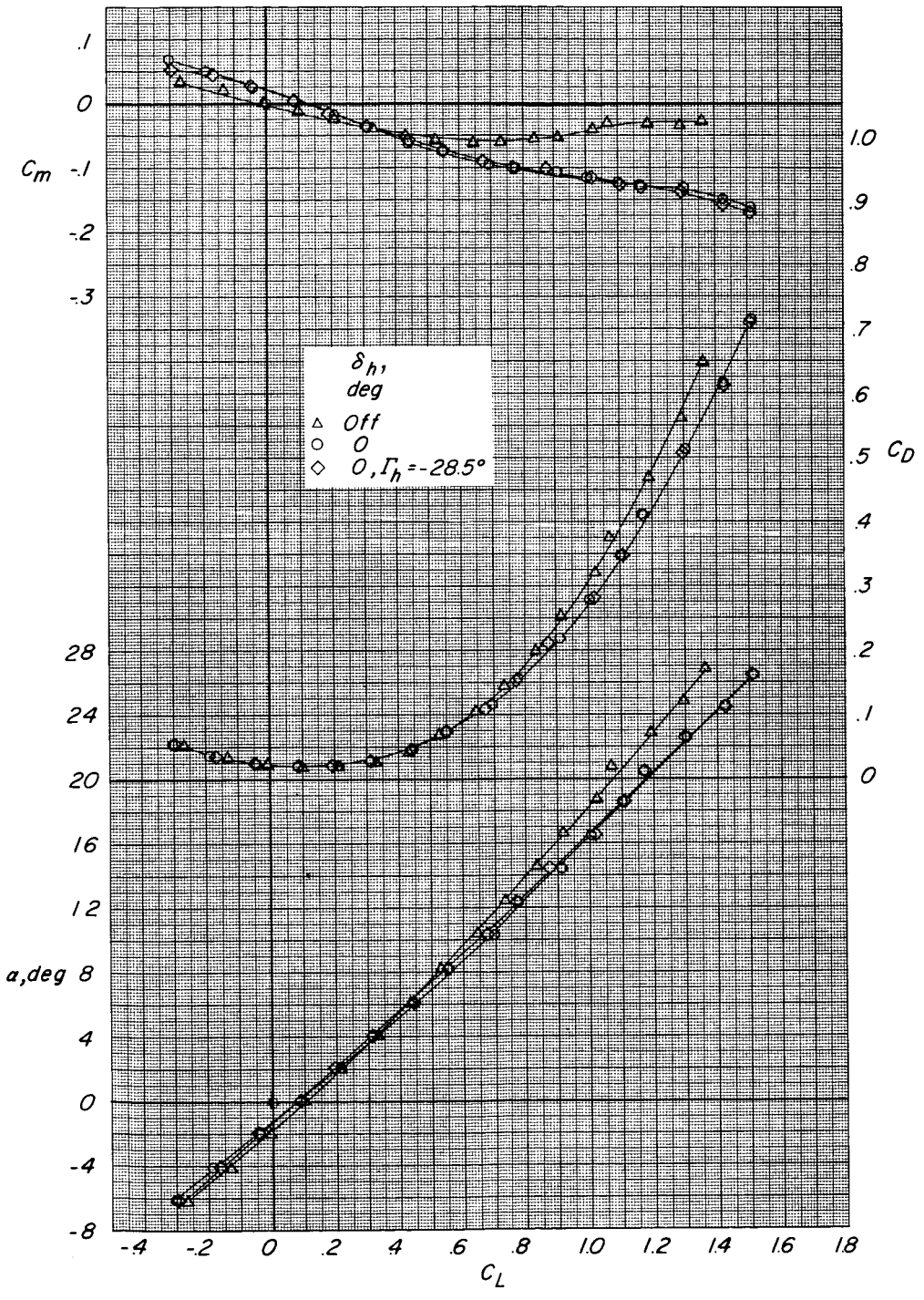

(b) $\Lambda = 45°$.

Figure 13.- Continued.

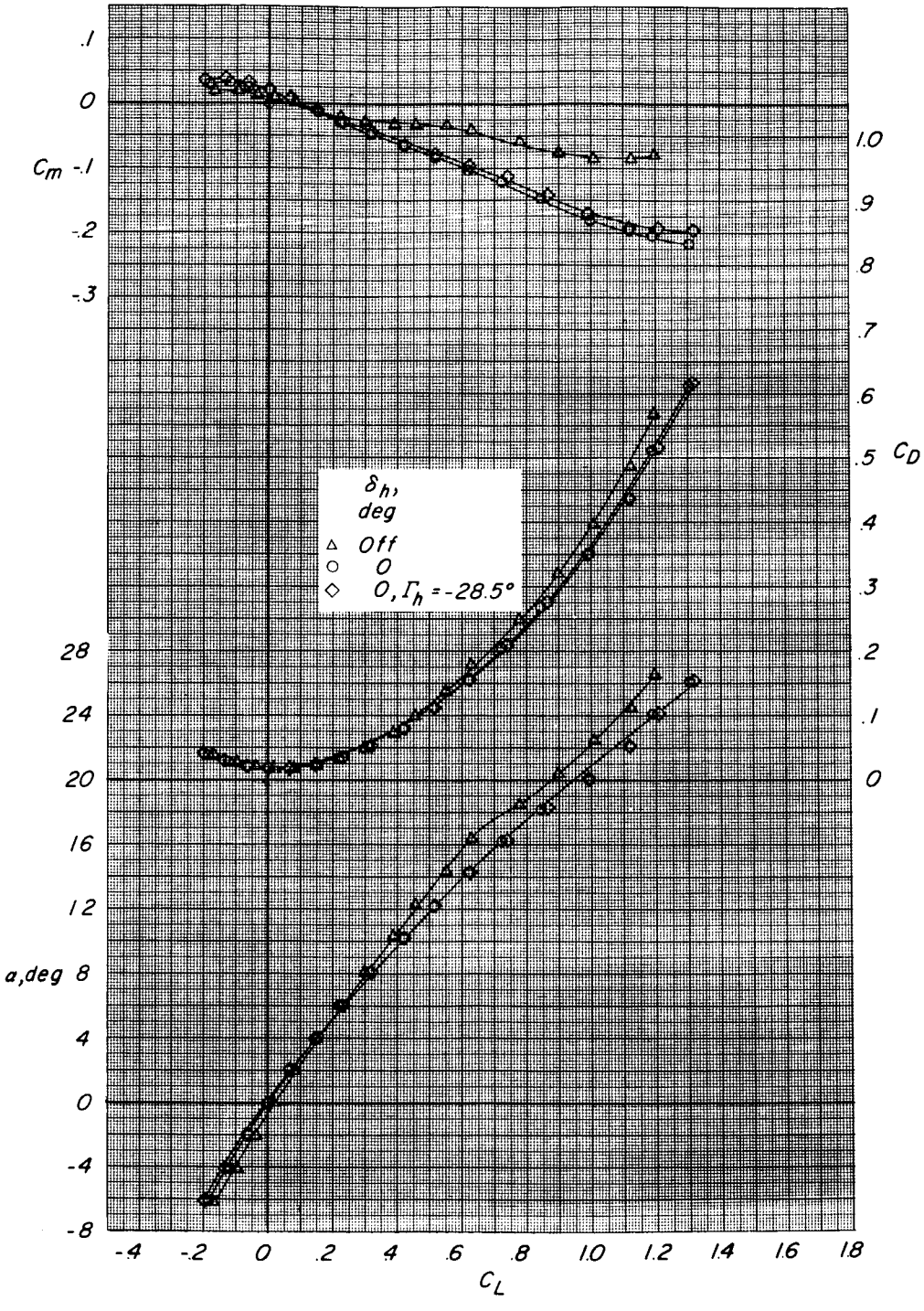

(c) $\Lambda = 75°$.

Figure 13.- Concluded.

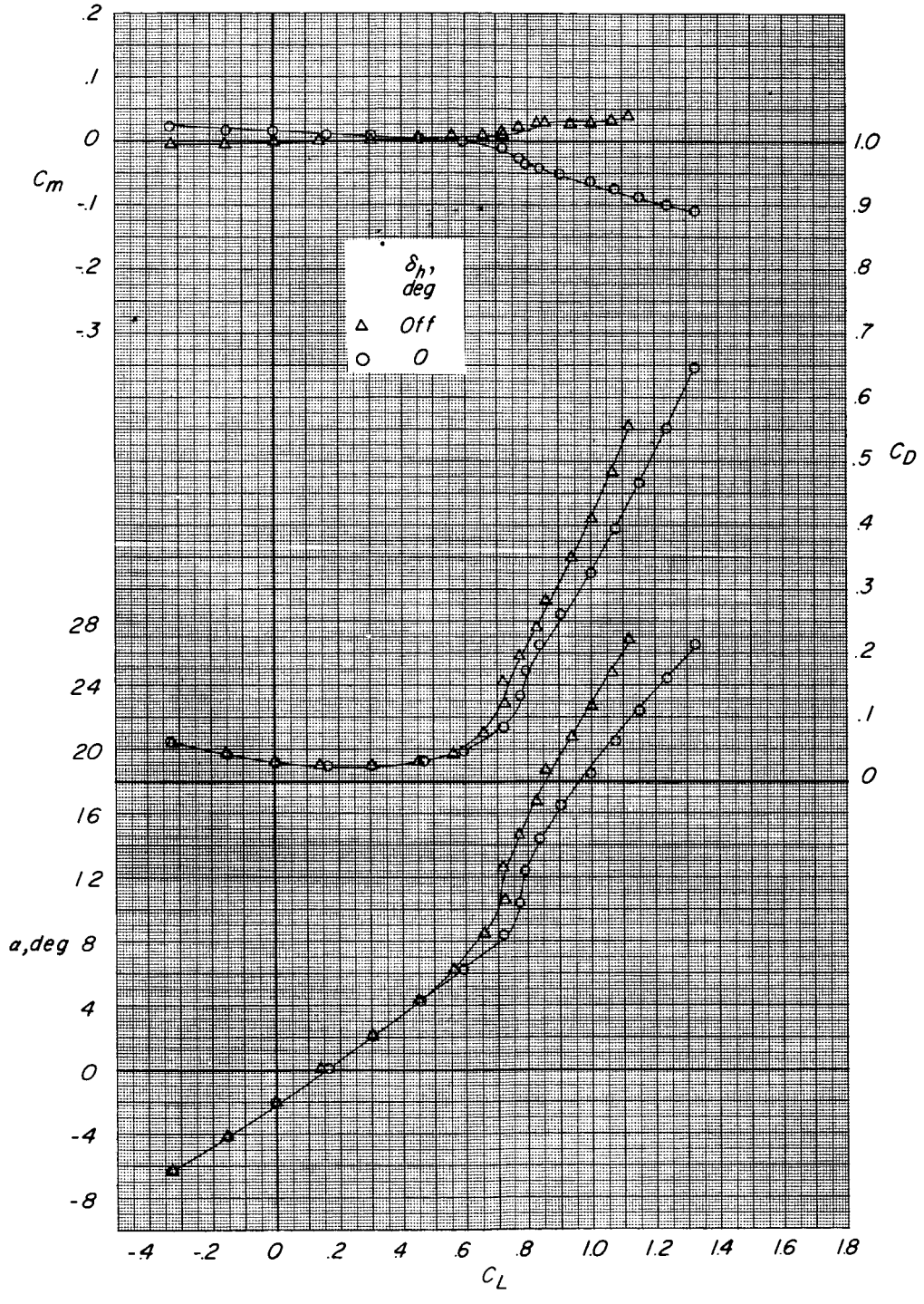

(a) $\Lambda = 13.5^{\circ}$.

Figure 14.- Effect of horizontal tail on aerodynamic characteristics in pitch. FW_2HV; WF = $70^{\circ}s29^{\circ}$.

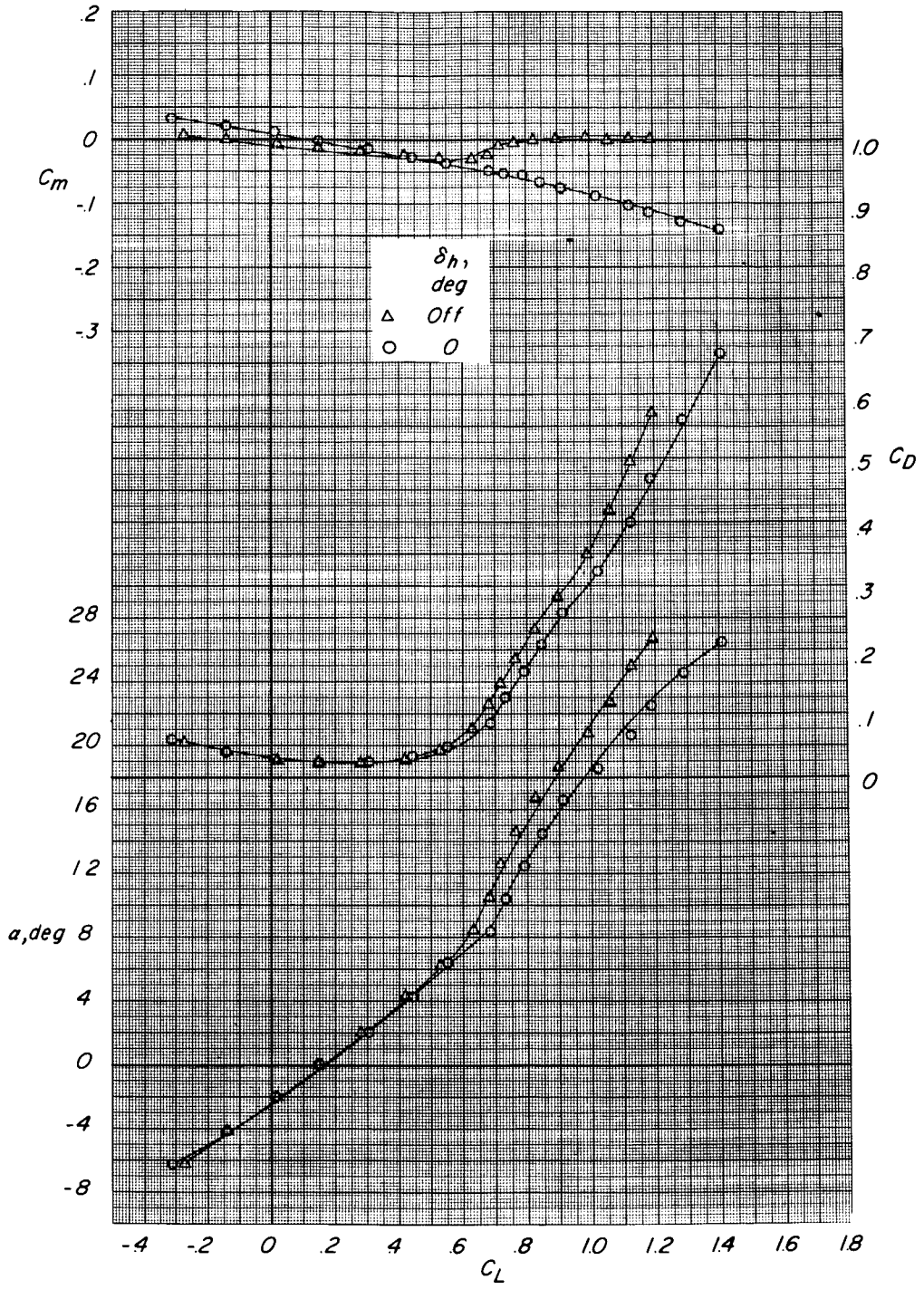

(b) $\Lambda = 25^\circ$.

Figure 14.- Continued.

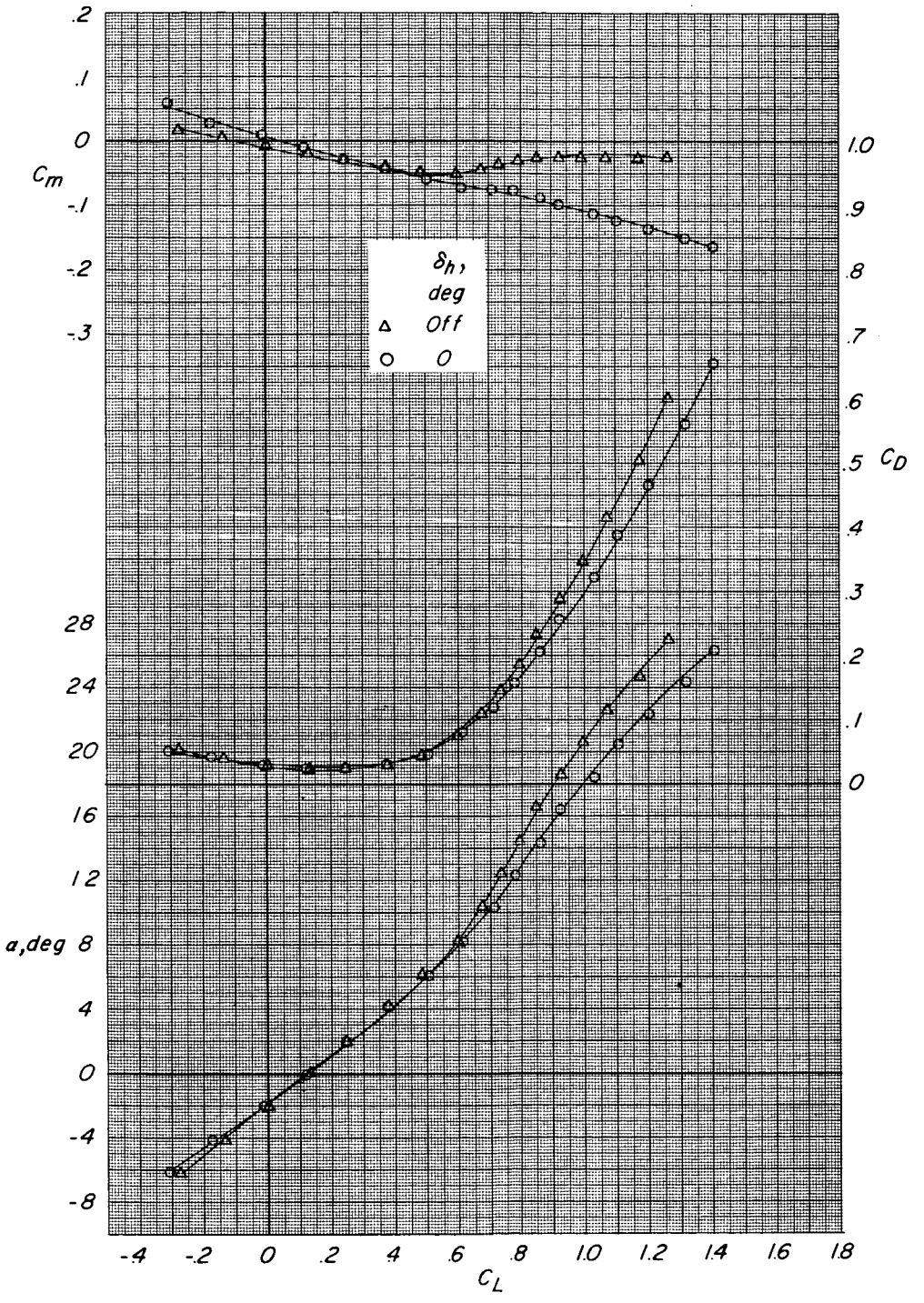

(c) $\Lambda = 35^{\circ}$.

Figure 14.- Continued.

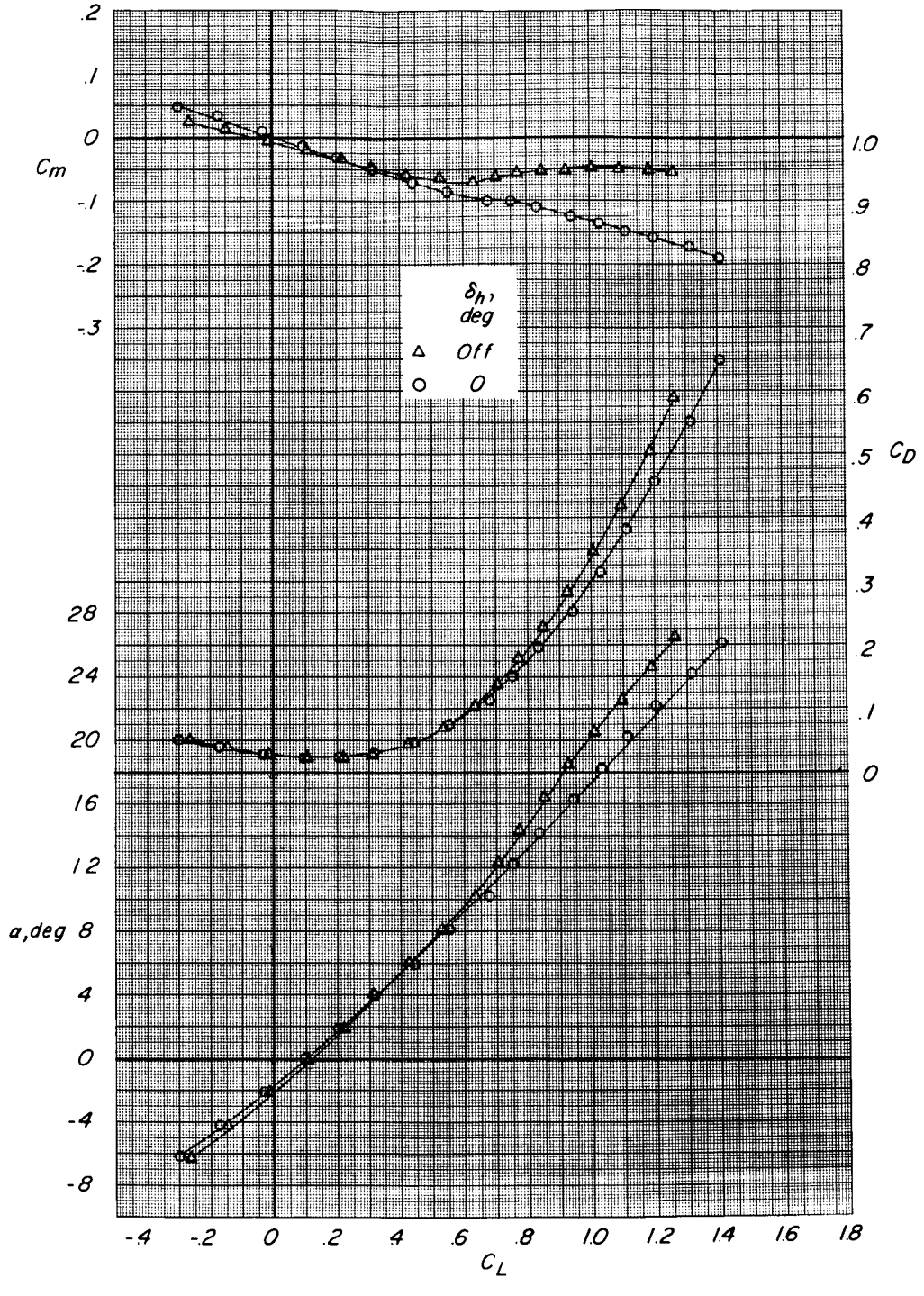

(d) $\Lambda = 45°$.

Figure 14.- Continued.

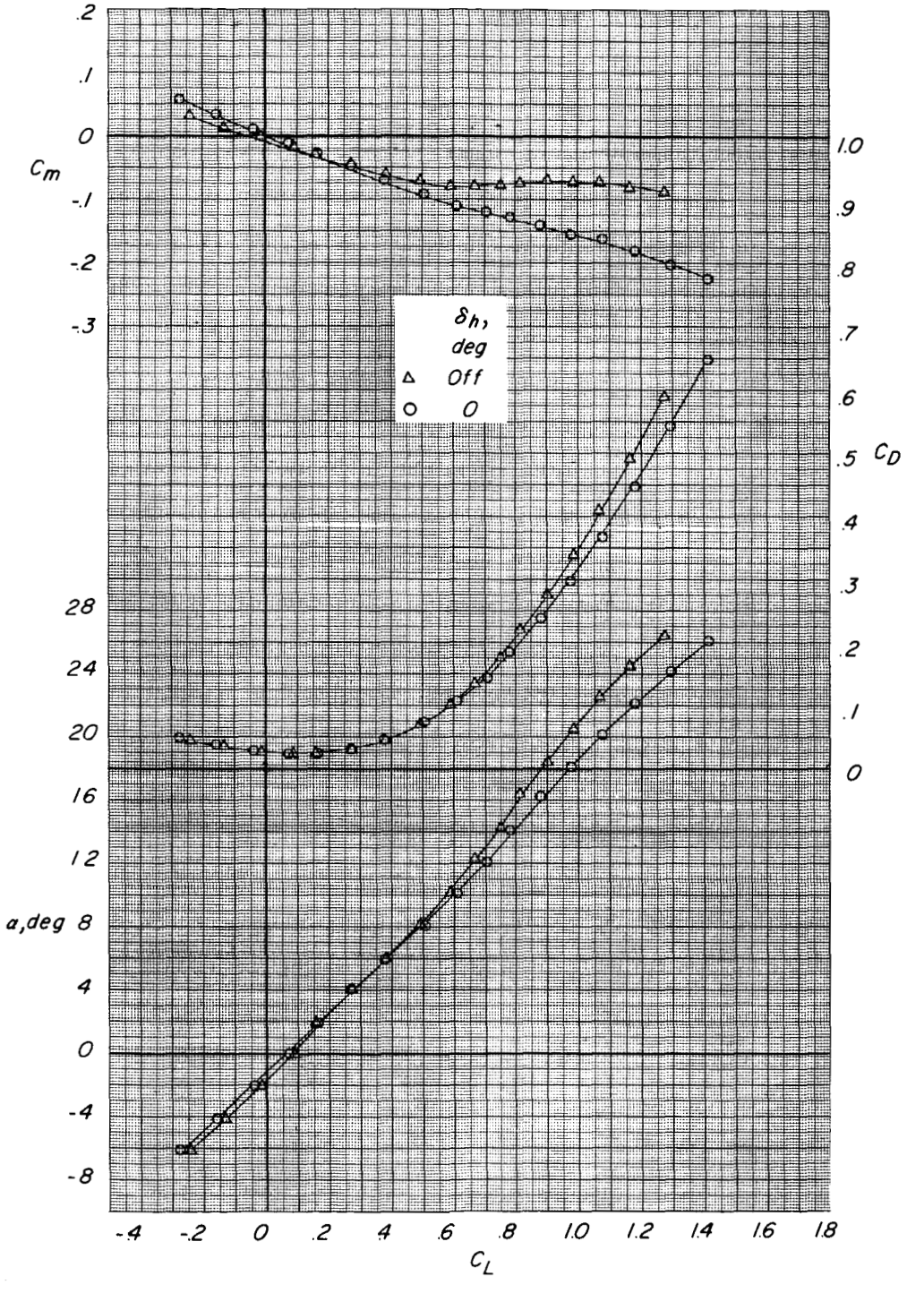

(e) $\Lambda = 55^\circ$.

Figure 14.- Continued.

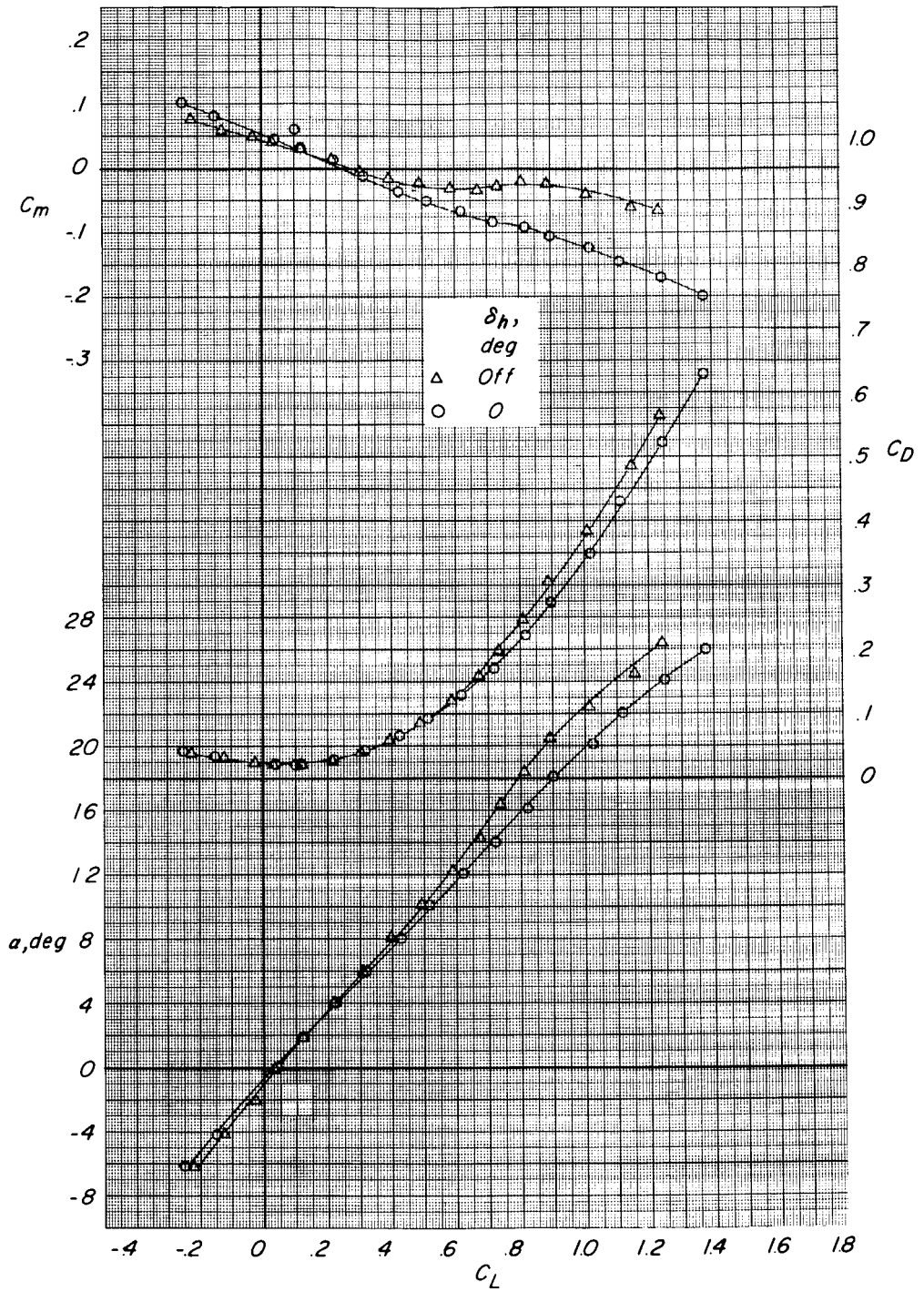

(f) $\Lambda = 65°$.

Figure 14.- Continued.

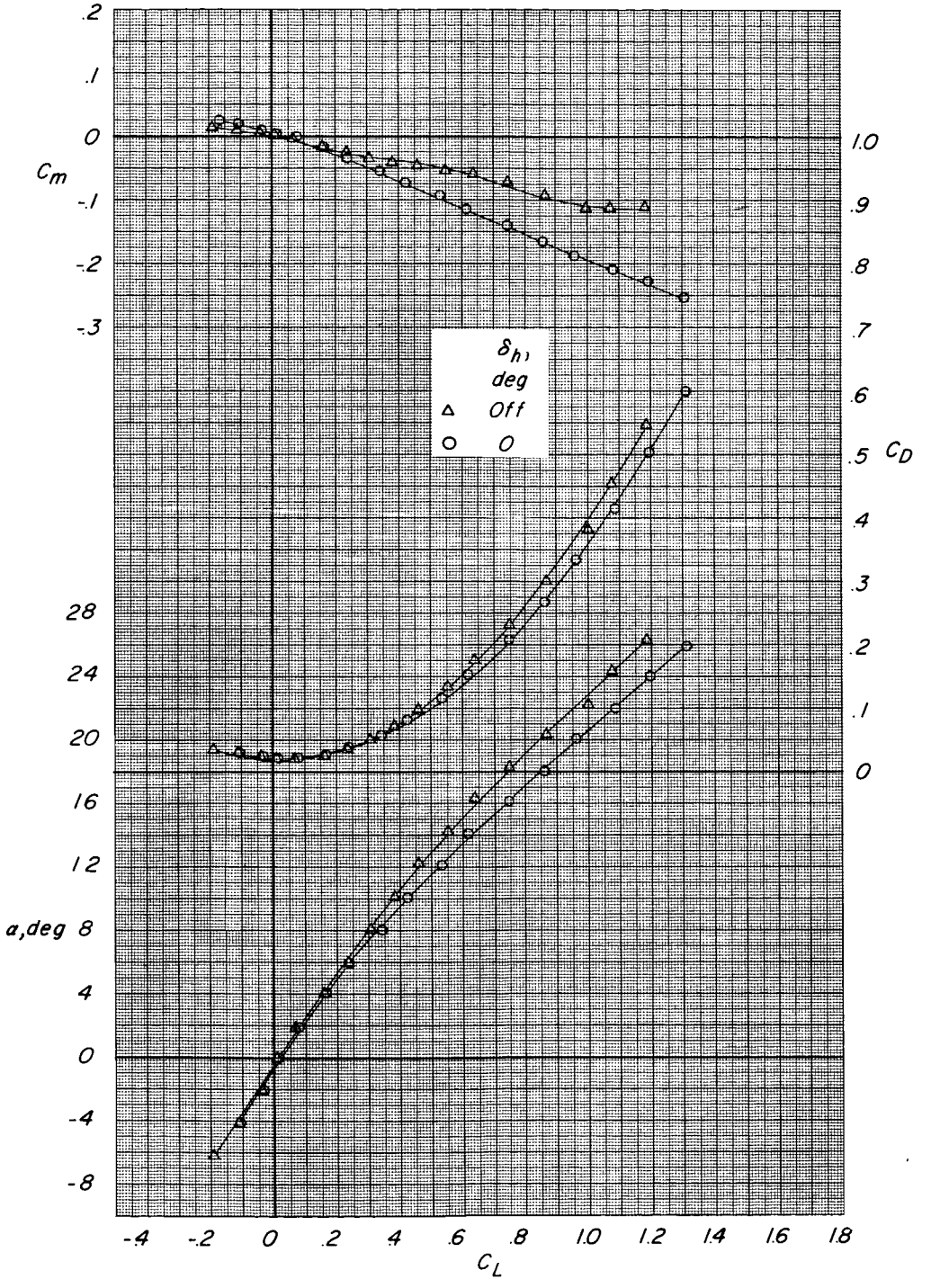

(g) $\Lambda = 75°$.

Figure 14.- Concluded.

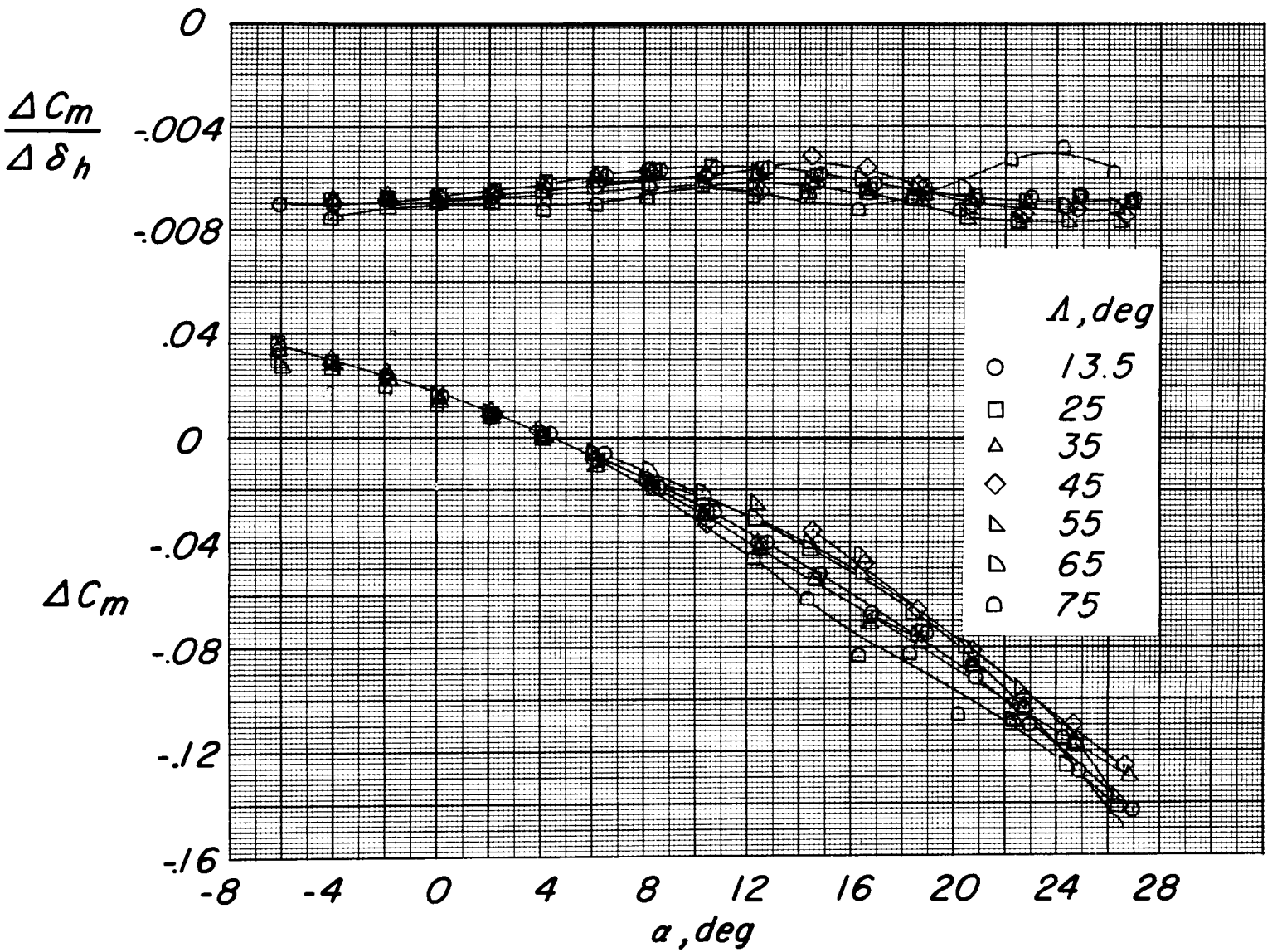

Figure 15.- Effect of wing sweep on the increment in pitching-moment coefficient due to addition of horizontal tail ΔC_m and horizontal control effectiveness $\Delta C_m/\Delta\delta_h$ for configuration FW_1H. WF = $70^o r0^o$.

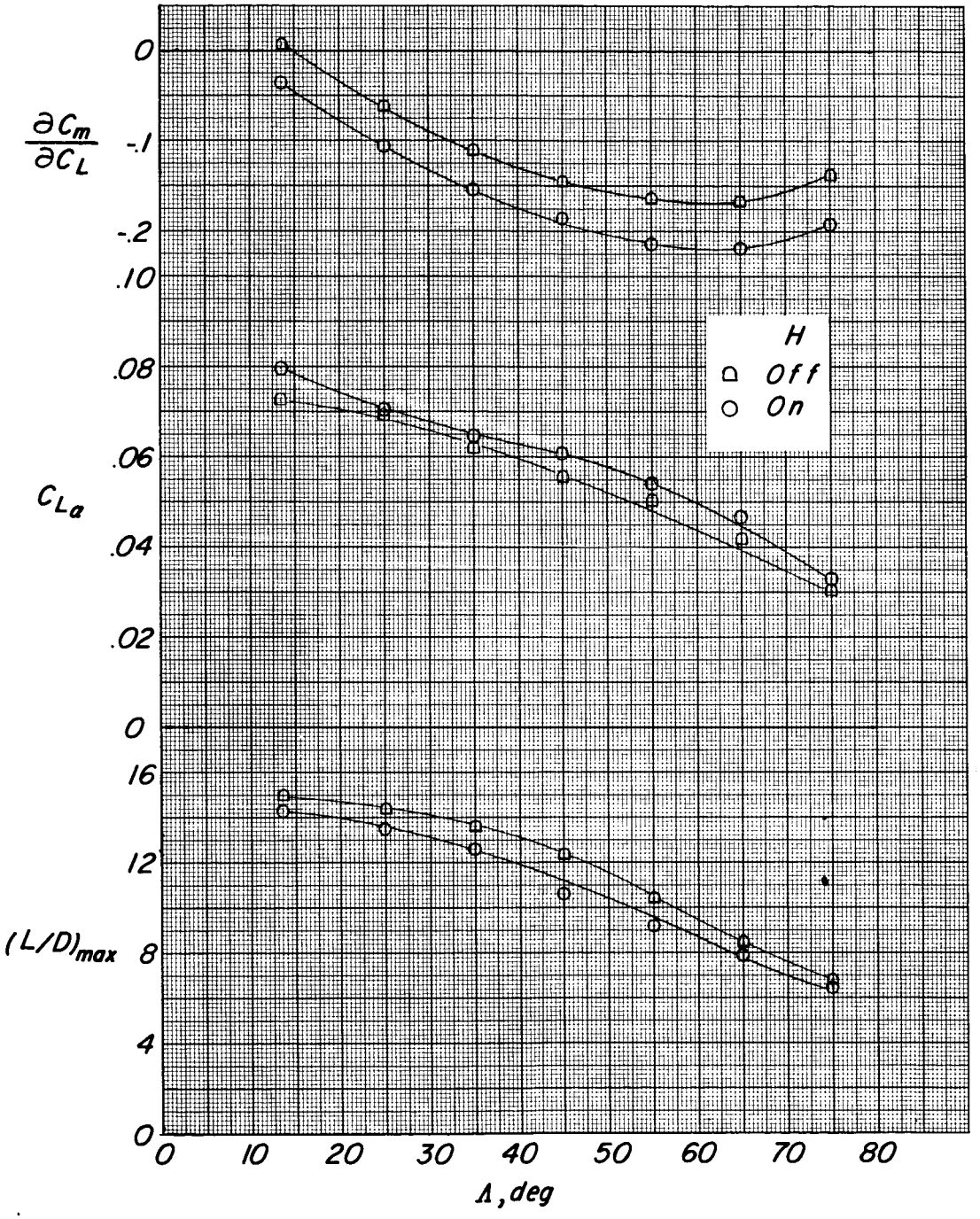

Figure 16.- Effects of horizontal tail on lift parameters $\frac{\partial C_m}{\partial C_L}$, C_{L_α}, and $(L/D)_{max}$. FW_1V; WF = 70°r0°.

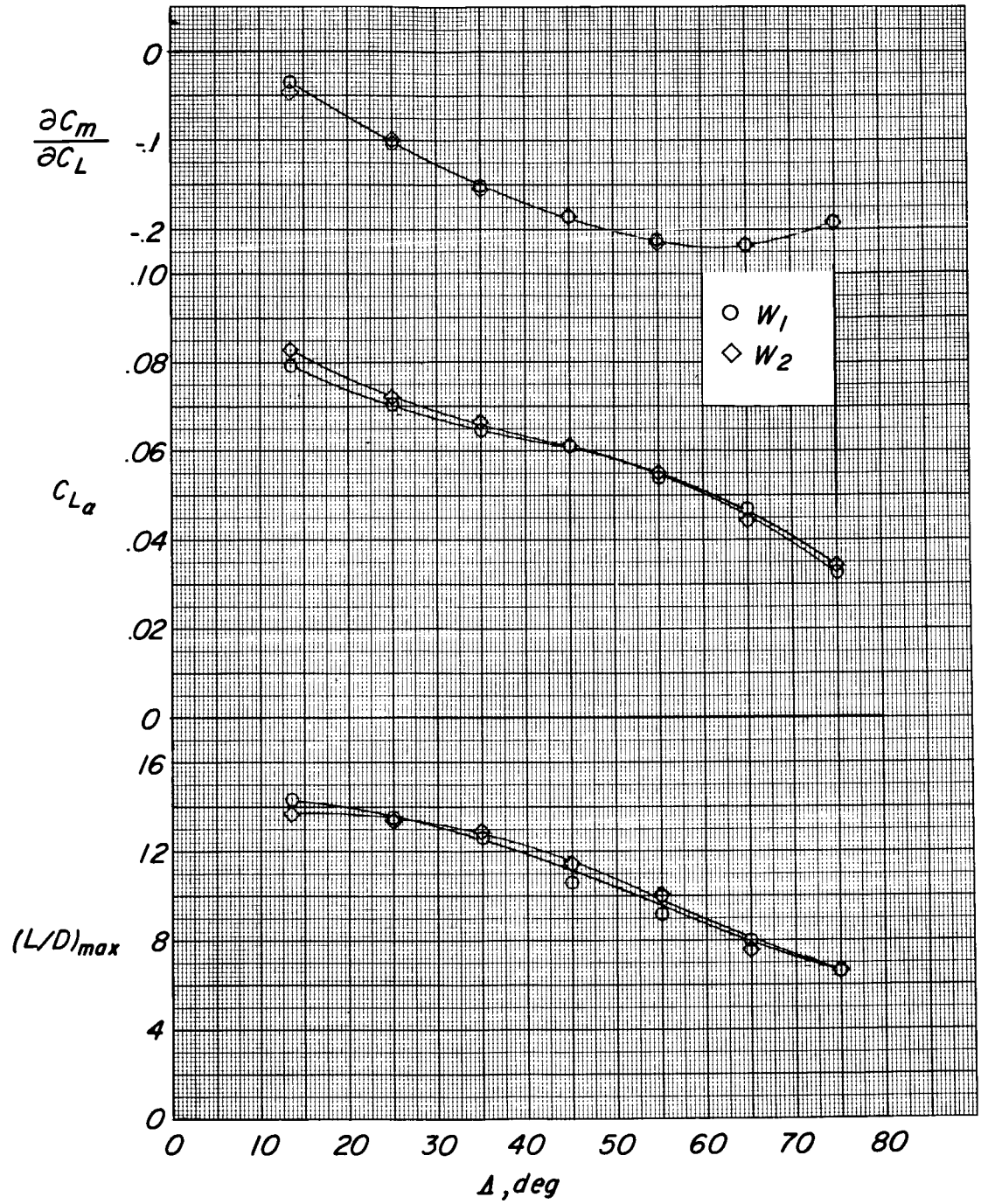

Figure 17.- Effect of wing twist on parameters $\frac{\partial C_m}{\partial C_L}$, C_{L_α}, and $(L/D)_{max}$.

FWHV; $\delta_h = 0^o$; WF = 70°r0°.

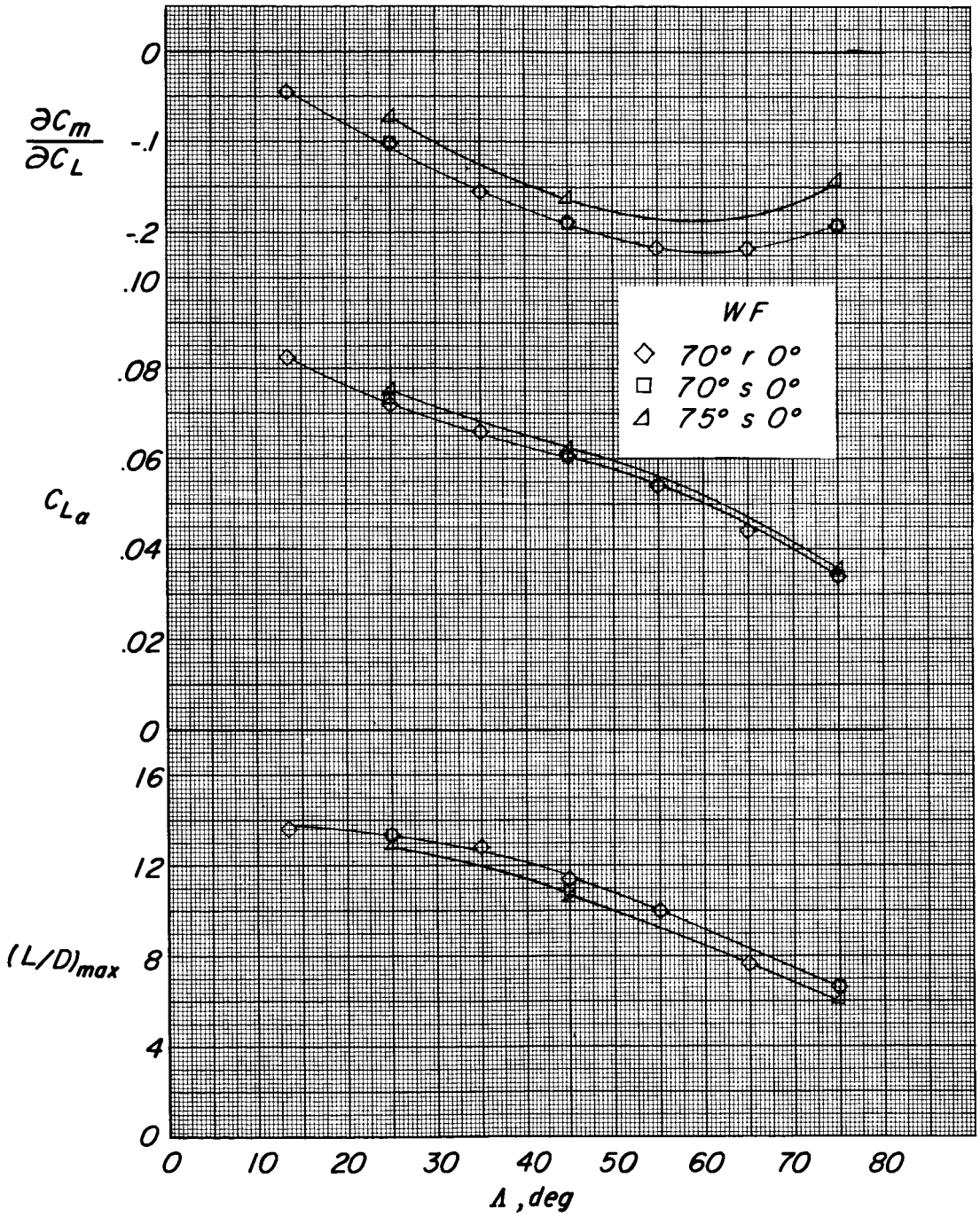

Figure 18.- Effect of wing-fuselage flap geometry on parameters $\frac{\partial C_m}{\partial C_L}$, C_{L_α}, and $(L/D)_{max}$. FW_2HV; $\delta_h = 0°$.

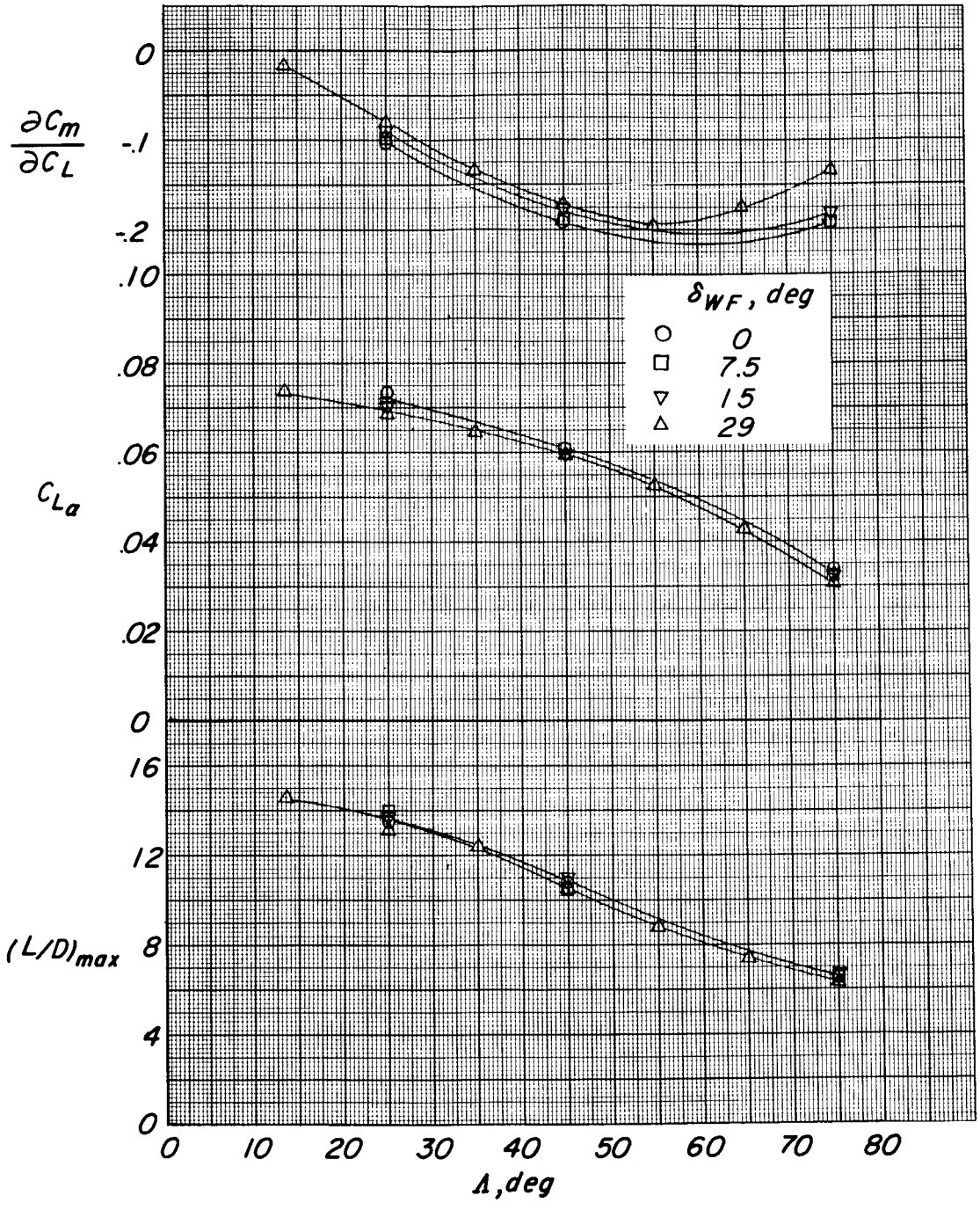

Figure 19.- Effect of wing-fuselage flap deflection on parameters $\frac{\partial C_m}{\partial C_L}$, C_{L_α}, and $(L/D)_{max}$. FW_2HV; $\delta_h = 0^\circ$; WF = 70°s.

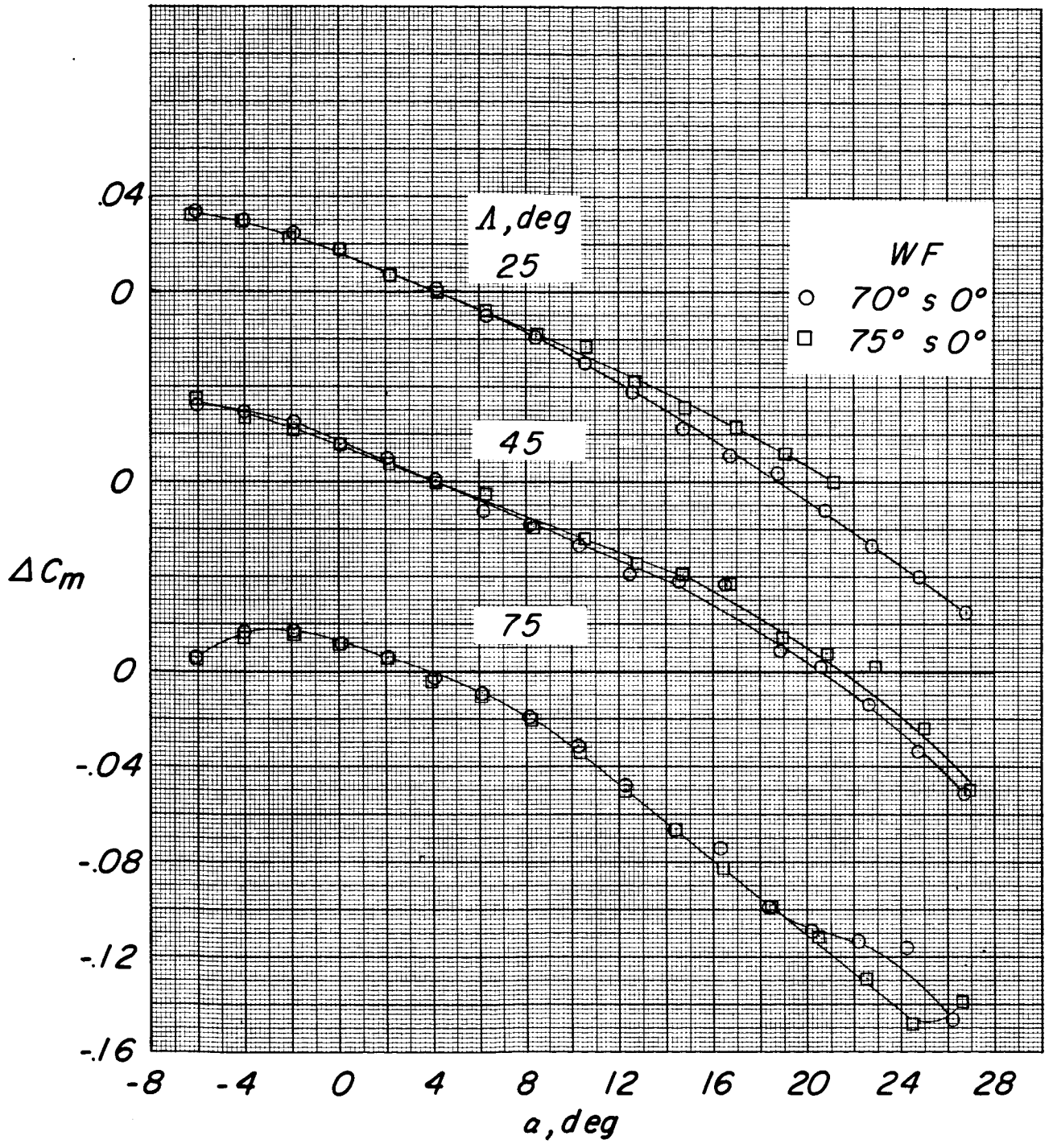

Figure 20.- Effect of wing sweep and wing-fuselage flap geometry on the increment in pitching-moment coefficient due to addition of the horizontal tail ΔC_m for configuration FW_2V.

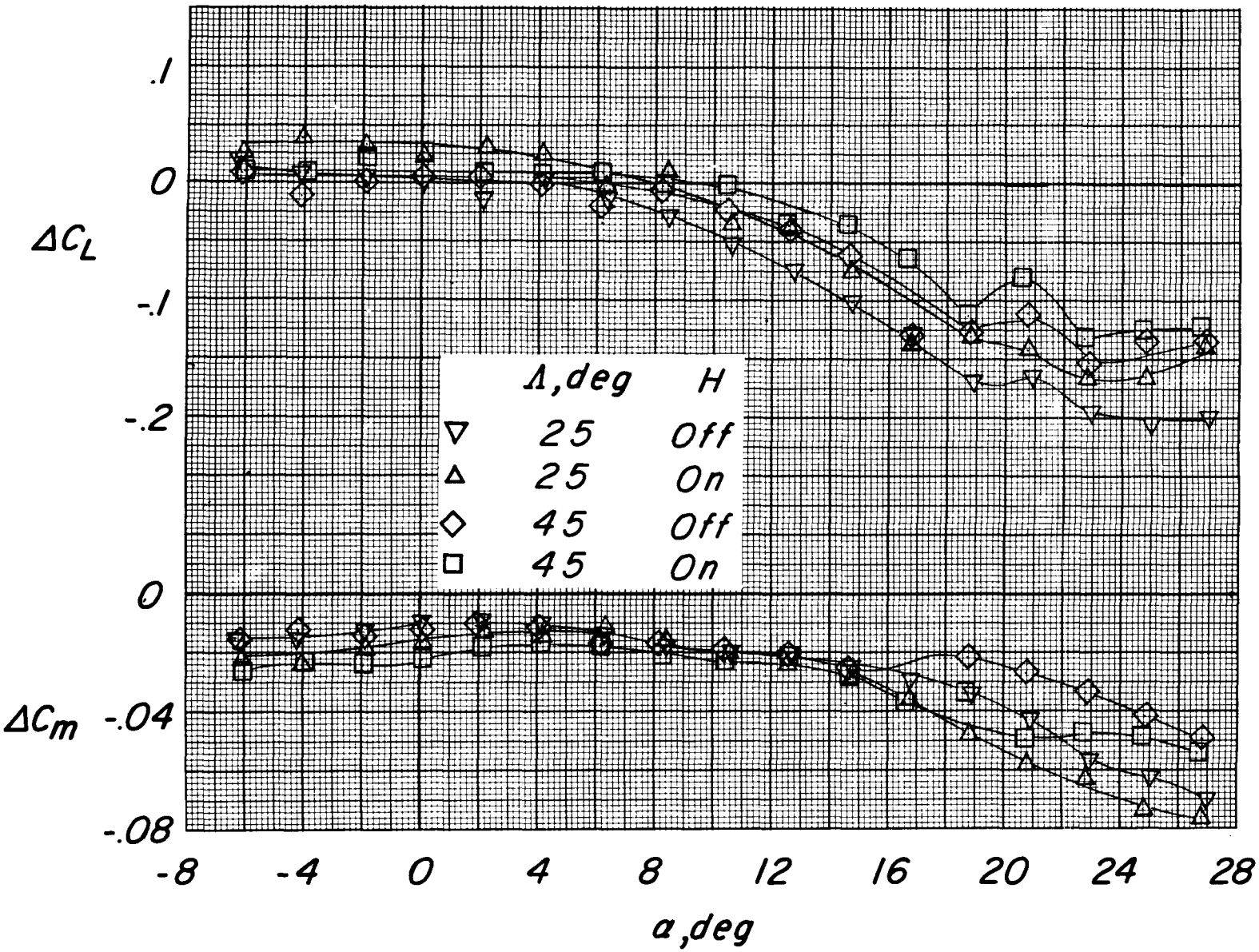

Figure 21.- Increment in pitching-moment and lift coefficients due to the deflection of the wing-fuselage flap. WF = $70^{o}s29^{o}$; FW_2HV.

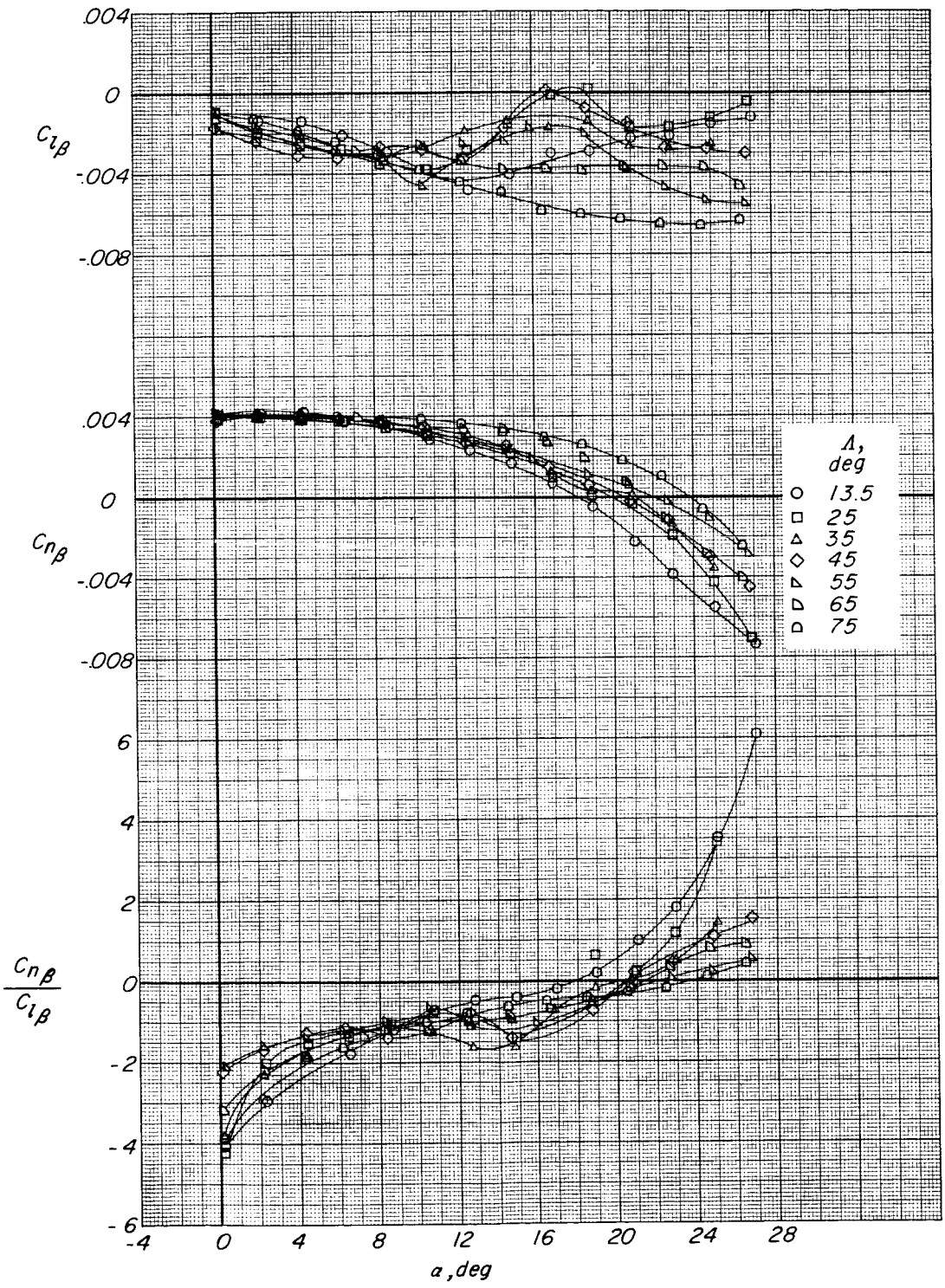

Figure 22.- Effect of wing sweep on lateral stability characteristics in pitch. FW_2HV; $\delta_h = -10^\circ$; WF = 70°s0°.

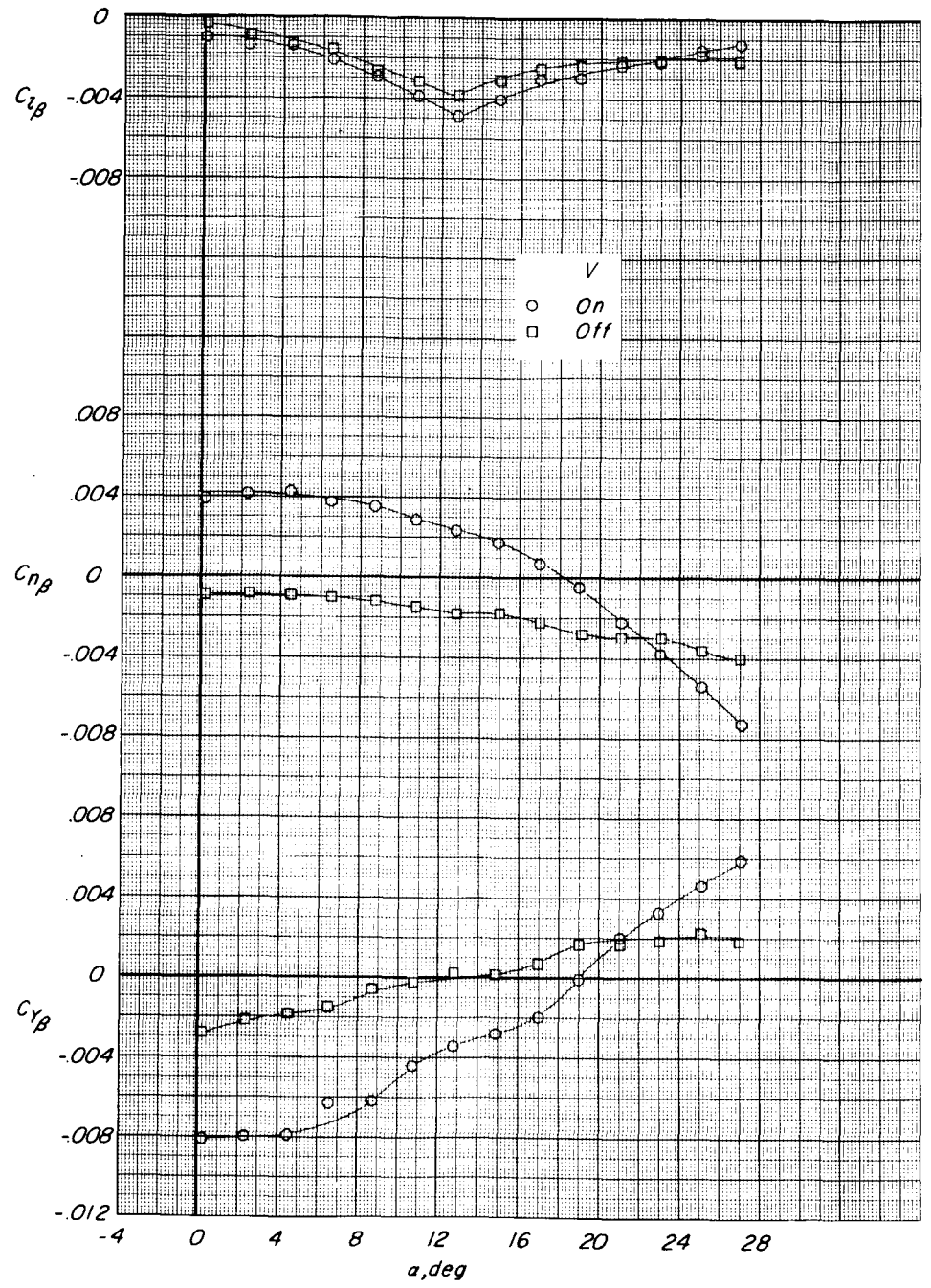

(a) $\Lambda = 13.5^{\circ}$.

Figure 23.- Effect of vertical tail on lateral stability characteristics in pitch. FW_2H; $\delta_h = -10^{\circ}$; WF = 70s0°.

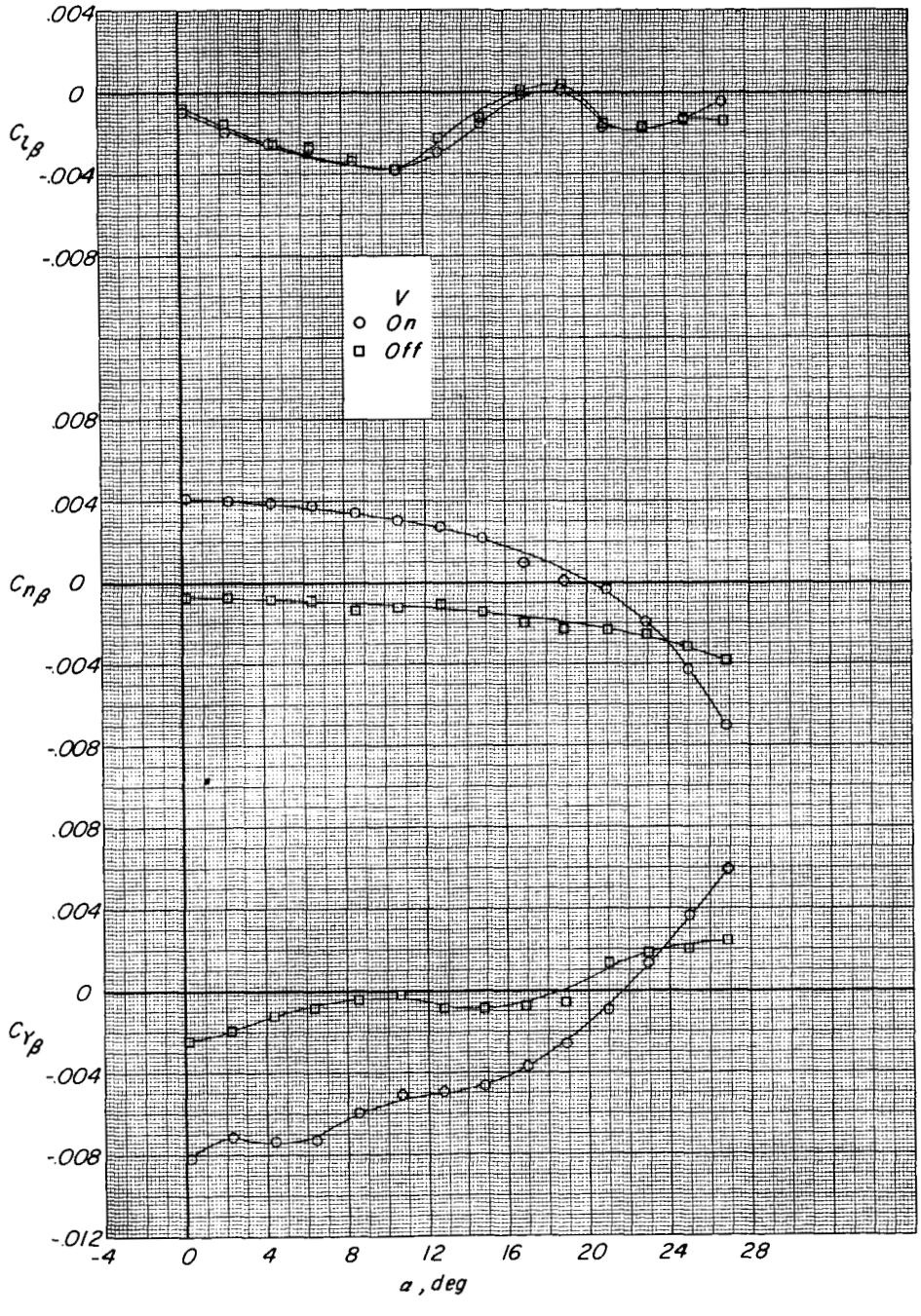

(b) $\Lambda = 25^\circ$.

Figure 23.- Continued.

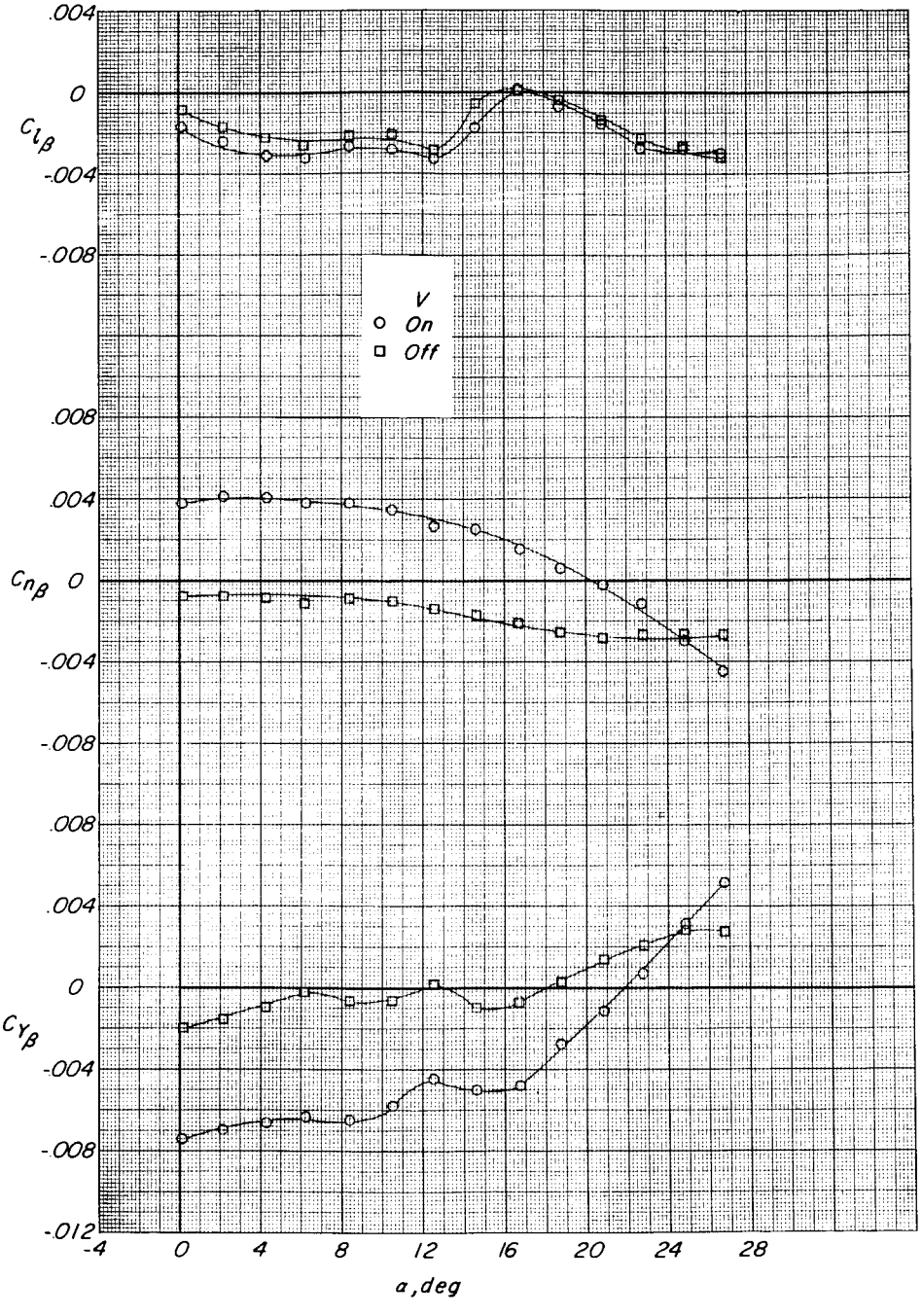

(c) $\Lambda = 45^\circ$.

Figure 23.- Continued.

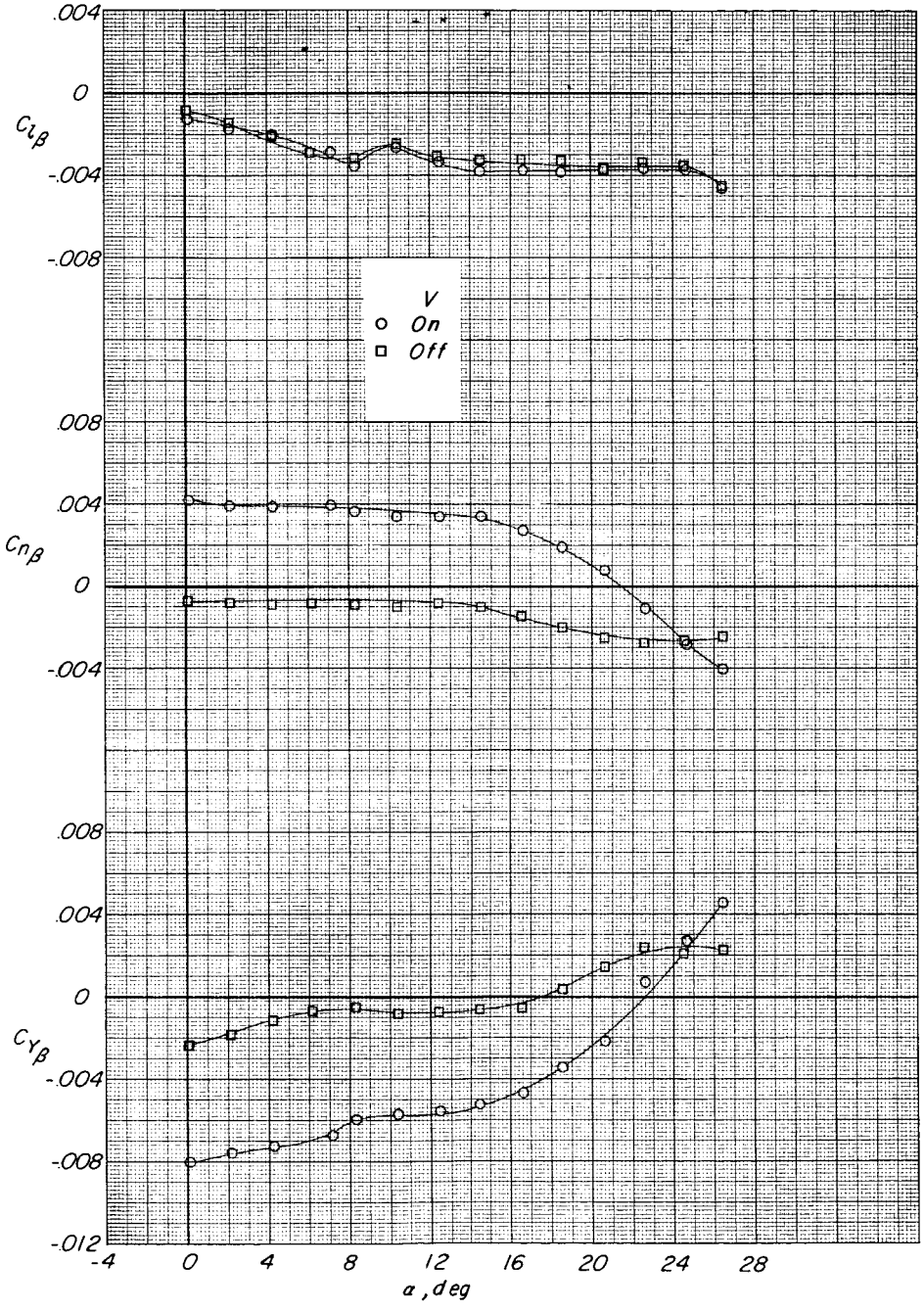

(d) $\Lambda = 65^\circ$.

Figure 23.- Continued.

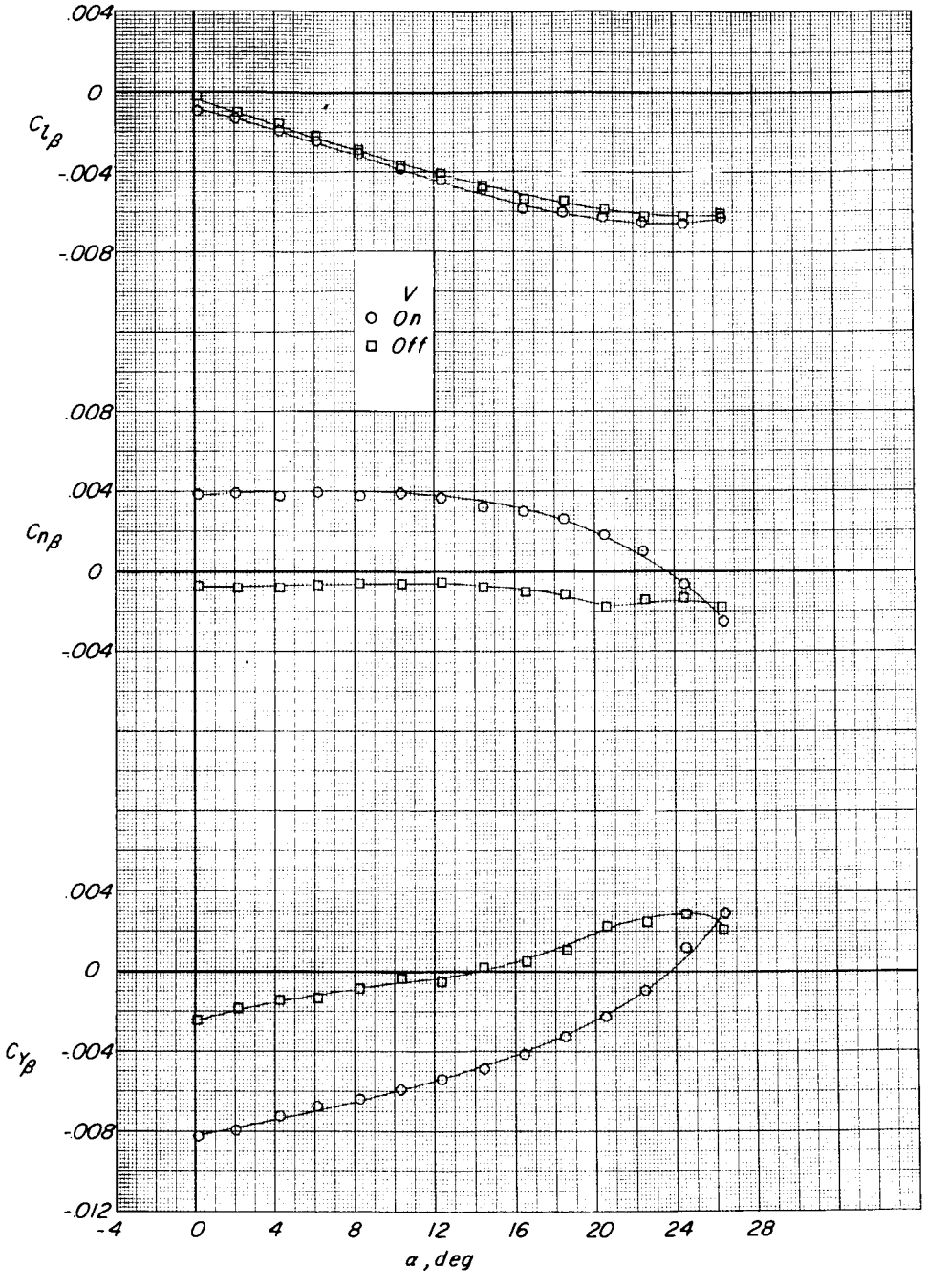

(e) $\Lambda = 75^\circ$.

Figure 23.- Concluded.

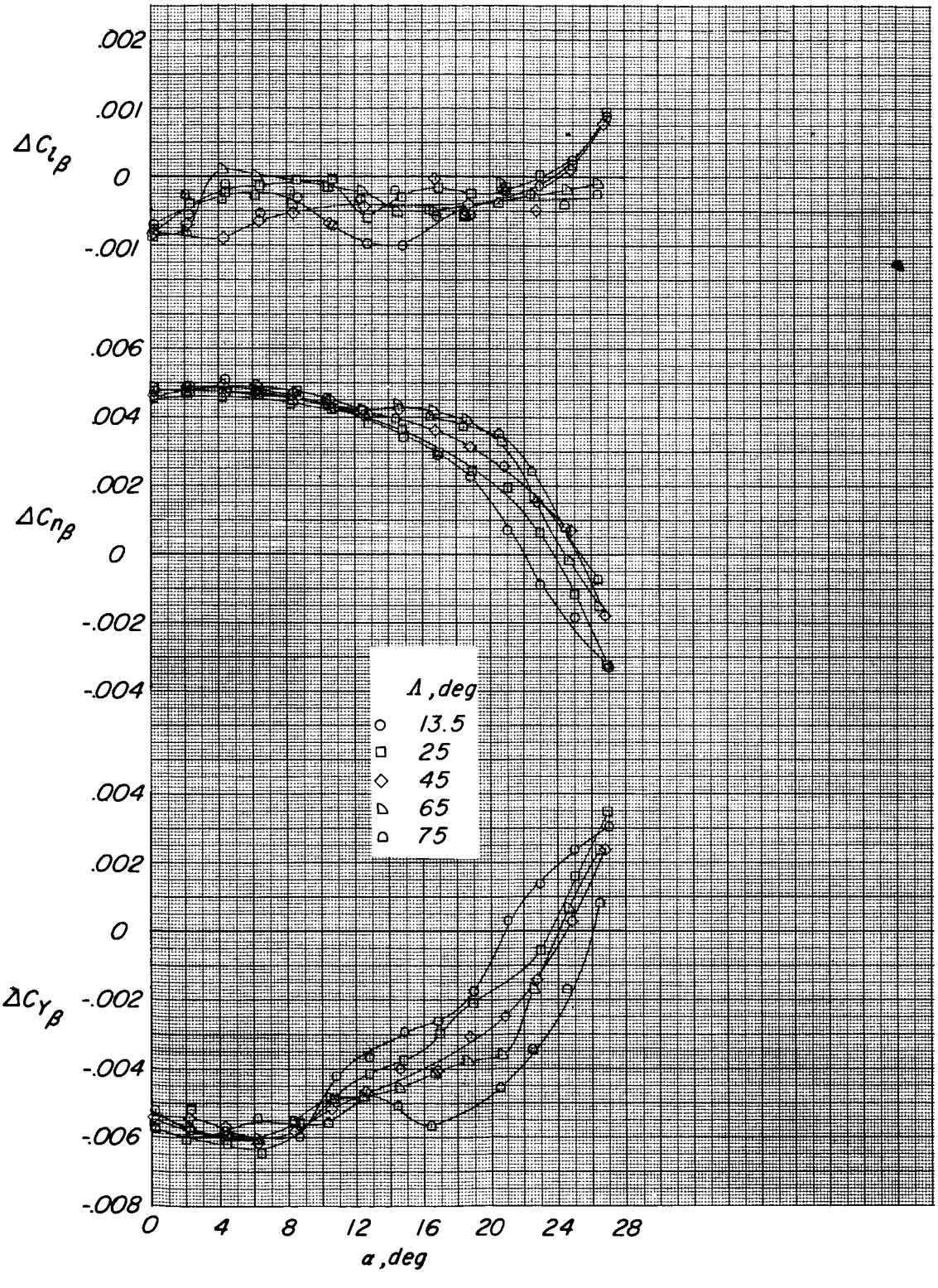

Figure 24.- Effect of wing sweep on vertical-tail contribution. FW_2H; δ_h = -10°; WF = 70°r0°.

[redacted] 8/18/67

"The aeronautical and space activities of the United States shall be conducted so as to contribute . . . to the expansion of human knowledge of phenomena in the atmosphere and space. The Administration shall provide for the widest practicable and appropriate dissemination of information concerning its activities and the results thereof."

—NATIONAL AERONAUTICS AND SPACE ACT OF 1958

NASA SCIENTIFIC AND TECHNICAL PUBLICATIONS

TECHNICAL REPORTS: Scientific and technical information considered important, complete, and a lasting contribution to existing knowledge.

TECHNICAL NOTES: Information less broad in scope but nevertheless of importance as a contribution to existing knowledge.

TECHNICAL MEMORANDUMS: Information receiving limited distribution because of preliminary data, security classification, or other reasons.

CONTRACTOR REPORTS: Technical information generated in connection with a NASA contract or grant and released under NASA auspices.

TECHNICAL TRANSLATIONS: Information published in a foreign language considered to merit NASA distribution in English.

TECHNICAL REPRINTS: Information derived from NASA activities and initially published in the form of journal articles.

SPECIAL PUBLICATIONS: Information derived from or of value to NASA activities but not necessarily reporting the results of individual NASA-programmed scientific efforts. Publications include conference proceedings, monographs, data compilations, handbooks, sourcebooks, and special bibliographies.

Details on the availability of these publications may be obtained from:

SCIENTIFIC AND TECHNICAL INFORMATION DIVISION

NATIONAL AERONAUTICS AND SPACE ADMINISTRATION

Washington, D.C. 20546

[redacted]